TRW Document No. 18353-6006-R0-00

APTD-1345

DEVELOP HIGH CHARGE AND DISCHARGE RATE LEAD/ACID BATTERY TECHNOLOGY

Environmental Protection Agency Contract No. 68-04-0028

APRIL 1972

FINAL REPORT

Prepared for

ENVIRONMENTAL PROTECTION AGENCY
OFFICE OF AIR PROGRAMS
Advanced Automotive Power Systems Development Division
Ann Arbor, Michigan 48105

TRW
SYSTEMS GROUP OF TRW INC.
ONE SPACE PARK • REDONDO BEACH, CALIFORNIA 90278

TRW Document No. 18353-6006-R0-00

DEVELOP HIGH CHARGE AND DISCHARGE RATE LEAD/ACID BATTERY TECHNOLOGY

Environmental Protection Agency Contract No. 68-04-0028

APRIL 1972

FINAL REPORT

Prepared for

ENVIRONMENTAL PROTECTION AGENCY
OFFICE OF AIR PROGRAMS
Advanced Automotive Power Systems Development Division
Ann Arbor, Michigan 48105

TRW
SYSTEMS GROUP OF TRW INC.
ONE SPACE PARK • REDONDO BEACH, CALIFORNIA 90278

FORWARD

This report represents a summary of the work performed by the TRW Systems Group, TRW Inc. The work was performed for the Environmental Protection Agency (EPA), Office of Air Programs, Advanced Automotive Power Systems Development Division under Contract Number 68-04-0028. Performance period was 28 April 1971 through 18 March 1972.

Dr. H.P. Silverman, Program Manager, was responsible for the overall direction of the project. Dr. E. T. Seo was responsible for the TRW tasks. Other major contributors from TRW were N.R. Garner, Dr. G.H. Gelb, R.S. Margulies, M.L. McClanahan and Dr. R.R. Sayano. B. Berman and H. K. Gehm designed the test equipment.

Dr. R.E. Biddick, Manager, Battery Development, Gould Laboratories, Gould Inc., was responsible for the work performed by Gould Inc. on Subcontract Number 029DH1 with TRW Inc. Other major contributors from Gould were Dr. M.H. Little, Dr. F.L. Marsh, G.A. Mueller, R.J. Rubischko and B.J. Sobcjzak.

The Environmental Protection Agency Project Officer was W.A. Robertson of the National Aeronautics and Space Administration, Lewis Research Center. Mr. Robertson worked for the EPA under a special technical assistance agreement between NASA and EPA. The Environmental Protection Agency program manager was Dr. J.T. Salihi.

SUMMARY

TRW adopted two approaches to the development of a lead-acid battery compatible with the requirements of a hybrid heat-engine/electric vehicle. The first approach, a near term plan, was designed to have in production a suitable battery within two years. The goals of this near term approach were to develop a lead-acid battery capable of producing a peak power of 200 W/lb without seriously altering the conventional manufacturing processes, cost or lifetime of the battery. The approach adopted, therefore, was to optimize conventional pasted-plate technology for power.

A state-of-the-art Gould 22F-GP-61 SLI battery (Group Size 22F, 61 A hr, 12 V) was evaluated by tests using both direct current (dc) and the TRW electromechanical transmission (EMT) chopper modes. Discharge currents during dc testing were 50 and 365 A and charge currents were 25 and 180 A. During the EMT testing with a nominal 1-kHz chopper frequency, the average discharge currents were 54 and 350 A at a 50% duty cycle and the average charge currents were 27 and 40 A. Overall energy efficiency at steady state was 79% for both dc and EMT tests. However, during start-up, more gas was evolved in the EMT tests resulting in a lower initial efficiency for the EMT mode.

By modifying current pasted-plate design and refining present production techniques it appeared probable that a battery meeting the performance and cost objectives of the Environmental Protection Agency could be in production by the end of 1972. An analysis of state-of-the-art batteries showed that significantly higher specific power could be achieved by modifying cell components. In order to obtain quantitative data which would permit a closer approach to an optimum design, component parameters were tested in statistically designed experiments. The experiments were designed to indicate optimum plate thickness, paste density, grid design and material. The results established that thin light-weight plates using a low density paste and a lithium-lead alloy provided an optimum power configuration. Based on these results, a computer program was used to predict the current and potential distributions in various plate configurations and to optimize the power to weight ratio.

As a result of these studies the cell element was redesigned. Grid resistance was reduced by redistributing the load. More vertical structure

elements were provided and tapered elements were used to provide more lead in the areas carrying the most current. The current collecting lug was relocated, the plate was shortened and a more conductive alloy was used. Electrolyte resistance was reduced by the use of thinner plates and separators.

Lead-acid cells using the modified design were built that demonstrated specific powers of 150 W/lb for 75 sec (3 W hr/lb) and 204 W/lb for 20 sec, double the output of conventional prismatic cells. This improvement in power was accomplished without requiring any major change in present production methods and without seriously impacting costs. Modified batteries based on these cells can be delivered on a production basis by 1973 at a cost comparable to the cost of conventional batteries.

The performance of the test cells exceeded the power requirements of EPA specifications for a 550-lb battery system and approached those for the 450-lb goal with respect to both average and peak power.

Service life for these test cells was estimated by subjecting them to a stringent, accelerated life test based on the EPA power requirements and compatible with the performance time period of this program. The test cycle contained 365- and 50-A discharges that corresponded to the 70.5- (and 55-) and 10-kW rates of the EPA service-life requirements. The ratio of high-rate to low-rate discharges was 1 to 29 and the charge rate was one-half the discharge rate with the low-rate charge time adjusted to provide a 5% net overcharge. Based on 1.5 V as the failure voltage for the high-rate discharges, our test cells lasted 8,000 to 10,500 total cycles or 260 to 400 high-rate cycles.

Failure analysis indicated shorting through the separator. Incomplete charging due to the shorting through the separators resulted in shedding of the active material. Further tests will be carried out using a more conservative separator material which is thicker and less porous to prevent shorting. In fact, single-plate test cells, using a more conservative separator have survived 600 cycles at twice the current density of the high-rate discharges of the cell tests.

On the basis of the test results, a cell of identical design, except using thicker separators and 17 instead of 21 plates, is expected to meet EPA specifications. The full-size battery would consist of 22 six-cell units connected in series to give a nominal 264 V. Weight and volume would

be 525 lb and 5.5 ft^3, respectively. Life of the battery is expected to be three to five years.

TRW's second, or longer term approach, was to consider advanced technology that could lead to batteries producing 300 W/lb. The bipolar plate, because of its minimum electrical resistance, absence of intercell connectors, maximum current capability, and minimum volume and weight appeared to be a good choice for further development. The feasibility of the lead-acid bipolar battery had been shown in earlier studies by Gould which demonstrated average power levels in the range desired. However, several technical developments were required before it could be used. These included the development of

- a light-weight electronically conductive substrate to which active material could be firmly attached and which would be inert in the cell environment,
- a method of attaching the active material utilizing Planté formation or pasting techniques, and
- a method of constructing a bipolar battery so that individual cells are sealed from each other.

The performance goals were to sustain a 2 $A/in.^2$ (0.3 A/cm^2) discharge rate for 60 sec with a cell voltage $\geq$1.5 V and a recharge time of twice the previous period.

Achievements under this program included:

- Fabrication of thin (0.06 cm), conductive vitreous carbon-epoxy substrates, chemically inert to lead-acid cell environment, and with a resistivity of $\leq$1 Ω cm and a density of $\sim$1.4 g/cm^3,
- method for applying (pasting) the active material onto the substrate,
- negative bipolar plates that exceeded our performance target of 2 $A/in.^2$ (0.3 A/cm^2) at 1.5 V for 60 sec and outperformed standard pasted plates on the basis of a figure of merit, and
- positive bipolar plates that met the performance goal of 2 $A/in.^2$ (0.3 A/cm^2) at 125 °F (52 °C).

Pasted positive bipolar plates performed about the same as average conventional pasted-plate positives. Cycle life of the best bipolar positive plate was 6,000 cycles including 600 deep discharges to 1.0 V. This is believed to be about equivalent to what would be expected from a good conventional positive plate.

The Planté formation of positive active material in a sufficient quantity to meet performance requirements of 2 A/in.^{2} (0.3 A/cm^2) for 60 sec is a major technical obstacle. The difficulty is shedding of the positive material after only a limited thickness is achieved. Efforts to produce more adherent material have failed, thus far. However, it is expected that procedures now under consideration will produce a pasted positive bipolar plate that will have a long life capability at 2 A/in.^{2} (0.3 A/cm^2). This would lead to a projected battery producing 230 W/lb. It is estimated that a prototype battery with these characteristics could be built by 1975.

CONTENTS

	Page
1. INTRODUCTION	1
1.1 PROGRAM GOALS AND APPROACHES	1
1.2 ACHIEVEMENTS	3
2. ANALYSIS OF PROBELM	7
2.1 HYBRID-VEHICLE BATTERY REQUIREMENTS	7
2.2 STATE-OF-THE-ART OF CONVENTIONAL (PRISMATIC) BATTERIES	10
2.2.1 Factors Affecting Specific Power Output	10
2.2.1.1 Effect of Current on Terminal Voltage	10
2.2.1.2 Influence of Design of Battery Requirements	11
2.2.2 Influence of Duty Cycle on Battery Performance	14
2.2.2.1 Overcharging	14
2.2.2.2 Undercharging	16
2.2.2.3 Charge Rate	16
2.2.2.4 Depth of Discharge	17
2.2.3 Analysis of an Available SLI Battery	18
2.2.3.1 Performance Characteristics	18
2.2.3.2 Testing of a 61-A hr Group Size 22F Battery	22
2.2.4 Discussion	33
2.2.4.1 Identification of Technical Problems	33
2.2.4.2 Conclusions	36
2.3 ADVANCED (ALTERNATE) CONCEPT BATTERIES	37
2.3.1 Bipolar Battery	37
2.3.2 Tubular Plate Battery	38
2.4 APPROACH TO SOLUTION	40
3. OPTIMIZATION OF CONVENTIONAL (PRISMATIC) BATTERIES	43
3.1 GRID STRUCTURE	43
3.1.1 Mathematical Modeling	43
3.1.1.1 The Model	43
3.1.1.2 Results	45
3.1.2 Accelerated Corrosion Tests of Selected Alloys	46
3.1.2.1 Approach and Selection of Alloys	46
3.1.2.2 Experimental Procedure	48
3.1.2.3 Results and Conclusions	51

CONTENTS (Continued)

Page

3.2 COMPONENTS-LEVEL TEST PLATES 62

3.2.1 Concept Requirements and Performance-Test Design. 62

3.2.2 Test Plate Fabrication. 66

3.2.3 Test Equipment. 68

3.2.4 Performance Tests and Results 71

3.2.4.1 Preliminary Check-Out. 71
3.2.4.2 Performance Tests. 78
3.2.4.3 Cycle-Life Tests 89

3.3 TEST CELLS 89

3.3.1 Cell Design and Fabrication 89

3.3.2 Test Procedures 96

3.3.3 Tests and Results. 99

3.3.3.1 Performance. 99
3.3.3.2 Cycle Life 104

3.3.4 Summary and Recommendations 107

4. DEVELOPMENT OF BIPOLAR BATTERIES. 109

4.1 ELECTRODE STUDIES. 109

4.1.1 Objectives. 109

4.1.2 Conductive Substrates 109

4.1.3 Electrode Development 116

4.2 ELECTRODE AND BATTERY EVALUATION 125

4.2.1 Fabrication 125

4.2.2 Tests and Results 127

4.3 SUMMARY AND RECOMMENDATIONS. 131

5. PROJECTIONS AND RECOMMENDATIONS 133

5.1 PRISMATIC CELLS. 133

5.1.1 Duty Cycle and Design Requirements. 133

5.1.1.1 Battery Power Requirements 133
5.1.1.2 Battery Weight and Volume. 138

5.1.2 Projected Characteristics of Cell and Full-Size Battery .138

5.1.3 Availability and Development. 138

CONTENTS (Continued)

Page

5.2 BIPOLAR BATTERY. 140

5.3 FUTURE WORK. 141

5.3.1 Program Plan. 141

5.3.2 Work Statement. 142

APPENDIX A. 147

APPENDIX B. 153

LIST OF TABLES

Number		Page
1	Plate Capacity in Terms of Electrolyte Specific Gravity for Several Temperatures	15
2	Weight Breakdown for 61-A hr Group Size 22F Battery.	19
3	Electrolyte Distribution in 61-A hr Group Size 22F Battery Cell	20
4	Resistances of Components in a 61-A hr Group Size 22F Battery.	23
5	Percent of Total Resistance for Components in a 61-A hr Group Size 22F Battery	24
6	Steady-State DC Performance of 61-A hr Group Size 22F Battery.	27
7	Losses Due to Resistance during DC testing for a 61-A hr Group Size 22F Battery	32
8	Discharge and Charge Cycles for a 55-kW Battery.	41
9	Resistances of Pasted-Plate Cells during Accelerated Corrosion Test at 71 °C.	52
10	Capacities of Pasted-Plate Cells during Accelerated Corrosion Test at 71 °C.	53
11	Growth of Pasted-Plate Specimens during Accelerated Corrosion Test at 71 °C.	54
12	Growth-Rate Constants for Pasted-Plate Specimens at 71 °C.	55
13	Estimated Growth-Rate Constants and Life Times for Pasted Plates.	59
14	Comparison Data for Rod, Bare-Grid and Pasted Plate Specimens Obtained during Accelerated Corrosion Test	61
15	Test Plan Layout for Components Level Test Plates at One Temperature.	63
16	Test Sequence of Test Plates	65
17	75-Second Discharge Currents for Pb 660 Positive Plates.	74
18	Summary of $i_{75}\bar{V}$ Values for Pb 660 Positive Plates.	75
19	Average $i_{75}\bar{V}$ Values for Pb 660 Positive Plates	76

LIST OF TABLES (Continued)

Number		Page
20	Analysis of Variance for Power (Pb 660 Positive Plates)	77
21	Properties of Components-Level Test Plates	79
22	Distribution of Components-Level Test Plates between Replicate Groups	80
23	Figures of Merit for Specific Power Based on Plate Weight, W/g	81
24	Figures of Merit for Specific Power Based on Paste Weight, W/g	82
25	Figures of Merit for Charge Acceptance for Components-Level Test Plates	83
26	Summary of Burn-In and Temperature Effects for Components-Level Test Plates	84
27	Analysis of Variance for Specific Power for Components-Level Test Plates	85
28	Figures of Merit for Specific Power for Components-Level Test Plates from Test Run 2 by Grid Type and Temperature	87
29	Summary of Components-Level Performance Tests on Negative Plates	88
30	Cycle-Life Test Data for Components-Level Test Plate P089 at 52 °C	90
31	Group Weights for Type IA Cells	92
32	Group Weights for Type IB Cells	94
33	Summary of Performance Test Data for Pasted-Plate Cells	100
34	Summary of Peukert-Plot Test Data for Pasted-Plate Test Cells	101
35	Averaged Specific Power Values for Pasted-Plate Cells	102
36	Anodic Corrosion Test Data on Substrate Material	112
37	Results of Conductive Plastic Fabrication Experiments	113
38	Formation and Performance of Planté-Type Positive Plates Formed on Conductive Epoxy-Vitreous Carbon Substrates	117

LIST OF TABLES (Continued)

Number		Page
39	Fabrication of Pasted-Plate Positives with Epoxy-Vitreous Carbon Substrates.	.119
40	Formation and Performance of Pasted-Plate Positives with Epoxy-Vitreous Carbon Substrates	.120
41	Performance Data for Bipolar Positive Electrode PA12	.123
42	Single Bipolar Electrode Weights	.126
43	Type II (Bipolar) Battery Electrode Weights.	.128
44	Performance Test Data on Bipolar Plates.	.130
45	Battery-Weight Constraints for Hybrid-Vehicle Systems (92.5-kW Peak Power Demand).	.139

LIST OF FIGURES

Number		Page
1	Power Profile for Revised EPA Battery Performance Requirements	9
2	Time vs. Voltage Trace during DC Test of 61-A hr, Group Size 22F Battery	26
3	EMT Transient Waveforms during Test of 61-A hr, Group Size 22F BAttery	29
4	Gas Evolution during Test of 61-A hr, Group Size 22F Battery	31
5	Outline of Grid for Pasted-Plate Test Cell	47
6	Accelerated Corrosion Test Assembly for Bare Grids and Rods.	49
7	Growth Rate Plot for Li and Sb-As Alloys	56
8	Second-Order Growth-Rate Plots for Sb-As Alloy	57
9	Outlines of Grids Used in Components-Level Test Plates	67
10	Block Diagram of Components-Level Tester	69
11	Schematic of Component-Level Test-Cell	72
12	Type IB Test Cell.	95
13	Battery Test Equipment	98
14	Typical Peukert Plot for Type IA Test Cell	103
15	End-of-Discharge Voltage for Cycle B vs. Cycle Number for Test Cells	105
16	IR Loss in Bipolar Substrate at 0.31 A/cm^2 vs. Substrate Resistivity at Various Substrate Thicknesses	110
17	Resistivity vs. Vitreous Carbon Content of a CIBA 1139/972 Substrate	115
18	Two-Cell Bipolar Battery	129
19	Wheel Power Demands for a 4,000-lb	134
20	EPA Battery Power Profile for a 4,000-lb Series Hybrid Vehicle.	135
21	Typical Histogram of Battery Current during a Driving Cycle.	137

1. INTRODUCTION

The objective of this program is to develop a high charge rate, high discharge rate lead-acid battery compatible with the requirements of a hybrid heat-engine/electric vehicle. Because the power requirements and charge-discharge profiles for a hybrid-vehicle battery are sufficiently different than those for a conventional lead-acid battery, a development program was undertaken to optimize the lead-acid battery for hybrid-vehicle use. The goals of the program are to maximize specific power without significantly affecting cost, lifetime or maintenance, As a result of this program ten test cells producing specific powers of 150 W/lb for a 75-sec discharge and 204 W/lb for a 20-sec discharge were developed and tested.

1.1 PROGRAM GOALS AND APPROACHES

As a result of examining the lead-acid battery problem, a program plan was developed which comprised two approaches to developing batteries that can satisfy the hybrid-vehicle requirements. One approach was to adapt conventional pasted-plate technology to a 55-kW battery (original EPA specifications) with further optimization leading to a 200-W/lb battery system, an anticipated requirement confirmed during the course of the program by EPA's revised specifications. This approach was selected to provide a near term solution with batteries being ready for production in two years. (EPA specifications are detailed in Section 2.1.) The second approach, a longer term effort, was to develop a bipolar battery which ultimately could lead to a 300-W/lb battery.

The revised power-time specifications were evaluated in terms of vehicle velocity-time characteristics for a 4,000-lb family car. The EPA specifications allow a series hybrid vehicle to accelerate to 60 mph in slightly over 12.5 sec and reach almost 90 mph in 25 sec. This performance is in line with EPA's vehicle design goals.

A state-of-the-art Gould 22F-GP-61 SLI battery (Group Size 22F, 61 A hr, 12 V) was evaluated by tests using both direct current (dc) and the TRW electromechanical transmission (EMT) chopper modes. Discharge currents during dc testing were 50 and 365 A and charge currents were 25 and 180 A. During the EMT testing with a nominal 1-kHz chopper frequency, the average

discharge currents were 54 and 350 A at a 50% duty cycle and the average charge currents were 27 and 40 A. Overall energy efficiency at steady state was 79% for both dc and EMT tests. However, during start-up more gas was evolved during the EMT tests, resulting in a lower initial efficiency for the EMT mode.

By adjusting conventional pasted-plate design and by refining present production techniques it appeared probable that the performance and cost objectives of the original EPA specifications could be met by 1972. However analysis showed that by optimizing components, higher specific power was realizable. In fact, TRW had tested pasted-plate batteries with a specific power exceeding 200 W/lb but their recharging characteristics were not satisfactory. In order to obtain data which would permit a closer approach to an optimum design, various design concepts, component modifications, and parameters were tested in statistically designed experiments on single electrodes and cells. Those experiments were designed to indicate optimum plate thickness and paste density, and elucidate to some degree a preferred grid design and material.

Accelerated corrosion tests were used to evaluate selected, more conductive alloys. Both extensive and intensive tests were performed to find improved alloys and evaluate their life by means of accelerated tests.

Computer programs were used to predict the current and potential distributions in various plate configurations, with the objective of optimizing the weight, uniformity of potential, and ease of fabrication of the battery.

Development of the bipolar battery which was recognized to be a longer term effort, was undertaken because it offered the advantages of minimum electrical resistance, absence of intercell connectors, maximum current capability, and minimum volume and weight for use in a hybrid heat-engine/electric family automobile. The feasibility of the lead-acid bipolar battery had been demonstrated in rather long-term tests lasting from several months to over a year at average power levels in the range required for the hybrid car.

1.2 ACHIEVEMENTS

Prismatic lead-acid cells that produce specific powers of 150 W/lb for 75 sec and 204 W/lb for 20 sec were built and tested. This is almost double the output of conventional prismatic cells. The improved specific power is achieved by accommodating a larger number of thin, light-weight plates with the volume and weight of a conventional battery. These thin light-weight plates are the result of the development of highly conductive alloys which are more corrosion resistant than the standard grid alloy, and a new grid structural design. The optimization studies which led to the improved design were accomplished using a factorial experiment and a TRW-developed computer program. No major change in present production methods or serious impact on costs is anticipated. Modified batteries based on these cells can be delivered on a production basis by 1973 at a cost comparable to the cost of conventional batteries.

The performance of the test cells exceeds the power requirements of the revised EPA specifications for the 550-lb battery system and approaches those for the 450-lb goal with respect to both the 70.5-kW average and 92.5-kW peak power. The EPA power requirements translate into the following specific powers and currents:

Power, kW	Weight, lb	Minimum Voltage, V	Specific Power, W/lb	Current, A
92.5	550	200	168	462
92.5	450	200	206	462
70.5	550	200	128	352
70.5	450	200	157	352
55	550	150	100	367

Our test cells sustained currents of 418 to 500 A for 75 sec, which corresponded to specific powers of 143 to 170 W/lb for a 75-sec discharge and peak currents of 600 A for 20 sec which corresponded to 204 W/lb (4.7-lb packaged cells). Thus in a 550-lb system the test cells would exceed the original 55-kW and the revised 70.5-kW requirements for average power for a discharge time which is 25-sec longer than the two 25-sec discharges of the EPA requirement. The 204-W/lb peak power for 20 sec at an average cell voltage of 1.6 V approximates the two 9-sec discharges of the EPA specifications. Both average and peak specific power values approach the goal of a

450-lb battery system.

Service life of the test cells was estimated by subjecting them to a stringent, accelerated life test based on the EPA power requirements and compatible with the performance time period of this program. The test cycle contained 365- and 50-A discharges that corresponded to the 70.5- (and 55-) and 10-kW rates of the EPA service-life requirements. The ratio of high-rate to low-rate discharges was 1 to 29 and the charge rate was one-half the discharge rate with the low-rate charge time adjusted to provide a 5% overcharge. Based on 1.5 V as the failure voltage for the high-rate discharges, the test cells failed after 8,000 to 10,500 total cycles or 260 to 400 high-rate cycles. The 10-kW level did not place a burden on the cell performance. Failure analysis indicated shorting through the separator and softening and shedding of the positive active material. Softening resulted from incomplete charging due to the shorting through the separators and the very stringent cycling conditions which are useful for comparing various cell designs but hardly permit estimation of battery life in a hybrid vehicle. Further tests should be carried out under conditions more representative of hybrid vehicle duty, with more shallow cycles, and a more complete charge after an occasional high-rate discharge.

Because thin, porous separators were used, we feel confident that the shorting through the separator can be corrected by a more conservative test cell design using thicker, less porous material to prevent shorting. In fact, a components-level single-plate test cell survived 600 cycles at twice the current density of the high-rate discharges during the test cell cycling. Test cells are now being retrofitted with more conservative separator material. However, the testing of the cells will not be completed in time to be included in this report.

On the basis of the test results, a cell of identical design, except using 17 instead of 21 plates, is expected to meet EPA specifications. The full-size battery would consist of 22 six-cell units connected in series to give a nominal 264 V. Weight and volume would be 525 lb and 5.5 ft^3, respectively. Life of the battery is expected to be three to five years based on accelerated corrosion tests on new grid alloys and past experience.

The development of bipolar batteries is a longer term effort than the optimization effort, but could lead to a long-life, 300-W/lb battery. The objectives of this program were:

- a light-weight electronically conductive substrate to which active material could be firmly attached and which would be inert in the cell environment,
- a method of attaching the active material utilizing Planté formation or pasting techniques, and
- a method of constructing a bipolar battery so that individual cells are sealed from each other.

The performance goals were to sustain a 2 A/in.^{2} (0.3 A/cm^2) discharge rate for 60 sec with a cell voltage $\geq$1.5 V and a recharge time of twice the previous discharge period.

Achievements included:

- Fabrication of thin (0.06 cm), conductive vitreous carbon-epoxy substrates, chemically inert to lead-acid cell environment and with a resistivity of $\leq$1 Ω cm and a density of $\sim$1.4 g/cm^3.
- method for applying (pasting) the active material onto the substrate,
- negative bipolar plates that exceeded our performance target of 2 A/in.^{2} (0.3 A/cm^2) at 1.5 V for 60 sec and outperformed standard pasted plates on the basis of figure of merit and
- positive pasted bipolar plates that met the goal of 2 A/in.^{2} (0.3 A/cm^2) for 60 sec at 125 °F.

Positive pasted bipolar plates performed about the same as average conventional pasted-plate positives. Cycle life of the best bipolar positive plate was a total of 6,000 cycles including 600 deep discharges to 1.0 V at room temperature. This is believed to be about what could be expected from a good conventional positive plate.

The current density goal of 2 A/in.^{2} (0.3 A/cm^2) for 60 sec was met by the pasted positive bipolar plate in tests at 125 °F. Planté formed positive bipolar plates were not tested at high temperature because tests at room temperature indicated that a sufficient quantity of Planté-formed

positive active material could not be made to adhere to the plate. Active material shedding caused short cycle life and efforts to produce a more adherent structure by alloying the lead base material failed.

Based on single-plate results, it is conservatively estimated that a prototype bipolar battery with pasted plates of the type tested will have a specific power of 164 W/lb and 21 kW/ft^3 for a 75-sec discharge to 1.5 V per cell. We estimate that a prototype battery of this type weighing 430 lb and occupying 3.3 ft^3 could be built in 1973, with production in 1975.

Over a longer term it is expected that the overall long-life current capability can be increased to 2 $A/in.^2$, resulting in a 33% reduction in size, to four modules instead of six. This leads to a projected battery weighing 300 lb and having a volume of 2.2 ft^3. Specific power would be 230 W/lb and 31 kW/ft^3. It is estimated that a prototype battery with these characteristics could be built in 1975 or earlier.

The organization of this report is essentially by task number, except that for the sake of clarity the material covering the development and testing of bipolar cells has been separated from the material concerning conventional (prismatic) cells. Bipolar battery development is covered separately in Section 4.

2. ANALYSIS OF PROBLEM

2.1 HYBRID-VEHICLE BATTERY REQUIREMENTS

The impact of a hybrid-vehicle's operating profile on its battery system was discussed in Section 1.1. Design goals for the battery and the program plan to achieve the goals were dictated by EPA's original requirements in Exhibit I, RFP No. EHSD 71-Neg. 100 and TRW's realization that a much higher specific power (∿200 W/lb) was needed and attainable. During the course of the program, revised EPA requirements were provided by W.A. Robertson, Project Officer, in Technical Direction No. 3, 1 December 1971, which approximated our original ∿200-W/lb estimate.

Both EPA requirements of a lead-acid battery for a hybrid heat engine/electric automobile are given below.

Exhibit I, RFP No. EHSD 71-Neg. 100 (original requirements):

The full size vehicle battery shall be capable of the following performance:

Power:

1. 55-kW discharge rate sustained for 25 sec and performed for two such 25-sec periods within a 60-sec interval.
2. 30-kW recharge rate sustained for 90 sec directly following the two above discharges of Item 1.

Voltage:

200 to 220 V open circuit; 150 V minimum working voltage.

Life:

The battery should be capable of operating at the above power rates and durations after operating for 5 years and 200,000 cycles which include the following number and types.

Number of Cycles	Discharge Rate, kW	Charge Rate, kW	Energy transferred to and from battery, W hr
500	55	30	380
3000	55	30	130
3000	55	30	80
balance of 200,000	10	5	30

Weight:

550 lb maximum.

Cost:

The battery should be capable of a mass production cost of less than $550.

Operation:

Suitable for safe use in a family automobile without undue care and maintenance.

Technical Direction No. 3, 1 December 1971 (revised requirements):

The full size vehicle battery shall be capable of the following performance:

Power:

1. The power profile of Figure 1 with peak power of 92.5 kW and performed for two such 25-sec periods within a 60-sec interval.
2. A minimum recharge rate of 39 kW sustained for 90 sec directly following the two above discharges.

Voltage:

Minimum working voltage of 200 V. Minimum cell voltage of 1.5 V.

Life:

The battery should be capable of operating at the above power rates and durations after operating for 5 years and 200,000 cycles which include the following number and types:

Number of Cycles	Discharge Rate, kW	Charge Rate, kW	Energy transferred to and from battery, W hr
500	70.5	39	490
3000	55	30	130
3000	55	30	80
balance of 200,000	10	5	30

Weight:

550 lb maximum. (Goal 450 lb max.)

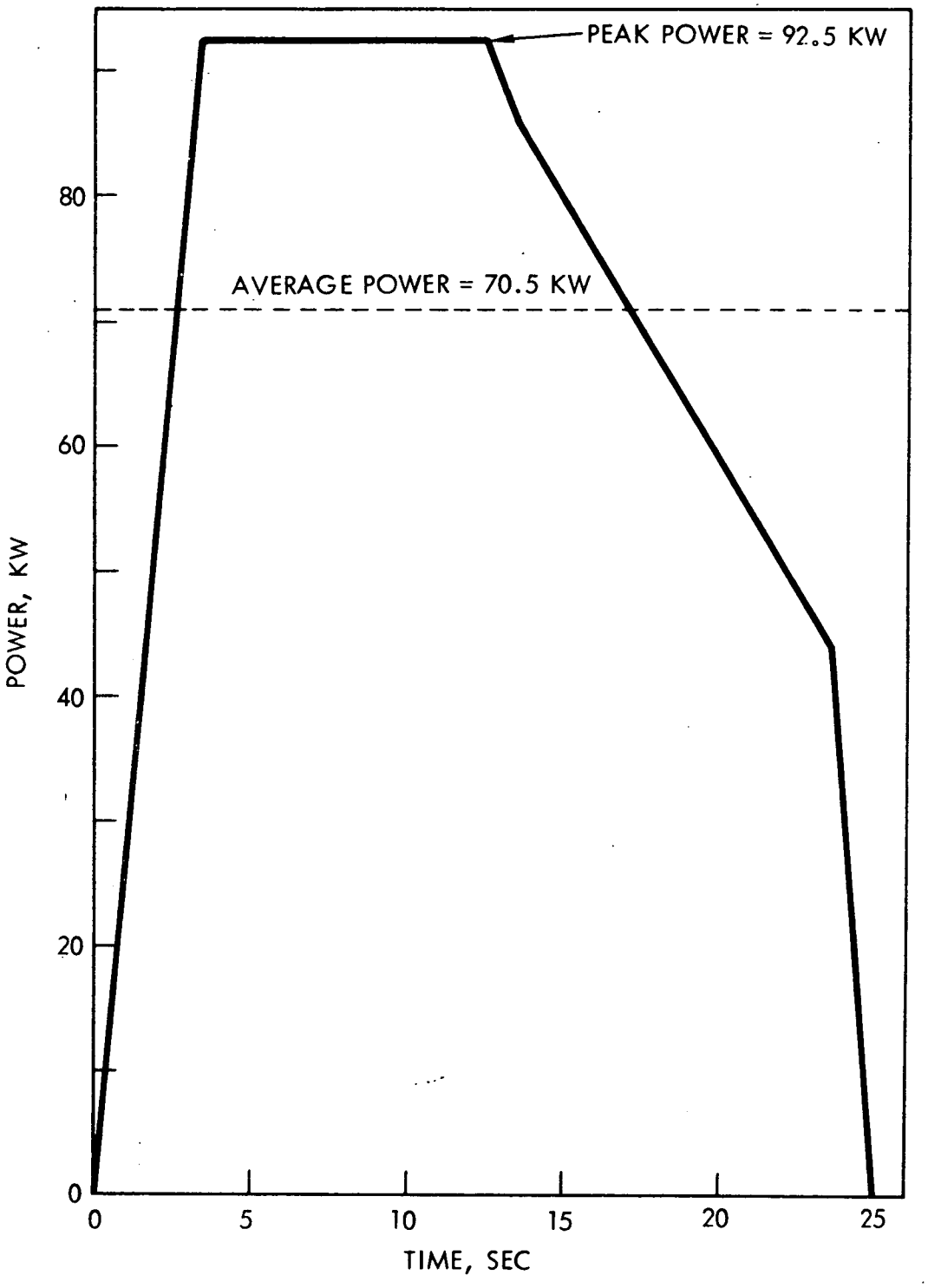

Figure 1. Power Profile for Revised EPA Battery Performance Requirements

Cost:

The battery should be capable of a mass production cost of less than $550.

Operation:

Suitable for safe use in a family automobile without undue care and maintenance.

2.2 STATE-OF-THE-ART OF CONVENTIONAL (PRISMATIC) BATTERIES

2.2.1 Factors Affecting Specific Power Output

2.2.1.1 Effect of Current on Terminal Voltage

Specific power output is determined by all the factors that govern the battery's terminal voltage under load, and by the weight of the battery itself. The following equation developed by Shepherd (C.H. Shepherd, "Theoretical Design of Primary and Secondary Cells," U.S. Naval Research Laboratory, Report No. 6129, AD 617 333, 1964) gives the relationship between the terminal voltage of a cell and certain fundamental parameters

$$E = E_s - iK\left(\frac{Q}{Q - it}\right) - iL$$

where E is cell voltage, V; E_s is the open-circuit voltage, V; K is a polarization constant, $\Omega\ cm^2$; i is current density, A/cm^2; Q is the limiting electrode's available capacity per unit area, C/cm^2; L is the internal resistivity per unit area, $\Omega\ cm^2$; and t is time, sec.

This equation was analyzed to determine the relative importance of its factors.

The current density, i, should be as low as possible. This means a maximization of the electrode surface area, requiring, therefore, the use of as thin a plate as possible consistent with maintaining physical integrity for long life under the stipulated cycle conditions. Physical integrity is also governed by the paste density.

The internal resistivity, L, should be as low as possible. This constant represents the net resistivity of the separator, grids, electro-

lyte, terminals and intercell connectors. Through-the-partition connectors in which the intercell connection is through the cell case wall, rather than across the top of the battery, effectively minimize this contribution to the overall internal resistance. The necessity of using thin grids disallows any freedom in changing grid resistance except through the antimony content and possibly by rearranging structural members. For example, pure lead at 20 °C has a resisitivty of 21.2×10^{-6} Ω cm, 4% antimony-lead alloy, 24×10^{-6} Ω cm, and 8% antimony-lead alloy 26.5×10^{-6} Ω cm. The interelectrode spacing is governed by the separator, and separator resistance depends on the construction material, the thickness of the backweb, size and pore-size distribution.

The factor Q/(Q - it) is essentially a measure of the state-of-charge, and is a term that modifies the current density, i. This means that as active material is electrochemically consumed, the current density becomes effectively larger. In the case of the present application, however, the state-of-charge is always at a comparatively high level, and the gross electrolyte concentration remains essentially unchanged during the shallow cycles.

The factor, K, is a coefficient of polarization, a highly critical term involving such parameters as paste densities (porosities) and electrolyte concentration. Concentration polarization is a source of voltage drop when the discharge current is high and prolonged, since the concentration of sulfuric acid in the immediate vicinity of the active material surface decreases.

2.2.1.2 Influence of Design on Battery Performance

Separators

The primary purpose of the separator in a lead-acid battery is to prevent electronic conduction between the plates of opposite polarity while permitting electrolytic conduction. A wide variety of separators is presently used in the industry. These include types made of wood veneer, perforated and slotted separators of hard rubber, microporous rubber and fibrous glass mats; additionally, separators made of micro-

porous plastics, fibrous materials impregnated with resins, regenerated cellulose films, and fabrics such as Saran, Dynel, and Vinyon are available.

As a general rule, ribbed separators are used in SLI batteries. This type of separator is flat on one side and ribbed on the other; in the construction of the battery elements, the flat surface is placed against the negative plate and the ribs against the positive. The ribbed separator construction, since it ensures the presence of free electrolyte in the vicinity of the positive plate, optimizes the high-rate discharge characteristic of the battery.

The positive electrode discharge is in accordance with this equation:

$$PbO_2 + SO_4^{=} + 4H^{+} + 2e^{-} = PbSO_4 + 2H_2O.$$

As can be seen, the reaction is such that not only is sulfuric acid consumed during the discharge but water is created serving to dilute the concentration further. By the use of the ribbed separator, which establishes a region of free-flowing electrolyte near the positive electrode, the transfer of liquid species is enhanced.

A resin-impregnated paper separator with embossed ribs coated with polyvinyl chloride is typically used in SLI batteries. It has an overall thickness of 0.052 in. (0.132 cm) with a resistivity of approximately 0.23 Ω cm^2 measured in accordance to the AABM test methods. In this test the separator resistivity is calculated by subtracting the resistivity between battery plates spaced a fixed distance apart without a separator from the resistivity measured with the separator between the plates; the specific gravity of the sulfuric acid for this test is 1.280. Other separators of lower resistivities are currently available, for example, 0.052-in. (0.132 cm) thick porous polyethylene separator recently tested was found to have a resistivity of 0.12 Ω cm^2.

Paste Density of Plates

Failure (incapability of the battery to deliver a stipulated percentage of capacity at a specified rate) occurs, in most instances, because of

the shedding of material from the positive plate, and grid corrosion. This condition is due, for the most part, to persistent overcharging and is accelerated by the use of plates not sufficiently dense for the service requirements. High-rate discharge polarization is particularly sensitive to the porosity of the positive plate (J.F. Dittman, "The Optimum Performance from the Lead-Acid Battery," SAE Paper 269C, 1961). As stated in the cited reference: ". . . the same amount of positive material at a low density of 50 g/in.^{3} would be capable of initially cranking an automobile twice as long at 0 °C as would the same element design, but with the positive active material at a high density of 70 g/in.^{3}." However, since plates of low density tend to limit cycle life, a compromise must necessarily be made by adjusting the density of the positive plate to achieve the desired life performance.

Specific Gravity of Electrolyte

The appropriate specific gravity of sulfuric acid must be selected to optimize performance. Since the capacity of a positive plate is sensitive, particularly at high rates, to the concentration of acid immediately available to it, the concentration selected should be as high as possible, but restricted by three considerations:

- In general, separators deteriorate faster at higher acid concentrations and temperatures. The maximum specific gravity to ensure separator integrity is 1.300 where the electrolyte temperature is maintained below 43 °C ("Battery Service Manual," 6th Ed., The Association of American Battery Manufacturers, Inc., East Orange, New Jersey, 1964, p. 32).
- At 25 °C the minimum resistivity of sulfuric acid is at 31.1%; at this point the resistivity is 1.213 Ω cm; 31.1% is equivalent to a specific gravity of 1.227 at 25 °C. For comparison, at 25 °C the resistivities of sulfuric acid of specific gravities of 1.185 and 1.265 are 1.261 and 1.231 Ω cm, respectively.
- The capacity of each of the plates varies with the specific gravity and the temperature.

The percent capacity with respect to the capacity at 25 °C of positive and negative plates at three electrolyte specific gravities (G.W. Vinal, "Storage Batteries," 4th Ed., John Wiley and Sons Inc., New York, 1966, pp. 224-225) is presented as a function of temperature in Table 1.

In summary then, the density of the positive plate should be adjusted to optimize the specific power and to maximize cycle life. If the battery is operated at elevated temperatures, e.g., 60 °C, a separator must be selected which will not deteriorate at that temperature under the specified cycle conditions, and finally, the specific gravity of the electrolyte should be adjusted so that its resistivity is at a minimum at the anticipated operating temperature.

2.2.2 Influence of Duty Cycle on Battery Performance

Cycle life in traditional service is affected by charge and discharge conditions.

2.2.2.1 Overcharging

Battery life is shortened by overcharging through the following mechanisms:

- Increased potential caused by overcharging a lead-acid battery corrodes the positive grids.
- The gases evolved by the decomposition of water tend to dislodge active material from the plates.
- The higher concentration of acid that results from the decomposition of water is harmful to the separators.
- Overcharging increases internal temperatures which accelerate the deterioration of the cell components.
- Overcharging, particularly, at high rates, by forcing electrolyte out of the cells can damage external components and associated equipment.

Table 1. Plate Capacity in Terms of Electrolyte Specific Gravity for Several Temperatures

Specific Gravity	Capacity/Capacity at 25 °C, %					
	Positives			Negatives		
	10 °C	0 °C	-10 °C	10 °C	0 °C	-10 °C
1.315	87	78	67	65	43	25
1.240	84	72	58	75	57	37
1.140	82	68	30	83	68	30

2.2.2.2 Undercharging

A battery that is repeatedly operated in an undercharged condition over a long period of time may develop a type of lead sulfate in the plates, which, being dense and coarsely crystalline, cannot be readily electrochemically converted into lead and lead dioxide. Frequently, the density of the lead sulfate is such that strains are set up, particularly in the positive plate, causing distortion and buckling.

2.2.2.3 Charge Rate

During overcharge, oxygen is evolved at the positive, and hydrogen at the negative plate. This can cause loss of active material and shorten the cycle life. In addition, in cells with antimony alloy grids, stibine is also liberated. An analysis was performed by Durant and co-workers (K. Peters, A.I. Harrison, and W.H. Durant, "Charge Acceptance of the Lead-Acid Cell at Various Charging Rates and Temperatures," in "Power-Sources 2," D.H. Collins, Ed., Sixth International Power Sources Symposium, Brighton, Sussex, Pergamon Press, Ltd., Oxford, 1968, pp. 1-16) on the charge acceptance of positive and negative electrodes at three temperatures, 0, 25, and 40 °C. The highest charge rate employed in their experiments was 0.8C, a rate substantially lower than what would be employed in the hybrid vehicle application. For example, with a 60-A hr battery charged at 180 A, as required after a 55-kW discharge, the charge rate would be 3C.

In the above study the charge efficiencies for the positive plate at 25 °C at the 0.8C rate were 99.1% at half-charge, and 71.1% at near 100% charge. For the negative plate under the same conditions, the efficiencies were 100% at half-charge and 83.8% at near 100% charge. At 0 °C the charging efficiency of the positive plate was reduced to 34.3% and the negative to 70% at near 100% charge. The authors suggest that the charge acceptance at the positive plate is influenced by the production and subsequent decomposition of persulfuric acid. It is apparent that charge acceptance at high rates of charge may present a serious problem in this application.

Some possible solutions to this problem would be:

1) Maintaining the state-of-charge of the battery at a level low enough to ensure a charge efficiency of close to 100% (about 75% state-of-charge).

2) Charging the battery in such a fashion that gas evolution is minimized. An example would be the imposition of high currents at the beginning of charge, tapering to lower levels as the state-of-charge increases. The control would be an empirically determined voltage cut off to ensure minimal gas evolution, probably on the order of 2.35 V per cell plus the iR voltage component.

2.2.2.4 Depth of Discharge

Although no specific information is currently available on the relationship between depth of discharge and cycle life for automotive batteries, an example taken from the testing of Gould Motive Power Batteries is useful. GSA Federal Specification W-B-133a for batteries of this type requires a minimum of 1000 cycles when discharged at the 6-hr rate to 80% of rated capacity and 2500 cycles when discharged to 45% of rated capacity at the same rate. Tests conducted by Gould's Industrial Battery Division have shown that the cycle life for the first mentioned test exceeds 1500 cycles, and for the second, 3500 cycles. The total time for each cycle in the first test is 12 hr, for the second, 8 hr.

An equation for expressing a semi-logarithmic relationship between cycle life and depth of discharge has been reported by Voss and Huster (E. Voss and G. Huster, "The Effect of Depth of Discharge on the Cycle Life of Positive Lead-Acid Plates," VARTA, Germany, unpublished communication) where the depths of discharge are 40 to 100%. If a 61-A hr SLI battery were used in a hybrid-vehicle application when the single-pulse discharge is about 2.5 A hr or 4.1% depth of discharge, the life of the 61-A hr battery would be calculated as 300 cycles, compared to 24 and 127 cycles at 100 and 40% depths of discharge, respectively. A more typical life at 40% depth of discharge would be 200 to 250 cycles at 40 °C. This would lead us to expect a cycle

life of at least the 500 cycles required for a hybrid vehicle.

No serious difficulty is envisaged in complying with the cycle life requirements for this application, provided that: 1) overcharge is kept to a minimum, 2) electrolyte temperatures are maintained at such a level that the separators are not deleteriously affected and corrosion is not excessive, and 3) the charge rate does not cause excessive gassing.

2.2.3 Analysis of an Available SLI Battery

2.2.3.1 Performance Characteristics

A battery must have minimum weight and ohmic resistance for optimum performance. Capacity, as such, is not important. With this in mind, the resistances and weights of various components of a 61-A hr, super premium grade Group Size 22F battery (Gould 22F-GP-61) were analyzed. Overall case dimensions of this unit are: 9 7/16-in. long × 6 7/8-in. wide × 7 5/8-in. high (24.0 cm × 17.5 cm × 18.7 cm) for a volume of 480 $in.^3$ (7870 cm^3) and a weight of 35.9 lb (16.3 kg). The specific energy and energy density are 18.7 W hr/lb (41.2 W hr/kg) and 1.52 W $hr/in.^3$ (0.093 W hr/cm^3), respectively.

Weight

Each cell element has six negative plates, 0.053-in. (0.135-cm) thick and five positive plates, 0.073-in. (0.185-cm) thick. The weight breakdown of various components of the battery (6 cells) is given in Table 2. The volume and weight distribution of electrolyte per cell in the 61-A hr Group Size 22F battery is given in Table 3. Using these values, a weight reduction of 2.04 lb (929 g) per battery could be achieved by designing the battery case so that sediment well and excess electrolyte above the separators is eliminated. In the current SLI batteries the sediment well is necessary in order to accommodate material which sheds, and the excess electrolyte provides for reserve capacity (at low-rate discharge). In hybrid application, due to low depth of discharge, shedding of active material should be small and reserve capacity is not required. Positive electrodes can be encased in a separator envelope to ensure against possible shorting due to some shedding which will occur.

Table 2. Weight Breakdown for 61-A hr Group Size 22F Battery

Component	Quantity	Mean Weight, lb (g)		Total Weight, lb (kg)		% of Total
Positive Paste	30	0.209	(95)	6.28	(2.9)	17.5
Negative Paste	36	0.174	(79)	6.26	(2.8)	17.4
Positive Grid	30	0.125	(57)	3.75	(1.7)	10.4
Negative Grid	36	0.106	(48)	3.82	(1.7)	10.5
Terminal Strap	2	0.187	(85)	0.37	(0.17)	1.04
Internal Strap	10	0.116	(53)	1.16	(0.53)	3.2
Cover	1	0.469	(213)	0.47	(0.21)	1.3
Container	1	1.52	(691)	1.52	(0.69)	4.2
Separators	60	0.014	(6.4)	0.84	(0.38)	2.3
Electrolyte	--			11.4	(5.2)	31.8
				35.87	(16.3)	100

Table 3. Electrolyte Distribution in 61-A hr Group Size 22F Battery Cell

Space	Weight, lb (g)	Volume, cm^3
Total	1.90 (864)	690
Sediment Well	0.168 (76)	66
Above Separators	0.271 (123)	98

Resistance

The intercell-connector resistance measured 0.08 mΩ, and since there are five connectors per battery, the total contribution for intercell connectors is 0.40 mΩ. Each of the two terminal connectors has a resistance of 0.08 mΩ.

Resistance contributions from interplate electrolyte and separators were calculated for 1.265 sp gr acid at 24 °C (which has a resistivity of 1.23 Ω cm), separator resistivity of 0.23 Ω cm^2, plate area of 177 cm^2 and plate separation of 0.135 cm. The total resistance of the separators and the electrolyte between two plates is 2.2 mΩ and since there are 10 separators in a cell, the resistance for a cell is 2.2 mΩ/10 or 0.22 mΩ.

The total of the terminal and intercell connector resistances and the electrolyte resistance of the battery is 1.9 mΩ. The measured resistance of a typical Group Size 22F battery at room temperature is 10.8 mΩ; the difference of 8.9 mΩ must be attributed to the grids, the active material, and the pores. The effective resistance of a grid is 2.5 mΩ or a grid resistance of 0.5 mΩ per grid group. Thus the sum of the resistance of the positive and negative grids is 1.0 mΩ per cell.

Since the thickness of the positive plate is 0.19 cm, by assuming a porosity of 40% and a tortuosity factor of 2, the electrolyte resistance per plate is 2.0 mΩ or 0.20 mΩ per cell. It should be noted that this calculation is not particularly accurate because of the assumption of the tortuosity factor.

The only remaining resistance is that of the active material. A typical pellet of active material is 0.19-cm thick and the total cross-sectional area of pellets in a plate is about 54 cm^2. Since on the average the current travels half the maximum distance through the pellet, and assuming a path tortuosity factor of 2.5 and porosity of 40%, the pellet resistance is estimated as 1.8ρ per cell, where ρ is the resistivity of the positive active material. If the positive plate is completely formed and charged, the active material is PbO_2 and the resistivity ρ, is about 10^{-2} Ω cm. This would yield

an estimated positive pellet resistance of 0.108 mΩ for a battery. In all likelihood the actual pellet resistance is greater than this and should fall in the range of 0.1 to 1 mΩ.

By comparison, resistance of negative active material should be entirely negligible, provided the battery is not entirely discharged, because of the high conductivity of metallic lead.

The calculated battery resistances are summarized in Tables 4 and 5.

The greatest uncertainty in these calculations is believed to be the estimate of active material resistance, but this is not likely to be in error by more than 0.5 mΩ.

It can be seen that the greatest source of resistance in a fully-charged battery at room temperature is the grid, amounting to about 60% of the total. Electrolyte resistance contributes another 30%, leaving only 10% contribution from connections and active material.

2.2.3.2 Testing of a 61-A hr Group Size 22F Battery

Testing was performed on the Gould 22F-GP-61 SLI battery (Group Size 22F, 61 A hr, 12 V) in order to establish performance behavior of lead-acid batteries cycled in a manner similar to EPA specifications. The Group Size 22F battery was selected for this test because it represents a "state-of-the-art" SLI battery with the specific power output and performance characteristics most nearly approaching the EPA requirements.

Test Method

The batteries were tested using the cycle routine developed from the original EPA specifications which require discharges at two power levels, 55 and 10 kW, based on a 200- to 220-V battery system. Furthermore, to simplify the cycling routine the shallow 55-kW discharges were replaced with deep (25-sec) discharges resulting in a much more stringent cycling routine. The batteries were cycled using both direct-current (dc) and the TRW electromechanical transmission (EMT) chopper modes. The cycle routines were as

Table 4. Resistances of Components in a 61-A hr Group Size 22F Battery

Component	Resistance, mΩ				
	-40 °C (-40 °F)	-18 °C (0 °F)	24 °C (75 °F)	52 °C (125 °F)	60 °C (140 °F)
Connectors and Terminals	0.44	0.49	0.56	0.62	0.65
Grids	4.7	5.4	6.0	6.6	6.9
Interplate Electrolyte and Separators	9.0	3.4	1.32	0.90	0.47
Electrolyte in Pores of Active Material	15.0	5.3	2.02	1.38	0.72
Active Material (est.)	0.50	0.50	0.50	0.50	0.50
Total	29.6	15.1	10.4	10.0	9.2
Measured					
Battery 1					
Fully Charged			10.8		
~75% Charged			11.1		
Battery 2					
Fully Charged			10.2		
~75% Charged			10.8		

Table 5. Percent of Total Resistance for Components in a 61-A hr Group Size 22F Battery

Components	Resistance %				
	-40 °C (-40 °F)	-18 °C (0 °F)	24 °C (75 °F)	52 °C (125 °F)	60 °C (140 °F)
Metal (Connectors, Grids, Terminals)	17	38	63	82	88
Electrolyte	81	58	32	13	6
Active Material (est.)	2	4	5	5	6

follows:

	Direct Current	EMT
Cycle A	Discharge at 50 A for 10.8 sec; charge at 25 A for 22 sec.	50 A for 10.8 sec; 25 A for 22 sec.
Cycle B	Discharge at 365 A for 25 sec; charge at 180 A for 50 sec.	365 A for 25 sec; 40 A for 225 sec.

The sequence involved thirty of Cycle A followed by one of Cycle B with the entire sequence then being continuously repeated. Due to the inability of the EMT to deliver a 180-A charging current for 50 sec, the Cycle B charging period was changed to 40 A for 225 sec. The following performance parameters were monitored:

- Battery discharge voltages,
- battery charge voltages,
- currents during charge and discharge,
- cell or electrolyte temperatures,
- outer skin temperature (the temperature of the outer surface of the battery case), and
- gas evolution rates.

A typical recorder chart showing terminal voltage during these cycles under dc testing is presented in Figure 2.

Results and Discussion

The steady-state test results for a battery cycled under dc conditions are shown in Table 6. The data represent a total of 6859 cycles (sum of "A" and "B" cycles, total test time 65 hours). Since the EMT had to be operated manually to achieve the average constant currents of the test cycles, the sequence was repeated only three times (total time, 62 min). Test results indicate that steady-state operation was achieved during this time. EMT results are similar to those obtained under dc conditions. That is, with the EMT the average voltages during a Cycle A charge and discharge were 13.8 and 12 V, respectively. During Cycle B, voltages of 14.2 and 9.2 V were observed for charge and discharge, respectively.

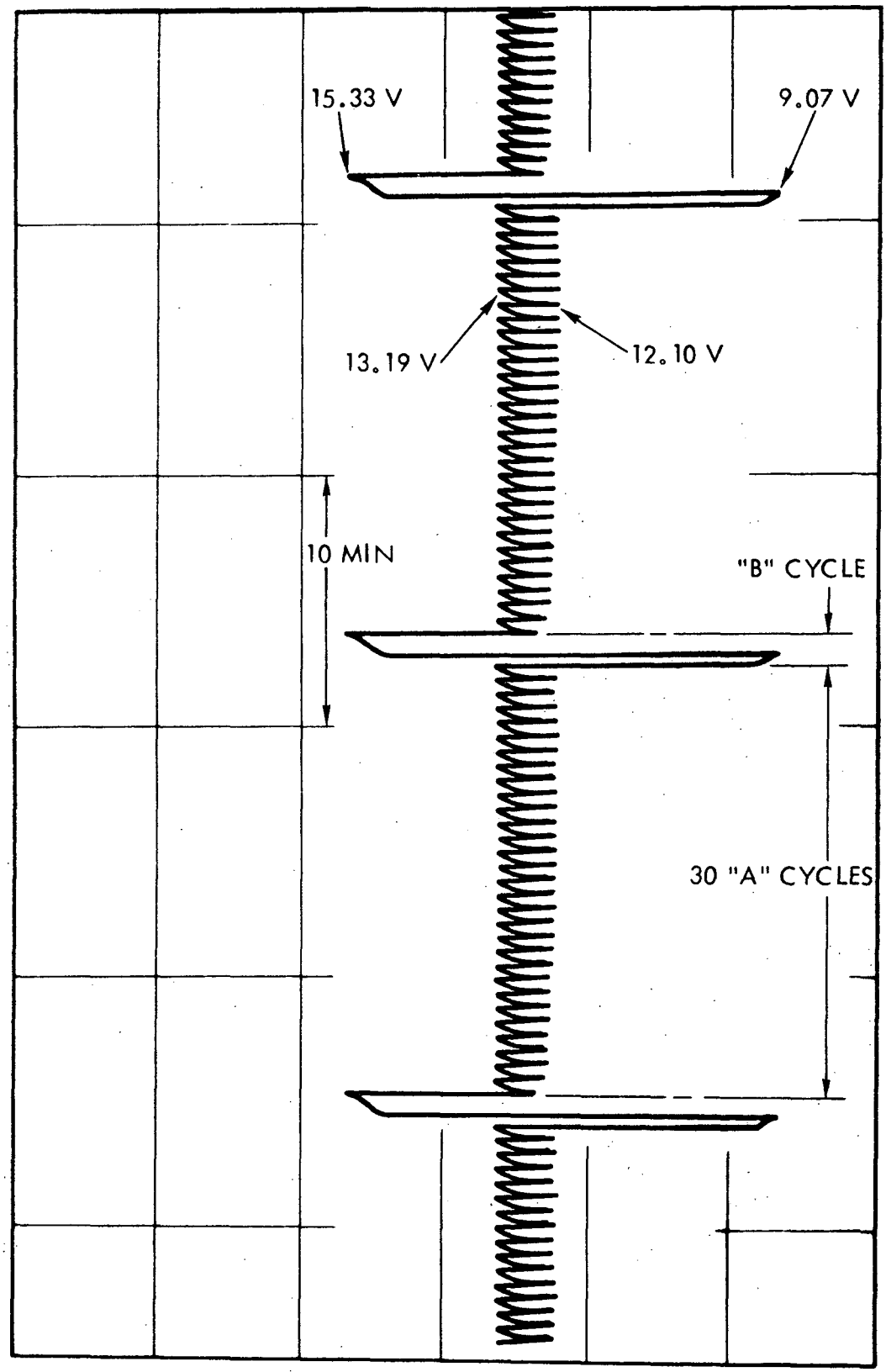

Figure 2. Time vs. Voltage Trace during DC Test of 61-A hr, Group Size 22F Battery.

Table 6. Steady-State DC Performance of 61 A-hr Group Size 22F Battery

	Cycle A		Cycle B	
	Discharge	Charge	Discharge	Charge
Voltage Range, V	12.1-12.4	13.1-13.2	9.0-9.1	15.2-15.4
Average Voltage, V	12.3	13.2	9.0	15.3
Current Range, A	50.5-51.5	25-27	350-395	166-200
Average Current, A	51	26	373	182
Equilibrium Cell Temperature, °F				
Cell 1	130-136	130-136	130	135
Cell 2	137-144	137-144	137	142
Cell 3	140-147	140-147	140	146
Cell 4	142-149	142-149	142	148
Cell 5	138-148	138-148	138	142
Cell 6	128-134	128-134	129	134
Equilibrium Skin Temperature, °F*				
Cell 4	124-126	124-126	124	125
Gas Evolution per Cycle, cm^3		0.60		17
Coulombic Efficiency, %		99.4		99.0

* Center of container side.

The average discharge and charge currents under EMT conditions were 54 and 27 A, respectively, for Cycle A, and 350 and 40 A for Cycle B. Typical peak currents during Cycle A were 105 A at 50% duty cycle during discharge and 90 A at 30% duty cycle during charge. Peak currents during Cycle B were 480 A at 73% duty cycle during discharge and 90 A at 45% duty cycle for charge. Figure 3 shows the transient waveforms observed under EMT conditions with a nominal 1-kHz chopper frequency.

When cycling of the battery was initiated at room temperature, because of the higher resistance of the battery (10.2 mΩ at 23 °C compared to 8.6 mΩ at steady-state operating temperature) the charge voltages were higher and the discharge voltages lower than at steady state. Initially, under dc conditions battery voltage during Cycle A was about 11.8 V on discharge and 14.2 V on charge; during Cycle B the battery voltage was 8.6 V on discharge and 18.3 V on charge. Similarly under EMT conditions, battery voltage for Cycle A charging decreased from 17.5 to 13.8 V during the first two sequences while the discharge voltage changed from 11.2 to about 12 V. Cycle B discharge resulted in a battery voltage of 8.9 V in the first sequence and 9.2 V for the next two sequences.

The average electrolyte temperature at steady state was higher during Cycle B than during the "A" Cycles. This temperature change was 3-4 °C for both dc and EMT test conditions. The temperature of the electrolyte during testing was 60-64 and 43-47 °C under dc and EMT conditions, respectively. The average differences between the electrolyte and skin temperatures were 8 and 5 °C for dc and EMT conditions, respectively. The tests were conducted under natural convection with the batteries set on a wooden board.

The average specific gravity after the charge portion of each cycle for dc tests was approximately 1.250. By comparison with the full-charge specific gravity of 1.280 the batteries were estimated to be operating at about 75% state-of-charge. Even though the specific gravity of the battery was not checked under EMT cycle test conditions, past experience with SLI batteries operating under EMT conditions indicated 90-95% state-of-charge.

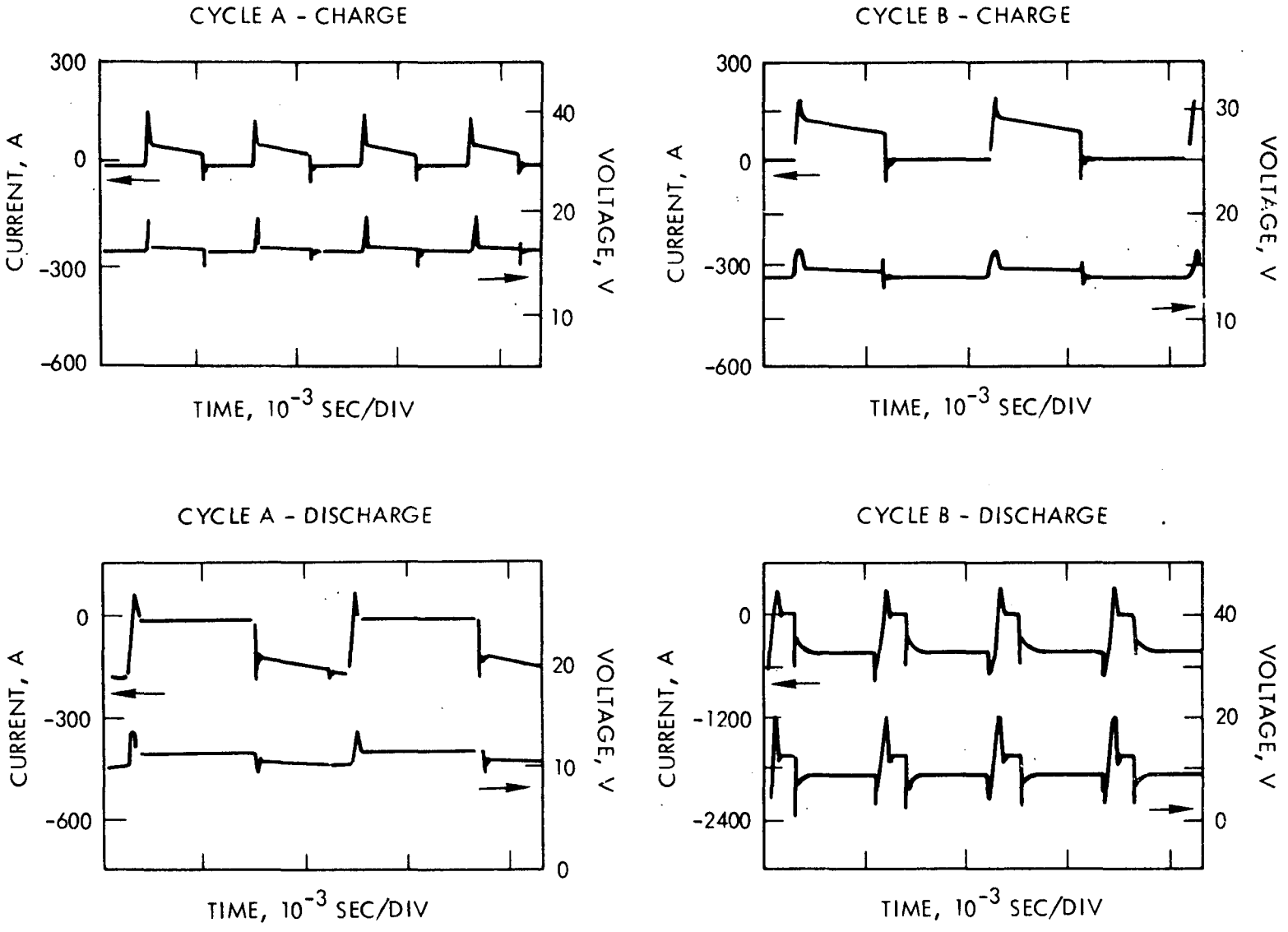

Figure 3. EMT Transient Waveforms during Test of 61-A hr, Group Size 22F Battery

The gas evolution during both the high and low rate charges at steady state was found to be surprisingly low. In both cases the coulombic efficiency was greater than 99%.

The rates of gas evolution under dc conditions were 0.60 and 17 cm^3 per cycle during Cycles A and B, respectively. Under EMT tests the rates were 3.7 and 50 cm^3 per cycle during Cycles A and B, respectively. This leads to a coulombic efficiency of greater than 99% for Cycles A and B for both dc and EMT test conditions. The gas evolution during start-up is shown in Figure 4. Coulombic efficiency during start-up was determined to be 91 and 78% for dc and EMT operations, respectively.

Overall energy efficiency at steady state for a single test sequence (30 Cycle A's and one Cycle B) was 79% for both dc and EMT. Average energy efficiencies for Cycles A and B were 90 and 61%, respectively, for dc conditions and 78 and 58%, respectively, for EMT conditions.

Power inputs for Cycles A and B under dc conditions were 0.34 and 2.8 kW, respectively, and the outputs, 0.63 and 3.4 kW. The specific power for Cycles A and B averaged 17 and 92 W/lb (38 and 206 W/kg), respectively. Similarly for EMT conditions, power inputs for Cycle A and B were 0.37 and 0.57 kW, respectively, and outputs were 0.65 and 3.2 kW, respectively. The specific power under EMT conditions becomes 18 and 88 W/lb (39 and 193 W/kg) for Cycles A and B, respectively. The energy losses due to resistance that occurred during the dc cycling regime were determined for the Group Size 22F battery as shown in Table 7. The internal resistance of the battery at the operating temperature of 63 °C was 8.6 mΩ. The total resistive energy losses are 0.10 and 12 W hr for Cycles A and B, respectively. These losses represent 5 and 32% of the total energy inputs of Cycles A and B, respectively.

These values are large compared to coulombic inefficiency losses of 0.55 and 0.97% for Cycles A and B, respectively.

In order to subject the batteries to more realistic operating conditions, the EMT was also operated under the following conditions:

Acceleration: 20 to 30 mph in 10 sec (average discharge current 45-95 A)

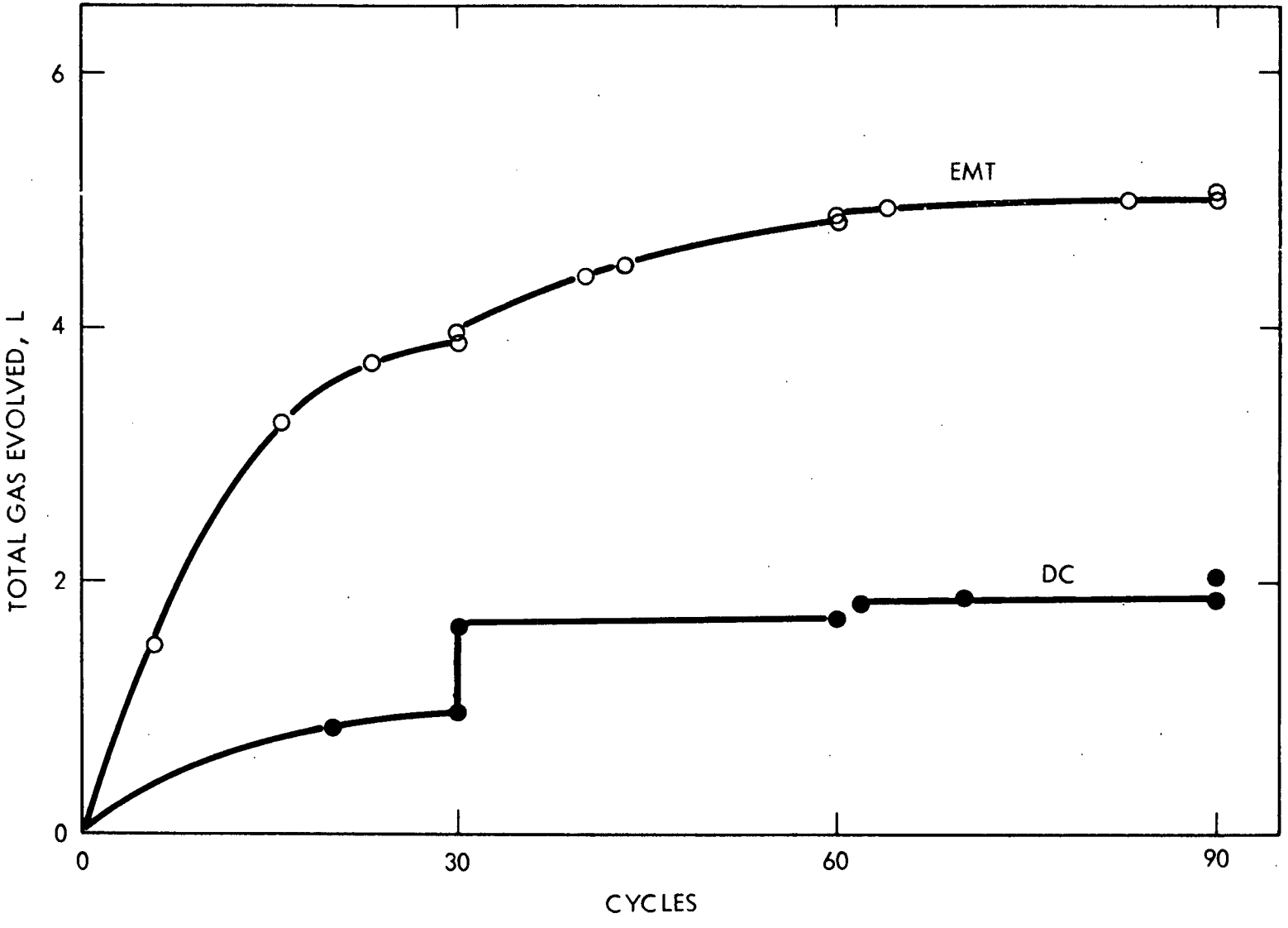

Figure 4. Gas Evolution during Test of 61-A hr, Group Size 22F Battery

Table 7. Losses Due to Resistance during DC Testing of a 61-A hr Group Size 22F Battery

	Cycle A		Cycle B	
Losses	Discharge (10.8 sec)	Charge (22 sec)	Discharge (25 sec)	Charge (50 sec)
Voltage, V	0.44	0.22	3.21	1.57
Power, W	22	5.8	1197	285
Energy, W hr	0.067	0.036	8.3	3.9

Deceleration:	30 to 20 mph in 20 sec (average charge current 20-65 A)
Idling:	75 sec (average charge current 45 A)
Drag:	30 ft lb at 30 mph
Vehicle Weight:	4,000 lb
Test Sequence:	accelerate-decelerate 15 times followed by idling (repeated 7 times, total time - 41 min).

At steady-state conditions the charge voltage was 13.6 to 13.3 V and discharge voltage was about 11 V. The coulombic efficiency was 95% (based on average discharge current of 55 A). Once again, the largest change in voltage and gas evolution was observed at the beginning of the test.

2.2.4 Discussion

2.2.4.1 Identification of Technical Problems

We have searched the literature to uncover information on the state-of-the-art of the lead-acid batteries germane to this application. No information was discovered that would permit us to predict with any degree of certainty the behavior of existing lead-acid batteries under the cyclic conditions specified. However, by analyzing the physical characteristics and behavior of existing batteries we were able to identify in general terms those parameters that would be critical. Possible problem areas which offer room for improvement are discussed in the following paragraphs.

Internal Resistance

Specific power for a particular battery can be improved by decreasing the internal resistance. Our component-by-component analysis of the internal resistance has identified the grids as the major contributory source of the overall resistance of the battery. This resistance can be reduced by a change in grid design and plate size and by use of a more conductive alloy. A second significant contributor to the internal resistance is the electrolyte which soaks into the active materials of the plates. This resistance is related to the porosity of the plates and a tortuosity coefficient. The more porous the plate the greater the conductivity; unfortunately we are unable at this time to relate the tortuosity coefficient to the porosity.

Our analysis also revealed that the cell interplate connectors, terminal straps, and the resistance of the electrolyte between the plates constitutes only about 17% of the battery's overall resistance.

Separators

The two most important characteristics of the separator are its resistivity and its physical integrity under the anticipated operating conditions. The resistivity can be lowered by increasing the pore size, but larger pores increase the chance of shorting through the separator. The resin-impregnated paper separator with embossed ribs has a resistivity of 0.23 Ω cm^2 and tends to deteriorate when operated at temperatures greater than 43 °C. Further, with an electrode spacing of 0.135 cm, it contributes about 58% of the overall resistance between plates. If, because of the high power drains, the anticipated operating temperature of the battery is greater than 43 °C, a separator must be selected capable of maintaining its physical integrity at that temperature, and further, in order to minimize the internal resistance of the battery, its resistivity should be as low as possible. Improved separators are available.

Weight of Electrolyte

Since present SLI batteries are designed for high reserve capacity, they contain approximately 14.5% of their electrolyte outside the element. Since this electrolyte is of no benefit in high-rate discharge, much of it could be removed thereby reducing the battery weight.

Charge Acceptance

Our exploration of the literature indicated that we would experience difficulty in charging a lead-acid battery efficiently at high rates (on the order of 3C). However, our experiments with 61 A hr Group Size 22F batteries revealed a surprisingly high coulombic efficiency, greater than 99% at the equilibrium temperature of 60 °C under the cyclic conditions employed. At lower operating temperatures we would expect the efficiency to be lower.

Energy Efficiency

Data from the experiments on the batteries mentioned above showed an overall energy efficiency of 80% as an average for one 55-kW deep cycle and 30 10-kW shallow cycles, with 63% for the 55-kW deep discharge, and 90% for the 10-kW shallow discharge. The major energy losses occurred in resistive heating. Using the cycle frequency routine of the EPA specifications, we estimate the average energy efficiency would be 86%.

Operating Temperature

The batteries were tested under a more severe routine than that specified by EPA, since all 55-kW discharges were of 25-sec duration, whereas for the EPA routine the average duration of the 55-kW discharges is only eight seconds. Under the test conditions used, the difference between the battery case temperature and ambient was about 36 °C at steady-state. We estimate that this difference would be reduced to approximately 14 °C under the EPA routine. Further, under the anticipated operating conditions of the hybrid vehicle, convective cooling would undoubtedly prevail and the temperature of the batteries would be kept at a temperature differential considerably below 14 °C, and probably below that of SLI batteries as they are currently used in automobiles where they are exposed to the engine's heat.

Cycle Life

It is known that in currently produced lead-acid batteries cycle life is related to the depth of discharge; the shallower the discharge, the longer the life. However, the literature search revealed no information on the relationship of depth of discharge to cycle life at depths less than 40%. Assuming, for example, a 61-A hr battery would be used in this application and the maximum capacity withdrawn on a single-pulse discharge would be 2.4 A hr, the depth of discharge would be approximately 4%. Any extrapolation from the relationship given in the literature for depths of discharge ranging between 40 and 100% and cycle life, to the levels anticipated for this application, is of questionable validity.

Cycle life is also affected by the corrosion rate of the positive grids which is highly sensitive to temperature. As noted above, we expect

the operating temperature of the battery pack in the hybrid vehicle to be at a level lower than that of present SLI batteries in automobiles so the corrosion rate would be lower. Because of the expected lower corrosion rate and the shallow discharge cycles, we feel batteries of the SLI type can meet the five-year life requirements. However, to insure meeting this requirement, a search should be carried out for alloys more resistant to corrosion than the 4.5% antimonial lead now used.

2.2.4.2 Conclusions

Our examination of the state-of-the-art of lead-acid batteries (which included the actual testing of super premium grade SLI batteries) considered two aspects of developing a battery system for hybrid-vehicle applications. One, to satisfy the original EPA specifications for a 100-W/lb battery, and two, to develop a 200-W/lb battery, the latter being a more realistic requirement based on TRW's experience with hybrid-vehicle systems. Problem areas which offered room for improvement were discussed in Section 2.2.4.1. The SLI battery studied embodies, in our opinion, the application of the highest level of technical knowledge to mass produced units. However, our detailed analysis of this battery showed that it could be improved and that the problems in designing a battery for the hybrid vehicle application are soluble.

With respect to the original EPA requirements, using 17 of these batteries in series yields a weight of 610 lb (277 kg), with a power output of 57 kW, at 1.53 V per cell and 365 A at the high-pulse load. With 16 batteries, the weight would be about 575 lb (261 kg), and the power output would be 53.5 kW. The specific power yield with these batteries is about 93.5 W/lb (206 W/kg); what is required to meet the weight requirement is 100 W/lb (220 W/kg), a difference of 6.5 W/lb (14.3 W/kg). A second successive high power pulse of 25-sec duration can be delivered readily.

An increase in specific power can obviously be effected by a decrease in weight and by a reduction in internal resistance. By reducing the weight of each of the Group Size 22F batteries by 1.5 lb (0.68 kg) and by using 16 of these batteries in series, the weight would be brought to an acceptable level. A reduction of this amount could be obtained simply by removing some of the electrolyte outside the element. However, a more funda-

mental approach lies in attempting to design a battery, by a careful consideration of all factors involved, in order to maximize the specific power. As was mentioned above, the grids are the major contributor to the internal resistance of the battery; however, merely increasing the conductivity of the grids by the addition of more cross-members, obviously does not solve the problem in optimum fashion because of the resultant increase in weight. Plate size, active material density, and separator should be optimized also. In other words, the optimization of the battery for specific power involves the use of a "systems" approach, preceded, naturally, by a thorough evaluation of all the individual parameters that affect specific power and their interrelationships.

2.3 ADVANCED (ALTERNATE) CONCEPT BATTERIES

In Section 2.2 attention was focused on the pasted-plate SLI (starting, lighting and ignition, or automotive) battery. A bipolar battery with Planté-formed plates and a tubular-plate battery were considered as possible alternatives to the pasted-plate SLI battery.

2.3.1 Bipolar Battery

A Planté plate is manufactured electrolytically by anodic oxidation of a pure lead substrate surface to active lead dioxide. The lead substrate ordinarily is deeply grooved to enhance its surface area. The greatest advantage of Planté plate batteries is their very long life of up to 40 years, due to the corrosion resistance of the pure lead substrate and the exceptional adherence of the active material to the substrate. However, because of their great weight they are presently used only in stationary applications.

In 1924, Kapitza [P. Kapitza, "A Method of Producing Strong Magnetic Fields," Proc. Roy. Soc., Ser. A, 105, 691-710 (1924)] described a bipolar battery from which a very high-power output was obtained for 10-20 msec. A bipolar battery utilizes positive and negative electrodes of adjacent cells as an integral electrically conducting sheet, which serves also as the partition between the cells. This arrangement provides the shortest possible current path between cells. Kapitza stacked thin lead sheets between U-shaped rubber gaskets and then formed a very thin layer of active material on either side of each sheet by the Planté process. He obtained current densities of 2 to 5 A/cm^2 at a power density of 500 kW/ft^3 (17.7 W/cm^3), withdrawing a capacity of about 0.047 A sec/cm^2 (0.3 A $sec/in.^2$) in 20 msec.

In 1968, Biddick and Nelson [R.E. Biddick and R.D. Nelson, "Lead-Acid Bipolar Battery for Multisecond Pulse Discharge," IECEC '68 Record (Proceedings of the Intersociety Energy Conversion Engineering Conference, Boulder, Colorado, Paper 689006) 47-51 (1968)] developed a higher capacity Planté bipolar electrode which sustained currents of 1 to 3 A/in.^{2} (0.16 to 0.48 A/cm^2) for several seconds. They also showed that the bipolar battery could be quickly and efficiently charged. A high state-of-charge was maintained during prolonged cycling with a discharge pulse of five seconds at 1 A/in.^{2} (0.16 A/cm^2) and a charge period of 20 sec. The battery employed a unique gasket design which allowed water to be added to all cells at once through a filling trough.

Under Navy sponsorship, a 300-V, 3.6-kW battery was constructed. It was made up of five 60-V modules ("Design and Fabrication of 300 Volt, 3.6 Kilowatt Pile-Type Bipolar Lead-Acid Battery for Pulse Duty," Final Report, 29 December 1967 to 29 September 1968, Contract No. N00123-68-C-0862, U.S. Navy Undersea Warfare Center). One of these modules was cycled 140,000 times at a discharge current density of 1 A/in.^{2} (0.16 A/cm^2) for one second and a charge period of 15 seconds. In addition, a three-cell bipolar battery was cycled 200,000 times at a five-second discharge current density of 1 A/in.^{2} (0.16 A/cm^2) and 20-second charge. A single cell was cycled for 425,000 times on the same duty cycle. These results established the feasibility of the bipolar battery concept for storing electrical energy to meet high power requirements. Power outputs exceeding 200 W/lb (440 W/kg) and 50 kW/ft^3 (1.77 W/cm^3) were obtained at an overall power efficiency of 80% using 0.032-in. (0.081-cm) thick lead sheet electrodes. It appears likely that specific power output can be increased significantly by use of a thinner and lighter electrode. However, the long-term life of these batteries has not been established.

2.3.2 Tubular Plate Battery

Tubular plates have three primary advantages over the pasted variety:

1) Tubular construction is very effective in preventing loss of the active material during cycling,

2) the weight of the grid is only about 50% of the weight of a pasted-plate grid giving equal life, and

3) a higher energy density is attained in comparison with pasted plates. (This was no longer true at the end of this program because of advances in pasted-plate technology.)

A conventional type of tubular plate utilizes either cylindrical or prismatic tubes to contain the active material. The positive active material is retained on the grid by means of a fabric sheath which is most often a woven Dynel or polyester material, but in some cases, may consist of braided fiberglass with a perforated polyvinyl chloride outer shield. The grid for this type of structure consists of a single "spine" of lead alloy along the axis of each tubular sheath. These spines are connected to a rather massive header at the top of the plate which is both a bus bar and a strengthening frame.

The tubular-plate battery is exemplified by Gould's 85T Motive Power cell. An improved tubular retainer recently developed has increased cycle life to about 3000 cycles at 40% depth of discharge and over 1000 cycles at 80% depth of discharge. This improvement is due to the use of a polyester material, specially tailored for resistance to sulfuric acid, resulting in excellent retention of active material within the cylindrical fabric sheath. With less resistant retainer materials, corrosion of the polymeric fiber results in reduction of thread diameter and increased porosity of the sheath so that small particles of lead dioxide permeate the sheath and collect in the sediment well. This results in loss of capacity and eventual shorting of the cell when active material accumulates to the top of the sediment well and contacts adjacent positive and negative plates. The specific energy of this type of battery at the six-hour rate is 11 W hr/lb (24 W hr/kg).

The tubular cell has been developed for ruggedness, dependability, and long life in motive power service (e.g., in fork-lift trucks where high specific power is not a requirement). At the present time, however, the smallest diameter tube is 0.275 in. (0.7 cm) as compared to an overall

plate thickness of 0.075 in. (0.19 cm) or less in pasted-plate SLI batteries. In order to achieve specific powers comparable to what is possible for pasted plates it would be necessary to radically modify the present design by reducing the diameter of the tube in order to decrease the mean distance between the active material and the spine. Additionally, since the spine diameter must also be reduced, mechanical problems associated with the introduction of active material into the tube can be anticipated.

Consequently, we did not feel that the tubular construction should be actively explored at this time. The pasted-plate design and the bipolar electrode concept appear to be the most promising for the hybrid-vehicle application.

2.4 APPROACH TO SOLUTION

As a result of examining the lead-acid battery problem, a program plan was developed which comprised two approaches to developing batteries that can satisfy the hybrid-vehicle requirements. One approach aimed at adapting conventional pasted-plate technology to a 55-kW battery (original EPA specifications) with further optimization leading to a 200-W/lb battery system. The second approach involved the development of a bipolar battery.

By adjusting present pasted-plate design and by refining present production techniques it appeared probable that the performance and cost objectives of the original EPA specifications (discharge and charge cycles summarized in Table 8) could be met by 1972. This design, was in all probability, not the optimum design for a pasted-plate battery. Higher specific power was realizable. TRW had tested pasted-plate batteries with specific power exceeding 200 W/lb but lifetime, cycle life and other characteristics had not been examined. It did appear probable that significantly higher specific power could be achieved by modifying cell components. In order to obtain data which would permit a closer approach to an optimum design we proposed to test various design concepts, component modification, and parameters in statistically designed experiments on single electrodes and cells as discussed in Section 3. Those experiments were designed to indicate plate thickness and paste density, and elucidate to some degree

Table 8. Discharge and Charge Cycles for a 55-kW Battery

Discharge					Charge			
Number of Cycles	Rate, kW	Energy, W hr	Time/Cycle, sec	Total Time, sec	Rate, kW	Energy, W hr*	Time/Cycle, sec	Total Time, sec
500	55	380	25	12,500	30	475	57	27,500
3,000	55	130	8.5	25,500	30	163	20	60,000
3,000	55	80	5.2	15,600	30	100	12	36,000
193,500	10	30	10.8	2,090,000	5	375	27	5,200,000
				2,143,600				5,323,500
				= 595 hr				= 1480 hr

* Assuming 80% energy efficiency.

a preferred grid design and material. Other factors to be studied included separator thickness and ribbing to provide good gas release from the cell on overcharge and the effect of electrolyte concentration on performance.

An important factor in determining battery life is the composition of the lead alloy used to fabricate the grid. Both extensive and intensive tests were planned in order to find improved alloys and evaluate their life by means of accelerated tests.

Computer programs were used to predict the current and potential distributions in various plate configurations, with the objective of optimizing the weight, uniformity of potential, and ease of fabrication of the battery.

The bipolar battery offered the following advantages for use in a hybrid heat engine/electric family automobile:

- Minimum electrical resistance
- Absence of intercell connectors
- Maximum current capability
- Minimum volume
- Minimum Weight.

Since the feasibility of the lead-acid bipolar battery had been demonstrated in rather long-term tests lasting from several months to over a year at average power levels in the range required for the hybrid car, its development was certainly worth pursuing.

The specific tasks required to develop the bipolar battery were:

- Develop a lightweight substrate material onto which thin layers of active material can be formed.
- Develop a method of forming active material on the substrate.
- Develop a method of sealing a plastic frame around the substrate, e.g., ultrasonic welding.
- Develop a method of sealing the plastic frames together to produce the battery.

Development of the bipolar battery is discussed in Section 4.

3. OPTIMIZATION OF CONVENTIONAL (PRISMATIC) BATTERIES

3.1 GRID STRUCTURE

3.1.1 Mathematical Modeling

3.1.1.1 The Model

A mathematical model was constructed for the optimization (maximization) of a figure of merit for the pasted-grid configuration of the positive plate. The figure of merit for the plate was defined as

$$fm = i[E - i(R_g + R_p + R_e)]/W$$

where i is the plate current, E is the half-cell potential of the positive plate (vs. Hg/Hg_2SO_4), R_g is the grid resistance, R_p is the paste resistance, R_e is the electrolyte resistance, and W is the weight of the plate. Thus, the figure of merit is seen to be the ratio of delivered power to weight. This figure of merit was optimized with the values of i and R_e remaining fixed, while R_g, R_p, and W varied with grid geometry. E is, of course, a physical constant.

A fairly detailed model of the current flow in the plate was constructed and implemented. Each paste element (pellet) was regarded as independent of all of the others. The current density flowing from electrolyte to paste was assumed constant, and Poisson's equation was set up and solved analytically for each rectangular pellet. This equation describes the steady-state distribution of current and voltage in an extended resistive medium.

The result of the analysis of Poisson's equation was a set of expressions for:

a) The equivalent resistance of a pellet,
b) the average voltage (iR) drop in a pellet,
c) the fraction of the pellet current which is delivered to each of its four bounding grid elements, and
d) the resulting voltage drop in each of the bounding grid elements.

The development of these expressions is shown in Appendix A.

Kirchhoff's laws were written for the distribution of voltage throughout the grid and of the currents delivered to the grid by the pellets. These laws express mathematically the conditions that the sum of the (positive and negative) currents entering any intersection of grid elements must be zero, and that the sum of the voltage drops around any closed path in the grid must also be zero. Calculation showed that collateral current flow in the paste elements and also in the electrolyte was small.

A computer program was developed, embodying the Kirchhoff and related equations. In the present model, the currents flowed to a single tab of arbitrary size and location on one boundary of the grid. The voltage distribution relative to this tab was computed, and its average value set equal to iR_g in the formula for figure of merit. Although the program contains the capability of specifying the current flow into each pellet individually, no use was made of this feature, due to the restricted scope of the present study.

The heart of the computer program is a set of Sparse Matrix Inversion subroutines developed at TRW. These are used to solve, in a highly efficient manner, the hundreds of simultaneous linear algebraic equations that arise from the use of Kirchhoff's laws. The computing machine used was the CDC 6500.

Although all of the most important physical effects have been included in the model, it was unfortunately necessary to omit from consideration a good many others. These include: variation of physical parameters with state of charge, temperature, current and age; any consideration of the negative plate or of the cell as a whole; variation of electrolyte composition (specific gravity) and volume; variation of separator parameters; variation of the current from pellet to pellet caused by voltage drops across the grid; reaction rates (mass action) and their dependence and effect on electrolyte concentrations; and effects of collateral current paths in the pellets and electrolyte. It would be desirable to include as many of these effects as possible in future modeling studies.

3.1.1.2 Results

A series of computer runs was made to optimize a grid design based on a square plate 4 1/4 in. (10.8 cm) on a side and 0.040 in. (0.102 cm) in thickness, having 24 vertical and 8 horizontal elements, a pair of tapered vertical elements (the 9th and 16th counting from one side) and a current-collector tab extending from the 8th to the 10th element at the top of the plate. The plate chosen was smaller than a conventional plate such as a Group Size 22F to minimize iR drop at high current densities.

The pellet size was the same as in conventional SLI battery grids. The width of the side and bottom frame members and the small end of the stiffeners was 0.040-in. (0.102-cm), corresponding to a 0.0016-$in.^2$ (0.01-cm^2) cross-sectional area. The cross-sectional areas of the vertical and horizontal elements were 0.0004 and 0.0008 $in.^2$ (0.0026 and 0.0052 cm^2), respectively. Parameters which were allowed to vary in the optimization were the taper of the 9th and 16th vertical elements (stiffeners) and the design of the upper horizontal portion of the frame. Corrosion of the elements was considered in the calculation.

The half-cell potential, E, was taken as 1.68 V and a plate current of 60 A was used. This is the approximate current that would be required for a Group Size 22F plate to meet the EPA specifications.

Computer runs were made on the uncorroded plate first. The figure-of-merit values for all of the tapered designs tried were found to lie within 1% of each other. This independence of the figure of merit on design results from the fact that at 60 A the iR term in the figure of merit is small compared to E. In the present case, a 10% decrease in grid resistance, R_g, produces only a 0.4% increase in the term $E - i(R_g + R_p + R_e)$ in the figure of merit. This increase is usually more than offset by the attendant weight penalty. This situation is characteristic of small plates where the figure of merit is governed largely by plate weight. Therefore, our figure of merit could be improved by adopting a plate with a larger (perhaps fiber reinforced) pellet size which would contain less lead and weigh less.

In the case of corroded plates, however, the situation is somewhat different. Corroded plates were simulated by decreasing all grid element cross-sectional areas, so that all of the vertical grid elements, except the frame and stiffeners, essentially disappear. Consequently, a comparison series of calculations was made on a plate with 4 vertical and 8 horizontal elements. The taper of the two inner vertical elements and dimensions of the upper frame were varied. Here, because of the much-increased value of the grid resistance, it was found possible to maximize the figure of merit. The maximum was "broad", however, and several grid designs that were tested had figure-of-merit values within 1% of the optimum.

The optimum design was found to be a 0.13-in. (0.33-cm) width for the top of the tapered stiffeners and the top frame element between the stiffeners, and a tapered width for the top element outside of the stiffeners. The outline of a grid actually cast is shown in Figure 5. The pellet size in the grid is the same as in standard SLI grids but the vertical and horizontal dimensions are interchanged.

3.1.2 Accelerated Corrosion Tests of Selected Alloys

3.1.2.1 Approach and Selection of Alloys

Six lead test alloys were prepared and cast into grids and rods. Bare grids and rods and positive plates incorporating test-alloy grids were exposed to 1.260 sp gr sulfuric acid electrolyte. Corrosion was accelerated by maintaining test cells at 71 °C (160 °F) and impressing upon the test specimens a potential of 0.075 V relative to the equilibrium potential of the alloy in the electrolyte. Dimensions of the test specimens and the capacity of the positive plates were measured periodically. Rod specimens were examined metallographically to determine corrosion patterns.

Compositions and selection criteria for the lead test alloys were as follows:

1. 3.08% Cd-2.8% Sb-0.15% Ag - High mechanical strength; feasible for using as extremely thin grids.
2. 0.013% Li - High electrical conductivity; superior electrochemical behavior.

Figure 5. Outline of Grid for Pasted-Plate Test Cells.

3.	4.5% Sb	- Standard alloy for battery grids.
4.	0.017% Li-0.90% Sn	- Improved castability and mechanical strength over 0.013% Li.
5.	2.5% Sb-0.45% As	- Contains less antimony than 4.5% Sb (standard alloy), but retains equivalent mechanical strength through use of arsenic.
6.	0.066% Ca-0.90% Sn	- Good corrosion resistance and improved castability.

The 4.5% Sb alloy (standard alloy) served as the comparison reference standard.

3.1.2.2 Experimental Procedure

Lead alloys of the compositions described above were cast into grids and rods. Grids were Group Size 22F size, 12.4 cm × 14.7 cm × 0.14 cm (4.9 in. × 5.8 in. × 0.055 in.) with the vertical and horizontal bars on 1.55-cm (0.61-in.) and 0.46-cm (0.18-in.) centers, respectively.

The positive plates were prepared by using conventional techniques and in the same manner as plates fabricated for component testing. These techniques are described in Section 3.2.2. The formation of plates was carried out with three-plate cells; i.e., one positive and two negative plates per cell with the cells connected in series. Plates were not dry charged.

Twelve corrosion test cells were set up, six of which contained two bare grids and two rods of one alloy in each cell. The other six cells each contained two positive plates prepared from one alloy. Each grid or plate was assembled in a three-plate electrochemical group (two standard negative plates with each positive plate and two bare standard Sb-alloy grids with each bare grid). Each test cell contained two grid (or plate) groups. The rods were placed between the two grid groups in each grid cell. A test cell containing two bare-grid groups and two rods is shown in Figure 6.

Tests were conducted at 71 °C (160 °F) in a manner similar to that used by Willihnganz [E. Willihnganz, "Accelerated Life Testing of Stationary

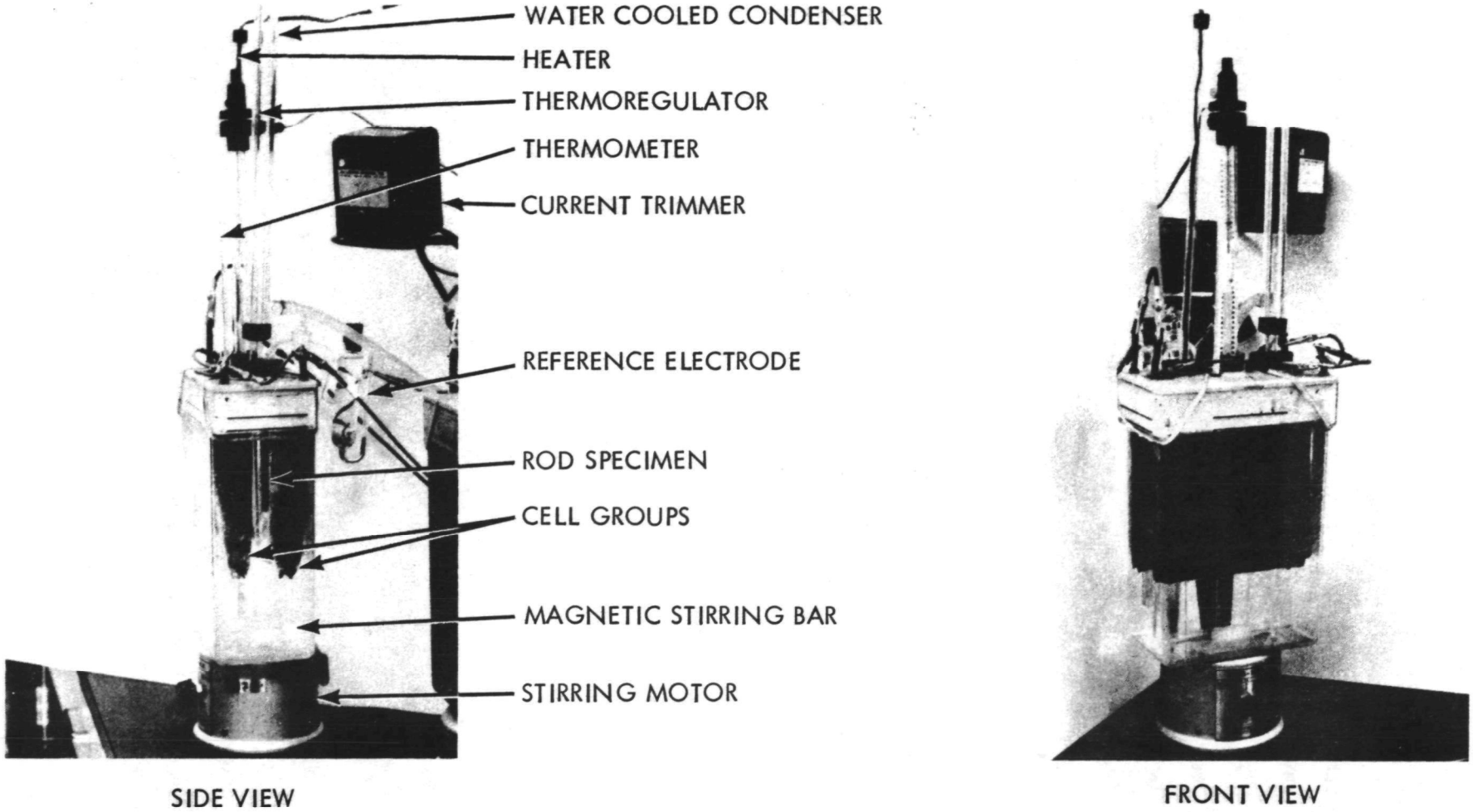

Figure 6. Accelerated Corrosion Test Assembly for Bare Grids and Rods

Batteries," Electrochem. Tech., 6, No. 9-10, 338-341 (1968)]. On the expectation that positive grids might warp during the test and could come in contact with the negatives, negative grids were enclosed with perforated Koroseal envelopes.

Each positive plate was separated from its two negative plates by standard PVC separators (Ethyl Corporation) and each plate group was clamped together as a unit to avoid excess warpage.

The cell containers used were oversize so that adequate stirring of the electrolyte could be accomplished by means of a magnetic stirring assembly.

All test components in an individual cell were connected in parallel and the test cells were in turn connected in parallel, each with its own current trimmer. Each cell was wired through a central panel so that cell voltage, positive electrode potential (vs. a saturated Hg/Hg_2SO_4 reference electrode containing 1.260 sp gr H_2SO_4) and current could be monitored through selection switching without the need for manual probes and without disturbing the wiring. Positive plate potential was maintained at 0.075 V relative to equilibrium plate potential at 71 °C in the 1.260 sp gr electrolyte. Potential of the bare grids was monitored with respect to the reference electrode and was maintained 0.075 V above the open-circuit value.

Cells were constructed so that they could be easily dismantled for growth and weight measurements on the test specimens. Growth measurements represent the mathematical averages of horizontal and vertical measurements made at three locations each (in center and ~1 cm from each edge). Rods were fitted into a Teflon (TFE) fixture which in turn was screwed into the cell cover. The length of the rod was measured from the end of the rod to the fixture. Diameter measurements were made on samples cut from the end of the rods for metallographic analysis.

Plate capacities were measured, normally at two-week intervals. The cells were allowed to cool to room temperature before the capacity and dimension measurements. Discharge rate was 60 A (0.16 A/cm^2) to a 0.95-V

(cell voltage) cutoff. Recharge rate (at room temperature) was 3 A (0.008 A/cm^2) until 110% of required charge was returned to each cell.

3.1.2.3 Results and Conclusions

Pasted-Plate and Bare-Grid Specimens

The accelerated corrosion test of pasted plates was terminated when the last surviving grid (Sb-As alloy) cracked during handling preparatory to measuring growth (138 days at 71 °C). The last pasted plate (Li alloy) failed after being on test for 128 days at 71 °C. Tables 9 and 10 summarize resistance and capacity data on the pasted-plate specimens. Sb-As and Li alloys had the best overall performance.

Cannone and co-workers [A.G. Cannone, D.O. Feder and R.V. Biagetti, "Lead-Acid Battery: Positive Grid Design Principles," Bell System Tech. J., 49, No. 7, 1279-1303 (1970)], have shown that plate growth can be described by one of two equations,

$$G = k_1 t$$

$$G = k_2 t^2$$

where G is the percent growth, t is the time and k is the rate constant.

Growth data for pasted plates are summarized in Table 11. Growth was linear for the Li, Sb and Li-Sn alloy plates and quadratic for the Sb-As alloy plate. Rate constants, obtained graphically, are given in Table 12. Growth curves for plates of the longest-lived alloys, Li and Sb-As, are shown in Figure 7. A quadratic plot for the Sb-As alloy plate is shown in Figure 8.

Vertical growth of plates is greater than horizontal growth on a percentage basis. Grid design (longer horizontal pellet section) and gravitational effects may account for this difference.

For the purpose of these measurements, growth was defined as enlargement of the grid (or plate) without cracking. Once a crack occurred in the grid frame, the frame was subject to further cracking during handling; a crack was not an isolated local occurrence. None of the bare grids cracked at the frame bar. For example, the interior members of the Cd-

Table 9. Resistances of Pasted-Plate Cells during Accelerated Corrosion Test at 71 °C[a]

	Resistance, mΩ								
Alloy	7 Jul	21 Jul[b]	4 Aug	1 Sep	14 Sep	24 Sep	22 Oct	27 Oct	11 Nov
Cd-Sb-Ag	4.8	---	6.0	---	---	---	---	---	---
Li	4.3	---	4.4	5.0	5.3	5.6	7.6	8.8	6.5[c]
Sb	5.7	---	6.4	8.0	8.7	9.2	8.6[c]	8.9[c]	---
Li-Sn	4.3	---	4.4	5.0	5.6	6.1	---	---	---
Sb-As	4.5	---	5.0	5.5	6.1	6.5	8.4	8.9	---
Ca-Sn	4.6	---	4.8	5.7	6.9	7.9	---	---	---

[a] Negative plates made with standard antimonial grids.

[b] No measurements made.

[c] Result from one plate; second plate broken.

Table 10. Capacities of Pasted-Plate Cells during Accelerated Corrosion Test at 71 °C[c]

Alloy	Capacity, A hr[a]								
	7 Jul	21 Jul	4 Aug	1 Sep	14 Sep	24 Sep	15 Oct	27 Oct	11 Nov
Cd-Sb-Ag	3.87	3.94	3.78	---	---	---	---	---	---
Li	4.34	4.45	3.37	3.53	4.08	3.88	3.01	2.16	1.17[b]
Sb	4.29	4.44	4.12	2.56	2.10	2.37[b]	2.08[b]	1.73[b]	---
Li-Sn	3.63	3.79	3.66	3.21	3.33	3.06	1.62[b]	---	---
Sb-As	4.04	4.05	4.15	4.42	4.16	3.88	2.22	1.83	---
Ca-Sn	4.30	4.32	4.08	2.25	2.38	1.84	---	---	---

[a] At 60-A (0.16-A/cm^2) rate to 0.95 V.

[b] Based on one plate only, second plate broken.

[c] Corrosion test carried out at 71 °C, but capacity measurements made at room temperature.

Table 11. Growth of Pasted-Plate Specimens during Accelerated Corrosion Test at 71 °C

Alloy	Time, days	Growth, %	
		Vertical	Horizontal
Li	39	1.3	0.9
	63	1.6	1.3
	84	2.0	1.9
	114	3.1	2.6
	128	3.6	3.5
Sb	39	2.0	1.2
	63	2.7	1.9
	84	3.6	2.8
	114	6.0	3.9
Li-Sn	39	0.9	0.5
	63	1.5	0.7
	84	1.8	1.3
Sb-As	39	1.2	0.6
	63	3.3	2.1
	84	5.5	4.1
	114	10.4	6.5

Table 12. Growth-Rate Constants for Pasted-Plate Specimens at 71 °C[a]

Alloy	Rate Constant × 10^2, %/day	
	Vertical	Horizontal
Li	2.8	2.4
Sb	5.0	3.3
Li-Sn	2.3	1.4
	Rate Constant × 10^4, %/day^2	
Sb-As	8.1	5.3

[a] Estimated graphically from Figures 7 and 8.

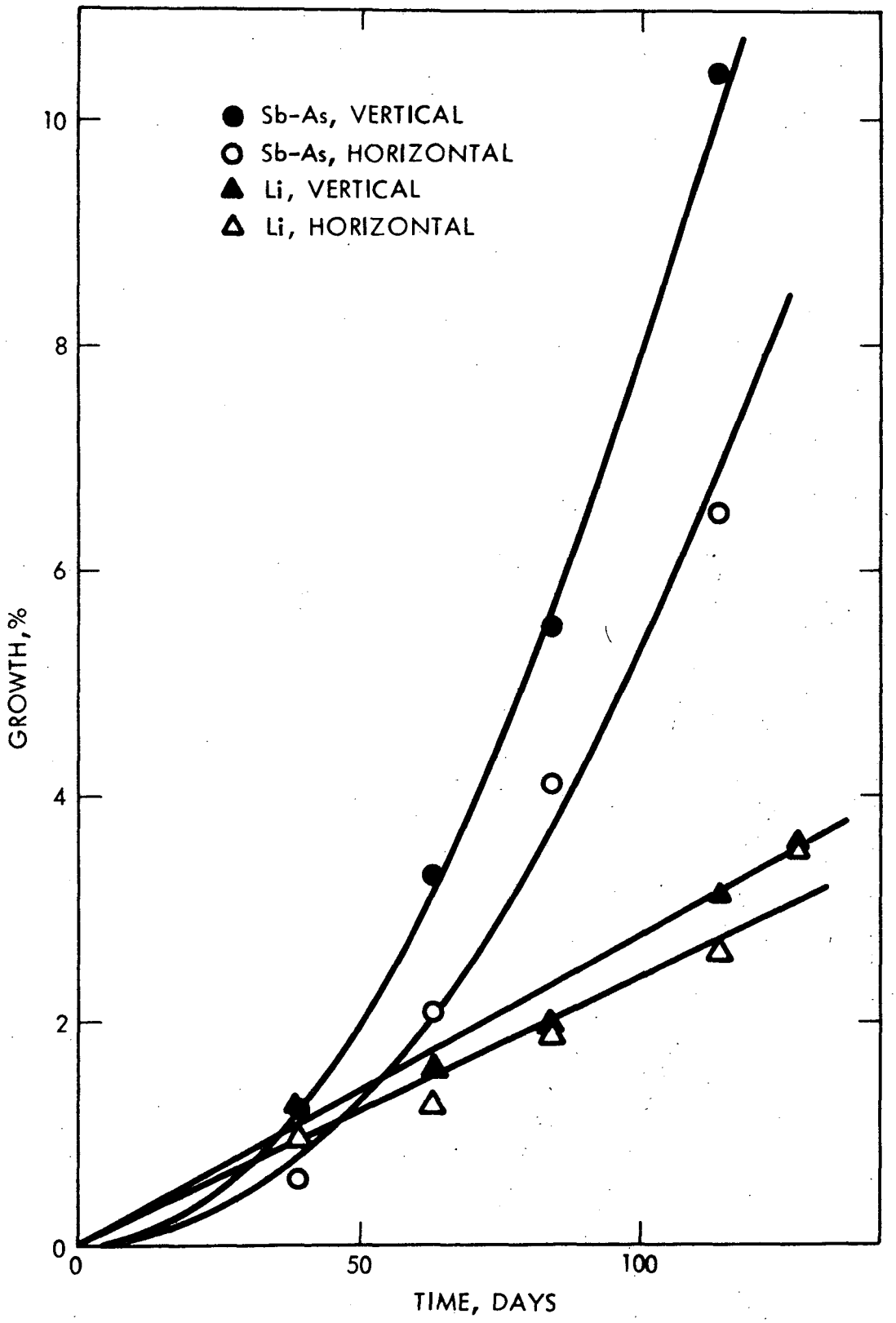

Figure 7. Growth-Rate Plot for Li and Sb-As Alloys

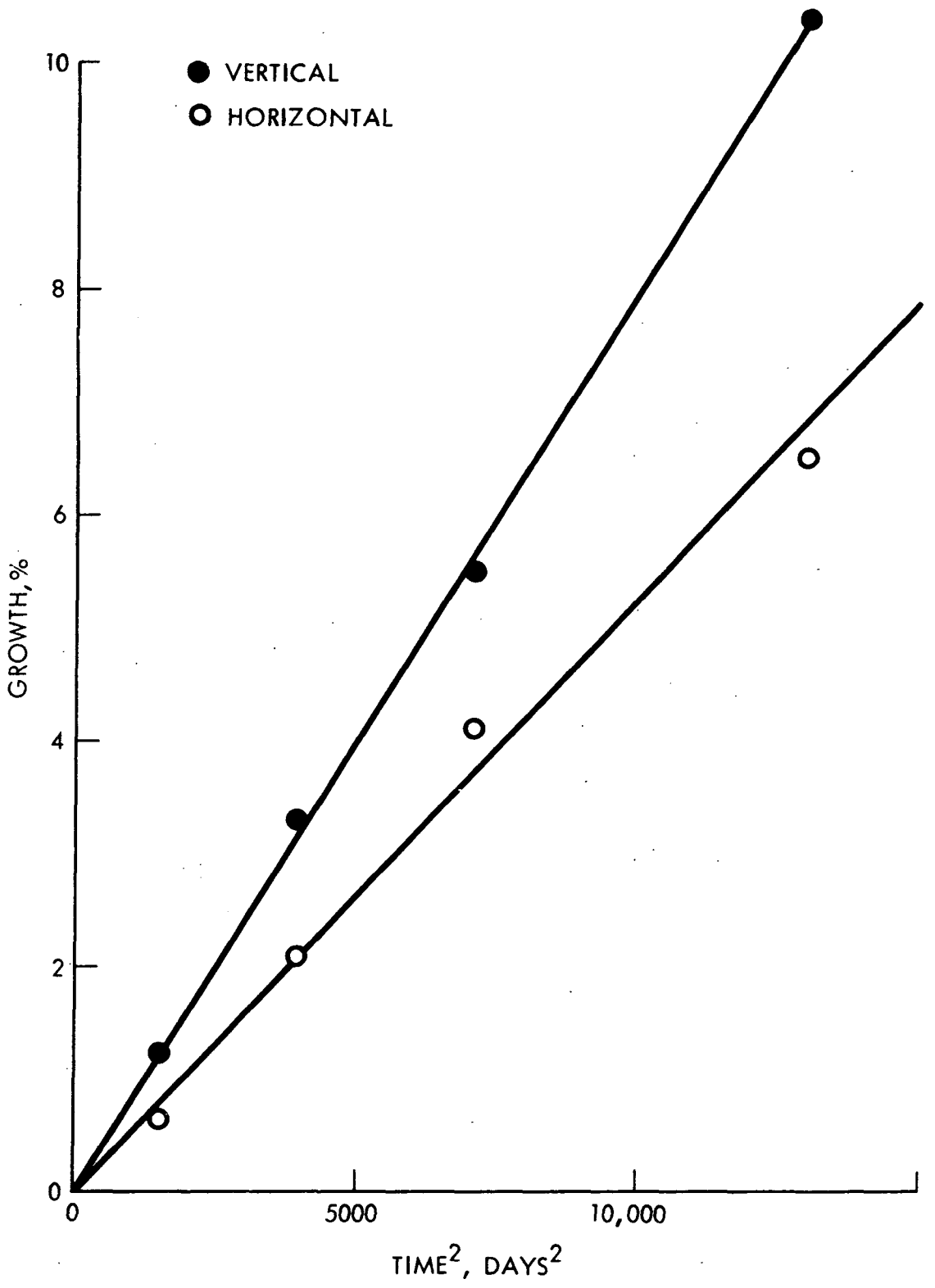

Figure 8. Second-Order Growth-Rate Plots for Sb-As Alloy

Sb-Ag alloy grid warped and pieces fell out, but the integrity of the frame was retained. Growth measurements on the Cd-Sb-Ag alloy grids were discontinued because of the warpage, difficulty of making measurements and failure of the corresponding plates.

Capacity, resistance and growth measurements were made at room temperature. The cooling, measuring and reheating period took 24 hours. This testing period is not included in the time scale of the growth curves. Since the Cd-Sb-Ag and Ca-Sn alloy plates were the first to fail, data for them were too limited for analysis.

Direct growth measurements on bare-grid specimens were difficult to make because waves or ripples had formed in the plane of the grid during expansion. Growth estimates were therefore made indirectly on projected grid images. These values, although erratic, seemed much less than those for pasted plates. Expansion of the pasted plates led to uniform bowing or dishing. Only the Sb-As alloy plate developed ripples which led to cracked and loosened pellets.

Estimates of growth rate constants and life times (times to failure) for 52 °C (125 °F) and 25 °C (77 °F) were made using the Arrhenius plot (log k vs. 1/temperature, °K) data of Cannone for pure lead (second-order rate; 162 kJ/mol) and 6% Sb-Pb alloy (first-order rate; 62.8 kJ/mol). The calculated values are summarized in Table 13. The approximations assume that the activation energy is the same for 1) lead alloys with the same reaction-rate order and 2) our test conditions. (Cannone used 1.210 sp gr sulfuric acid and maintained the plates at 0.080 V above the reversible $PbO_2/PbSO_4$ potential.) Growth rate is assumed to be independent of grid design.

These estimates of life times are optimistic because they do not take into account the effect of positive plate potential on corrosion-caused growth. Our tests were carried out at the minimum growth potential of 0.075 V with respect to open circuit. At open circuit or under cycling conditions the corrosion rates may be several fold greater. Therefore, grid corrosion is a likely cause of failure of a hybrid-vehicle battery. Perhaps the best way of estimating corrosion life is by examining the life

Tabl3 13. Estimated Growth-Rate Constants and Life Times for Pasted Plates at 52 and 25 °C[a]

Alloy	Temperature, °C	Rate Constant, %/day[b]	Rate Constant, %/day[2c]	Life Time, mo
Li	71	2.4×10^{-2}		4.0
	52	6.6×10^{-3}		14.5
	25	8.1×10^{-4}		119
Sb	71	3.3×10^{-2}		3.3
	52	9.2×10^{-3}		11.9
	25	11.2×10^{-4}		97
Li-Sn	71	1.4×10^{-2}		3.5
	52	3.9×10^{-3}		12.5
	25	4.7×10^{-4}		103
Sb-As	71		5.3×10^{-4}	3.8
	52		1.9×10^{-5}	20.0
	25		8.4×10^{-8}	300

[a] Horizontal growth.

[b] Based on activation energy of 62.8 kJ/mol.

[c] Based on activation energy of 162 kJ/mol.

of present-day SLI batteries which utilize antimony-alloy grids that are perhaps 50% thicker than grids projected for use in hybrid-vehicle batteries. Our corrosion tests indicate that lithium alloy is 20% more resistant to corrosion than antimony alloy, and antimony-arsenic alloy is perhaps 100% more resistant than antimony alloy. On this basis, the antimony-arsenic alloy would be expected to yield a life time in a hybrid-vehicle battery comparable to that of present SLI batteries.

Rod Specimens

Rod specimens were kept on test for 138 days at 71 °C until all plate and bare grid tests were terminated. Specimens did not show significant growth or pronounced curvature. Three alloys, Cd-Sb-Ag, Sb, and Ca-Sn, revealed casting defects (voids) not evident when rods were prepared for testing.

Weight loss (per unit of original exposed surface area) and change (decrease) in diameter are summarized in Table 14. Included in the table are the times to failure for pasted-plate and bare-grid specimens. Agreement among the results from the three types of corrosion tests was obtained only with the Cd-Sb-Ag alloy. However, in general, Sb-As and Li alloys appeared the best overall.

The alloys tested can be divided into eutectic (Cd-Sb-Ag, Sb and Sb-As) and noneutectic (Li, Li-Sn and Ca-Sn) alloys. Metallographic examination showed that corrosion in eutectic alloys is concentrated along the interdendritic network, whereas in noneutectic alloys, attack occurs preferentially along grain boundaries, the matrix being resistant to corrosion. Corrosion is more uniformly distributed in eutectic alloys because the interdendritic network is much finer than the grain boundary network. It is therefore less destructive because it is distributed over a large area, although it progresses more rapidly and results in greater weight loss. The behavior of Sb-As and Li alloys (Table 14 demonstrates the relationship between material loss and plate (or grid) life time for the two classes.

Table 14. Comparison Data for Rod, Bare-Grid and Pasted-Plate Specimens Obtained during Accelerated Corrosion Test

Alloy	Weight Loss, g/cm^2	Diameter Decrease, cm	Time to Failure, days	
	Rods[a]	Rods[a]	Plates[b]	Grids[c]
Cd-Sb-Ag	0.36	0.071	36	70[d]
Li	0.07	0.010	114 128	117 132
Sb	0.32	0.058	84 114	99[d]
Li-Sn	0.12	0.015	104[d]	99[d]
Sb-As	0.15	0.028	114[d]	132 138
Ca-Sn	0.14	0.018	84[d]	99[d]

[a] 138-Day test; nominal diameter, 0.25 in. (0.64 cm).

[b] Based on capacity determined at 60-A (0.16-A/cm^2) discharge rate to 0.95 V; failure defined as capacity of 2.00 A hr or less.

[c] Broke apart while measuring growth.

[d] Both specimens failed at the same time.

3.2 COMPONENTS-LEVEL TEST PLATES

3.2.1 Concept Requirements and Performance-Test Design

Plate thickness, T, paste density, P, and grid design were identified as variables in the component plates most likely to influence the performance of lead-acid batteries in a hybrid vehicle. For each matrix point shown in Table 15 four each of both positive and negative plates were fabricated with the following selected values (nominal) for the parameters:

Grid Design,	G_1:	Normally spaced members
	G_2:	Closely spaced members
Thickness,	T_1:	0.040 in. (0.10 cm)
	T_2:	0.060 in. (0.15 cm)
	T_3:	0.080 in. (0.20 cm)
Paste Density,	P_1:	3.3 g/cm^3
	P_2:	4.0 g/cm^3
	P_3:	4.7 g/cm^3

Based on the fabricated plates and the test condition variables, temperature(s), electrolyte specific gravity(ies) and replication, a test plan for positive plates was developed which included both grid designs, all three thicknesses, two paste densities (P_1 and P_3), two temperatures (27 and 52 °C) and replication. These variables were grouped to establish a statistically designed minimum test matrix. Evaluation of several implementation approaches resulted in selection of the test plan layout shown in Table 15.

Table 16 shows the sequencing of tests used to obtain the optimum information. Evaluation Period 1 represents two test runs on each of eight plates representing cell numbers shown in Table 15. (Four of these plates are run first at t_1 followed by a run at t_2 and four plates are run first at t_2 followed by a run at t_1.) For Evaluation Period 2, eight new plates (duplicates of the plates from Evaluation Period 1) are selected and the runs of Evaluation Period 1 are duplicated, except that the initial temperatures are reversed. In Evaluation Period 3, eight new plates are selected (two each for Cell Numbers 9, 10, 11 and 12 in Table 15) and run with the

Table 15. Test Plan Layout for Components-Level Test Plates at One Temperature

	G_1		G_2	
	P_1	P_3	P_1	P_3
T_1	1*	2	3	4
T_2	5	6	7	8
T_3	9	10	11	12

* Cell number denotes one of twelve matrix points for sequencing the test run (Table 16).

temperature sequencing shown in Table 16. It should be noted that the design of these evaluation periods is such that options are provided for reducing the total number of test runs. For instance, if all of the effects of temperature, paste density, plate thickness, and grid geometry are well defined after Evaluation Period 1, there is no need for Evaluation Periods 2 and 3. Likewise, Evaluation Period 3 is not necessary if the thinnest plate (T_1) is shown to be best in Evaluation Periods 1 and 2.

Figures of merit for specific power and charge acceptance were developed to provide a measure of battery performance on the components test plate level. The figure of merit for specific power is defined as

$$(fm)_{sp} = i_{75}\bar{V}/W$$

where i_{75} is the current required to discharge the test plate to 1.5 V in 75 sec, $\bar{V}$ is the average cell voltage for the 75-sec discharge, and W is the plate weight. Current rather than current density was used in the figure of merit because all the test plates have identical geometrical surface areas. Furthermore, the average cell voltage, $\bar{V}$, rather than the plate potential (vs. Hg/Hg_2SO_4) was used since preliminary performance tests on Gould Pb 660 positive plates of comparable size indicated that the difference in the cell voltage and plate potential values was only 25 mV. The current value required for 75-sec discharge was obtained from a Peukert plot (log discharge time vs. log discharge current).

The figure of merit for charge acceptance was defined as

$$(fm)_{ca} = \frac{\text{Capacity after cycling}}{\text{Capacity before cycling}}$$

where the capacities are measured at constant-current discharge of 20 A (0.28 A/cm^2) to 1.5 V.

Performance data is obtained with the following test sequence:

Peukert Plot (Specific Power)

1. Charge at 1 A (0.014 A/cm^2) for 1 hr (2.7 V limit).
2. Discharge at 30 A (0.42 A/cm^2) to 1.0 V.
3. Charge at one-half the discharge rate to 2.7 V; at 2.7 V for 5 min.

Table 16. Test Sequence of Test Plates

Evaluation Period	Test Run	Test Condition t_1	Test Condition t_2	Total Plates	Total Tests
1[b]	1	2	8		
		1	6		
		7	4		
		3	5		
	2[a]	8	2		
		6	1		
		4	7		
		5	3		
2[b]	1	8	2		
		6	1		
		4	7		
		5	3		
	2[a]	2	8		
		1	6		
		7	4		
		3	5		
3	1	10	12		
		9	9		
		11	10		
		12	11		
	2[a]	12	10		
		9	9		
		10	11		
		11	12		

[a] Test Run 2 is a rerun of Test Run 1 with the cell temperature t_1 and t_2 reversed.

[b] Test plates used in Evaluation Periods 1 and 2 correspond to plates in Replicate Groups 1 and 2, respectively, in Section 3.2.4.

4. Repeat Steps 2 and 3 for discharge currents of 20, 10 and 5 A (0.28, 0.14 and 0.07 A/cm^2).

Charge Acceptance

5. Discharge at 20 A for 10 sec.
6. Charge at 10 A for 20 sec.
7. Repeat Steps 5 and 6 nine times.
8. Discharge at 20 A to 1.0 V.
9. Charge at 2.5 A to 2.7 V; at 2.7 V for 5 min.

3.2.2 Test Plate Fabrication

Grids with the nominal thicknesses and separation of vertical members described in Section 3.2.1 were prepared from 4.5% Sb alloy. Those with normally spaced members (G_1) and 0.080- and 0.040-in. (0.20- and 0.10-cm) nominal thicknesses were cast in corresponding grid molds. One-half each of the 0.20- and 0.10-cm molds were combined for casting the 0.15-cm thick grid. A set of grids with closely spaced grid members (G_2) was cast after both sets of molds were recut to reduce pellets to one-half of their original size; i.e., three additional vertical members were added. In the G_1 and G_2 grids, the vertical members are on 3/4- and 3/8-in. (1.9- and 1.0-cm) centers, respectively. (Measurement note: the frame bar measurement is made from the outer edge.) Outlines of the fabricated grid types are shown in Figure 9. The actual grid thicknesses were 0.040, 0.066 and 0.088 in. (0.10, 0.17 and 0.22 cm) for the corresponding nominal thicknesses of 0.040, 0.060 and 0.080 in. (0.10, 0.15 and 0.20 cm), respectively.

Pastes were hand-mixed in the laboratory using standard automotive oxide, Gould SP102, and two standard automotive paste formulas each for positive and negative plates. The lowest-density paste in each case was obtained by adjusting a standard paste formula with water and sulfuric acid until the desired wet paste desity was obtained. Positive paste formulas were PF-62, PF-66, and PF-71G which correspond to the nominal densities of 3.3, 4.0, and 4.7 g/cm^3, respectively. The actual wet paste densities were 3.81, 4.08 and 4.36 g/cm^3, respectively. Negative paste formulas were PF-69, PF-73, and PF-76FG which correspond to actual wet paste densities of 4.24, 4.47 and 4.69 g/cm^3, respectively. Densities of negative paste are normally

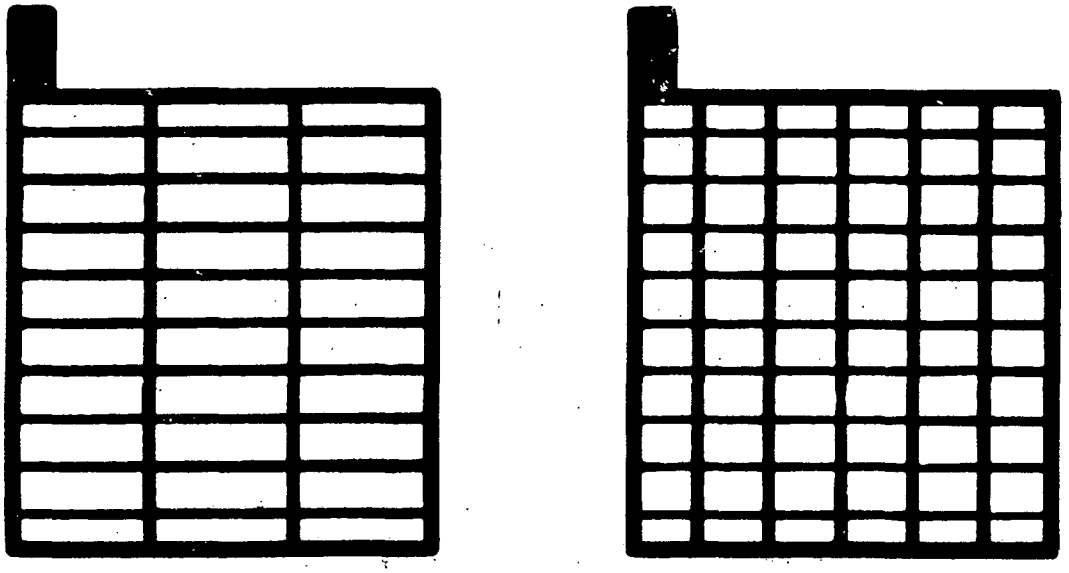

Figure 9. Outlines of Grids Used in Components-Level Test Plates.

slightly higher than positive densities. (All paste designations refer to proprietary Gould formulas.)

A total of 72 positive and 72 negative plates were fabricated. Individual grid weights, paste density, and dried (unformed) plate weights were obtained for those plates actually tested and are tabulated in Table 17, Section 3.2.4. The dry paste weights were obtained by subtracting the grid weights from the plate weights.

After pasting, the plates were cured and dried using conventional techniques. Pasted plates were interleaved with pasting paper, wrapped in plastic and allowed to cure at room temperature for 24 hr. Interleaved papers were removed and the stacked plates were rewrapped in plastic and curing was continued another two days. The plates were then unwrapped and racked to dry overnight in air.

Plates were then tank-formed. After formation, positives were washed in running water and then were racked and dried in room air for three hours. The negatives were first soaked in hot Stoddard solvent at 99 °C. When bubbling action ceased, the temperature rose to 127 °C and plates were removed. Plates were allowed to cool in the air. Actual density or porosity of the dry active material was not measured.

3.2.3 Test Equipment

Four components-level test stations were assembled. These stations were developed for controlled testing of the plate parameters defined within the statistically designed experimental matrix. The testers are capable of providing accurate current and voltage control through various charge-discharge sequences to provide data for calculating the figures of merit for test plates. One of the stations contains additional programming capability required for performing preliminary tests on plates to determine the effects of cycling and past history on the figures of merit.

Each components tester consists of the following major elements (Figure 10):

- A dc power supply with independent current and voltage controls for charge and discharge,

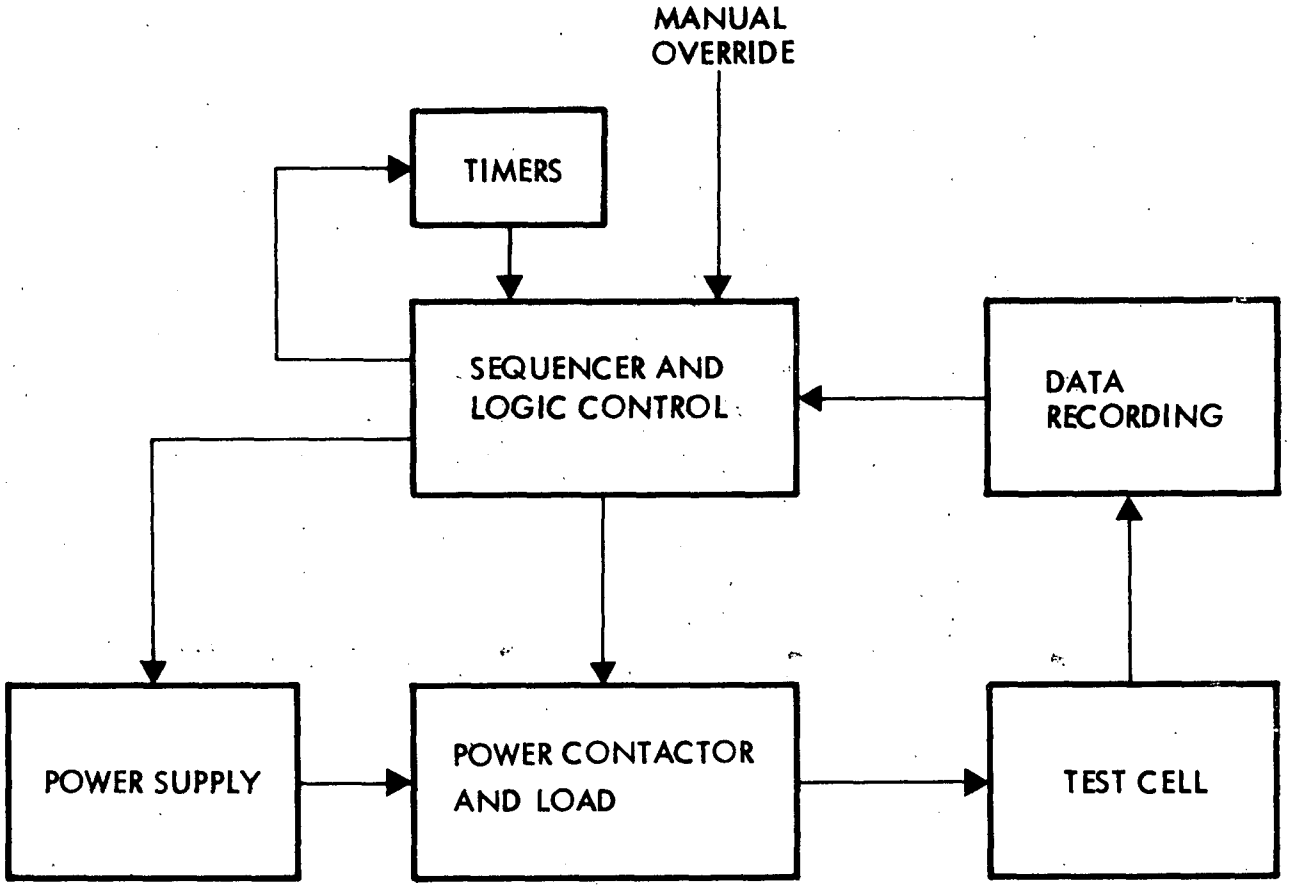

Figure 10. Block Diagram of Components-Level Tester.

- load resistors to absorb discharge power,
- power contactor to transfer power from power circuitry to the test cell and to select modes of operation (charge or discharge),
- sequencing and control logic, and
- data recording.

The programmed sequence for the components-level performance test was the following:

Step	Function
1	Off
2	Charge at 1.0 A for 1 hr (voltage limit set at 2.7 V)
3	Discharge at 30 A to 1.0 V
4	Charge at 15 A to 2.7 V
5	Charge at 2.7 V for 5 min
6	Discharge at 20 A to 1.0 V
7	Charge at 10 A to 2.7 V
8	Charge at 2.7 V for 5 min
9	Discharge at 10 A to 1.0 V
10	Charge at 5 A to 2.7 V
11	Charge at 2.7 V for 5 min
12	Discharge at 5 A to 1.0 V
13	Charge at 2.5 A to 2.7 V
14	Charge at 2.7 V for 5 min
15-20	Advance
21	Discharge at 20 A for 10 sec
22	Charge at 10 A for 20 sec
23-40	Repeat Steps 21 and 22 nine times
41	Discharge at 20 A to 1.0 V
42	Charge at 2.5 A to 2.7 V
43	Charge at 2.7 V for 5 min
44-60	Reset.

A schematic of the cell designed for components-level plate testing is shown in Figure 11. All surfaces exposed to the sulfuric acid electrolyte are Teflon (TFE) or glass except for rubber bands used to secure the plates and separators. Ports are provided in the Teflon cover for a thermometer, a mercury/mercurous sulfate reference electrode (No. 288, Koslow Scientific Co.) and addition or removal of electrolyte. Electrical lead to the plate is lead welded to the plate tab.

3.2.4 Performance Tests and Results

3.2.4.1 Preliminary Check-Out

Tests were conducted on standard lead-acid positive plates to check-out the procedures developed for determining the figures of merit. The plates were those used in a commercially available battery (Gould Pb 660, 3-A hr capacity at the 20-hr rate) and which have nominal dimensions of 2 1/4 in. in width × 2 7/16 in. in height × 0.080 in. (5.7 cm × 6.2 cm × 0.20 cm). The plate area is 11.0 $in.^2$ (71 cm^2). The test cells consisted of two negative plates and one positive plate with paper separators. A mercury/mercurous sulfate reference electrode (at the same temperature as the electrolyte) was used in measuring the plate potentials. The cell was maintained at a constant temperature with a thermostated water bath. Specific gravity of the sulfuric acid was 1.260.

After checking out the test equipment and the procedures for determining the figures of merit, tests were performed to determine the effect of previous cycling (discharging and charging) on a plate's Peukert plot. These tests were done by carrying out the performance test using several permutations of the discharge current sequence, 30, 20, 10, 5 A. The permutations selected for this check-out were the following:

Permutation	Discharge Current Sequence
1	30, 20, 10, 5 A
2	20, 10, 5, 30 A
3	10, 5, 30, 20 A
4	5, 30, 20, 10 A

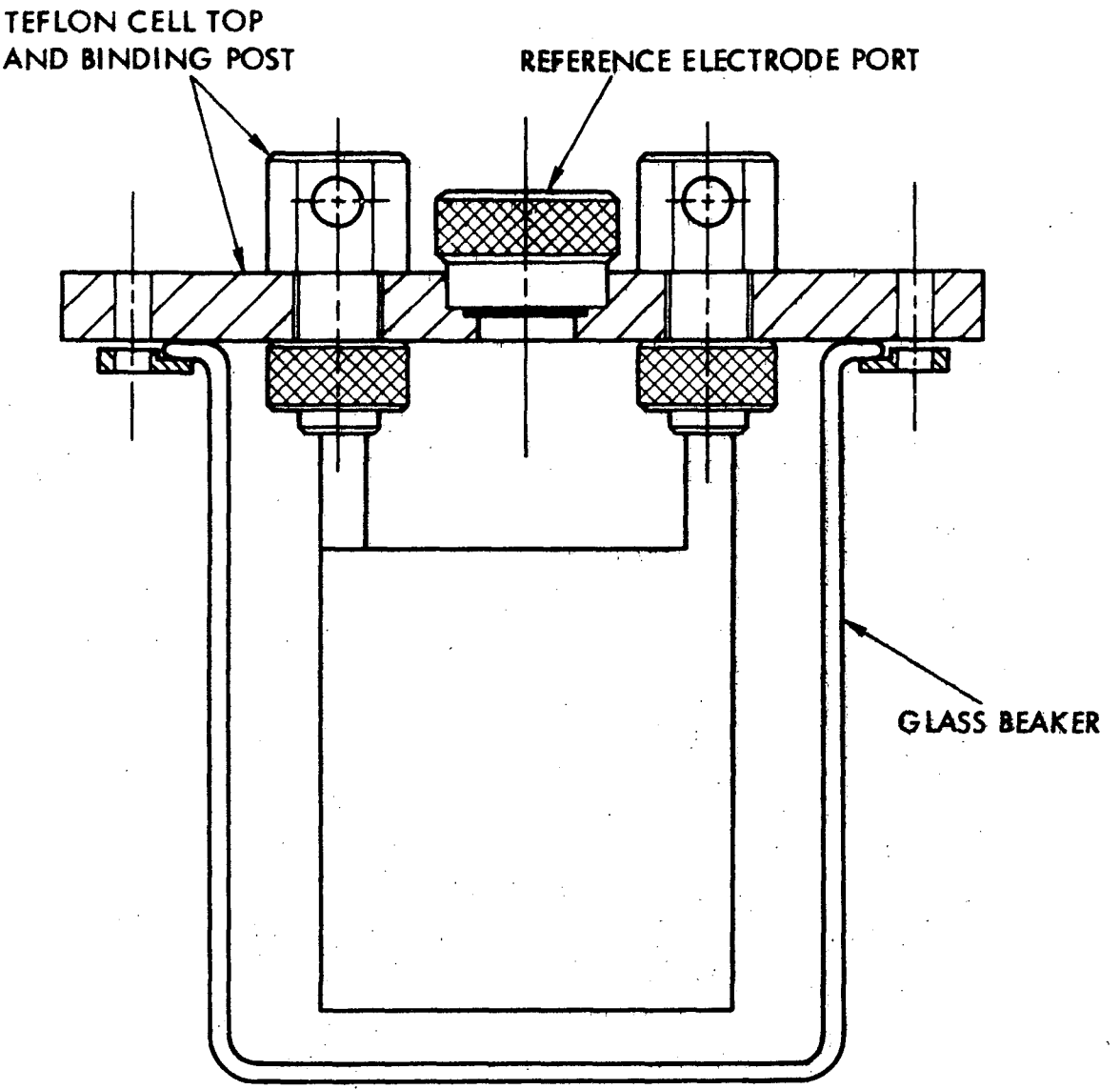

Figure 11. Schematic of Components-Level Test Cell.

Preliminary results from tests on used Pb 660 positive plates indicated that the Peukert plots were independent of the permutation used. However, to eliminate any doubt, four new plates were used in a test of broader scope in which each plate was run five times with the permutations sequenced as follows:

	Permutation			
Run	Plate 1	Plate 2	Plate 3	Plate 4
1	1	2	3	4
2	2	3	4	1
3	3	4	1	2
4	4	1	2	3
5	1	2	3	4

Note that Run 5 ends the test for each plate with the starting discharge current sequence and that although the permutation sequence is the same for all plates, the permutation for Run 1 for each plate is different. Altogether, twenty runs were made to establish the influence of previous cycling. The plates were charged after each discharge at one-half the discharge current until the test cell voltage reached 2.7 V, then for 5 min at 2.7 V. There was no additional charging between runs. The specific gravity of the sulfuric acid was 1.260 and the tests were conducted at 38 °C.

The results in terms of i_{75} and $i_{75}\bar{V}$ values are listed in Tables 17 and 18, respectively. The $i_{75}\bar{V}$ values averaged according to plate, permutation and run groups are listed in Table 19. The value of the product $i_{75}\bar{V}$ was used as the measurable output parameter and the results for the analysis of variance are given in Table 20. Sample calculations are given in Appendix B. Based on the F-ratio test it was concluded at the 95% confidence level that test runs and order of current application have no significant influence on the power output. Accordingly, all data were pooled and the best estimate of the standard error of experimental variation was calculated to be 2.02. Since the overall average was 37.4 W, the coefficient of variation was found to be 5.4%. Such a small coefficient of variation denotes a well run experiment. The data do indicate that there may be some influence of past history at low power levels.

Table 17. 75-Second Discharge Currents for Pb 660 Positive Plates

	Discharge Current, A			
Run	Plate 1	Plate 2	Plate 3	Plate 4
1	24.0	22.6	22.3	20.2
2	24.2	22.6	22.2	18.9
3	22.3	22.5	21.8	23.3
4	21.8	23.1	23.5	22.0
5	21.7	23.6	23.5	22.5

Table 18. Summary of $i_{75}\bar{V}$ Values for Pb 660 Positive Plates

	$i_{75}\bar{V}$, W			
Run	Plate 1	Plate 2	Plate 3	Plate 4
1	39.8	36.8	37.0	33.9
2	40.6	37.5	37.5	31.9
3	37.7	36.7	36.8	38.9
4	36.8	37.0	39.9	37.0
5	35.6	39.6	38.3	38.2

Table 19. Average $i_{75}\bar{V}$ Values for Pb 660 Positive Plates

Plate	Average Power, W
1	38.1
2	37.5
3	37.9
4	36.0
Permutation Order	
1	36.2
2	39.2
3	37.5
4	36.6
Run	
1	36.9
2	36.9
3	37.5
4	37.7
5	37.9

Table 20. Analysis of Variance for Power (Pb 660 Positive Plates)

Source of Variation	Degrees of Freedom	Mean Squares	F-Ratio
Plates	3	7.83	2.06
Runs	3	0.75	--
Permutations	3	6.74	1.78
Experimental variation	6	3.79	

3.2.4.2 Performance Tests

The physical properties of all the positive and negative plates that were tested are listed in Table 21. The positive plates were placed in two replicate groups according to the matrix shown in Table 22. Each replicate group was further divided into two test runs with one test run being made first at 27 °C (80 °F) and the other being made first at 52 °C (125 °F). Upon completion of the first test run, the temperatures of the cells were reversed and the test run was repeated. For the second replicate group, the initial temperature for each matrix point was reversed from that of the first replicate group.

Positive plates to be tested were assembled into cells using two standard negative plates of the same size as the positive plates and paper separators. The specific gravity of the electrolyte was 1.260. Results of the tests are shown in Tables 22, 24 and 25. Tables 23 and 24 show the figures of merit for specific power calculated as $i_{75}\bar{V}$ divided by the plate weight and paste weight, respectively. Table 25 summarizes the figure of merit for charge acceptance.

A "burn-in" effect was observed in that the second test run performance was found to be better than the first. In order to check the stabilization of the burn-in, two plates were subjected to additional tests. The results summarized in Table 26 demonstrate that no significant change occurs after the second run. An analysis of the results shows that the "burn-in" effect does not influence the selection of the optimum electrode configuration. The figure of merit was shown to improve with increasing temperature. The results of the analysis of variance for specific power are shown in Table 27 which indicates that all main effects are highly significant. A preliminary analysis showed that there were no significant interactions between the design parameters. Therefore, the optimum conditions were determined by a simple regression equation on the main effects. Sample calculations are given in Appendix B.

It was recognized that pellet area (size) is correlated to grid type, Therefore, rather than use dummy variables for grid type, the regression equation was run using pellet area as the variable for grid type. In addition, although temperature is not a design parameter, it was also included

Table 21. Properties of Components-Level Test Plates

Plate	Grid Type	Grid Weight, g	Thickness, cm	Paste Density, g/cm^3	Paste Weight, g	Plate Weight, g	Replicate[a] Group
P058	G_1	14.5	0.17	4.36	15.9	30.4	1
P059	G_1	14.6	0.17	4.36	15.9	30.4	2*
P062	G_2	17.0	0.17	4.36	15.8	32.8	1
P063	G_2	17.0	0.17	4.36	15.9	32.9	2*
P065	G_1	8.6	0.10	4.36	11.7	20.3	1*
P068	G_1	8.7	0.10	4.36	12.3	21.0	2
P069	G_2	10.1	0.10	4.36	11.7	21.8	1
P070	G_2	10.4	0.10	4.36	11.6	22.0	2*
P081	G_1	14.4	0.17	3.81	14.4	28.8	1
P082	G_1	14.5	0.17	3.81	13.6	28.1	2*
P085	G_2	16.8	0.17	3.81	13.7	30.5	2
P086	G_2	17.0	0.17	3.81	14.0	31.0	1*
P089	G_1	8.6	0.10	3.81	10.6	19.2	1*
P092	G_1	8.7	0.10	3.81	10.1	19.8	2
P093	G_2	10.1	0.10	3.81	9.1	19.2	1*
P094	G_2	10.4	0.10	3.81	9.5	19.9	2
N089	G_1	8.7	0.10	4.24	10.3	19.0	-
N092	G_1	8.8	0.10	4.24	10.8	19.6	-

[a] Asterisks denote plates first run at t_1 (27 °C), then at t_2 (52 °C); others run in reverse order.

Table 22. Distribution of Components-Level Test Plates between Replicate Groups

	First Replicate				Second Replicate			
	T_1		T_2		T_1		T_2	
	G_1	G_2	G_1	G_2	G_1	G_2	G_1	G_2
P_1	P089*	P093*	P081	P086*	P092	P094	P083*	P085
P_3	P065*	P069	P058	P062	P068*	P070	P059*	P063*

* Denotes plates run first at t_1.

LEGEND:

T_1 = 0.10-cm thickness
T_2 = 0.17-cm thickness
G_1 = normally spaced grid members (0.86-cm^2 pellet area)
G_2 = closely spaced grid members (0.39-cm^2 pellet area)
P_1 = 3.81-g/cm^3 paste density
P_3 = 4.36-g/cm^3 paste density

Table 23. Figures of Merit for Specific Power Based on Plate Weight, W/g

Test Run 1 for Each Plate

	t_1				t_2			
	T_1		T_2		T_1		T_2	
	G_1	G_2	G_1	G_2	G_1	G_2	G_1	G_2
P_1	1.27*	1.04*	0.97	0.78*	1.61	1.40	1.26*	1.18
P_3	1.00*	0.92	0.65	0.66	1.15	1.04*	1.14*	1.13*

Test Run 2 for Each Plate

	t_1				t_2			
	T_1		T_2		T_1		T_2	
	G_1	G_2	G_1	G_2	G_1	G_2	G_1	G_2
P_1	1.45	1.10	1.05*	0.93	1.77*	1.52*	1.42	1.20*
P_3	1.04	1.00*	0.89*	0.84*	1.37*	1.25	0.99	1.01

* Denotes plates from Replicate Group 1.

Table 24. Figures of Merit for Specific Power Based on Paste Weight, W/g

Test Run 1 for Each Plate

	t_1				t_2			
	T_1		T_2		T_1		T_2	
	G_1	G_2	G_1	G_2	G_1	G_2	G_1	G_2
P_1	2.29*	2.20*	2.00	1.73*	3.00	2.92	2.53*	2.62
P_3	1.73*	1.74	1.25	1.36	1.96	1.93*	2.17*	2.42*

Test Run 2 for Each Plate

	t_1				t_2			
	T_1		T_2		T_1		T_2	
	G_1	G_2	G_1	G_2	G_1	G_2	G_1	G_2
P_1	2.70	2.31	2.10*	2.06	3.21*	3.20*	2.93	2.66*
P_3	1.77	1.86*	1.69*	1.75*	2.37*	2.37	1.90	2.09

* Denotes plates from Replicate Group 1.

Table 25. Figures of Merit for Charge Acceptance for Components-Level Test Plates

Test Run 1 for Each Plate

	t_1				t_2			
	T_1		T_2		T_1		T_2	
	G_1	G_2	G_1	G_2	G_1	G_2	G_1	G_2
P_1	0.85*	0.22*	0.95	0.41*	1.02	1.11	1.00*	1.03
P_3	0.35*	0.23	0.26	0.59	1.10	1.10*	0.40*	0.83*

Test Run 2 for Each Plate

	t_1				t_2			
	T_1		T_2		T_1		T_2	
	G_1	G_2	G_1	G_2	G_1	G_2	G_1	G_2
P_1	0.86	0.42	0.87*	0.89	1.02*	0.93*	0.96	1.06*
P_3	0.82	1.06*	1.01*	1.09*	1.07*	1.13	1.05	1.05

* Denotes plates from Replicate Group 1.

Table 26. Summary of Burn-In and Temperature Effects for Components-Level Test Plates

Plate	Figure of Merit	Test Run 1	2	3	4	5	6[a]	7[a]
P089	Specific Power[b]	1.27[c]	1.77	1.71	1.75	1.72	1.22	1.37
	Charge Acceptance	0.85[c]	1.02	1.01	0.95	0.90	0.91	0.85
P092	Specific Power[b]	1.61[d]	1.45	1.87	1.90	1.88	1.52	1.58
	Charge Acceptance	1.02[d]	0.86	1.00	0.98	1.01	0.87	0.86

[a] Additional runs made at 27 °C.

[b] Based on plate weight, W/g.

[c] First run made at 27 °C, next four at 52 °C.

[d] First run made at 52 °C, second at 27 °C and next three at 52 °C.

Table 27. Analysis of Variance for Specific Power for Components-Level Test Plates. Figures of Merit Based on Plate Weights, W/g (Test Run 2 for Each Plate).

Sum of Variation	Degrees of Freedom	Sum of Squares	Mean Squares	F-ratio[a]
Temperature (t)	1	0.312760	0.312760	>39
Thickness (T)	1	0.296208	0.296208	>37
Grid type (G)	1	0.079665	0.079665	> 9
Paste density (P)	1	0.262400	0.262400	>32
Experimental variation	11	0.090537	0.008230[b]	

[a] F-ratio required for significance at 5% probability is 4.84.

[b] The standard error per measurement is $0.008230^{1/2} = 0.0287$. Since the average measurement was 1.1764, the coefficient of variation is 2.44%, indicating a well run experiment.

in the regression analysis to improve the predictive capability. The resulting equation is

$$(fm)_{sp} = 2.977 + 0.0112t - 3.887T - 0.4657P + 0.3003G.$$

The observed and predicted values are given in Table 28. Since no interactions were detected within the region of experimentation, we can only say that the region of optimum specific power is for a thin plate with low paste density on a grid having normally spaced members.

If it is assumed that specific power is functionally related to these parameters in a linear manner only, then the optimum combination is the thinnest plate, largest pellet size and minimum paste density possible consistent with design constraints of weight and cost, and fabrication capabilities. Since the thin plate provides the optimum specific power, it was decided not to run the additional tests with the thickest plates (0.20 cm).

In summary, within the scope of the experiment, the design for a positive plate that provides optimum specific power is the following:

Grid Type:	Normally spaced members, G_1 (0.86-cm^2 pellet area size)
Paste Density:	$3.81\ g/cm^3$
Thickness:	0.10 cm

Further experimentation around these points is necessary to more accurately pinpoint the combination of design parameters which would provide optimum specific power.

Components-level testing of negative plates was limited to the plate with physical parameters corresponding to those of the best positive plate. The physical parameters of the negative plate were given in Table 21. The results of the test, Table 29, show that for negative plates the figures of merit for specific power are slightly larger and those for charge acceptance slightly lower than those for the corresponding positive plate.

The effect of operating temperature on negative plate performance (Table 29) is a reduction in both specific power and charge acceptance with decreasing temperature.

Table 28. Figures of Merit for Specific Power for Components-Level Test Plates from Test Run 2 by Grid Type and Temperature

	G_1				G_2			
	t_1		t_2		t_1		t_2	
	T_1	T_2	T_1	T_2	T_1	T_2	T_1	T_2
P_1	1.45[b] 1.37	1.05 1.10	1.77 1.65	1.42 1.38	1.10 1.23	0.93 0.96	1.52 1.51	1.20 1.24
P_3	1.04 1.11	0.89 0.84	1.37 1.39	0.99 1.12	1.00 0.97	0.84 0.70	1.25 1.25	1.01 0.98

[a] Specific power in W/g based on plate weight.

[b] Top, observed value; bottom, predicted value.

Table 29. Summary of Components-Level Performance Tests on Negative Plates

Plate	Figure of Merit	Test Run[a] 1	2	3	4	5	6	7	8
N089	Specific Power[b]	1.96	1.90	1.89	1.39	1.46	0.87	1.02	--
	Charge Acceptance	0.92	0.92	0.86	0.66	0.74	0.48	0.43	--
N092	Specific Power[b]	1.90	1.82	1.81	1.35	1.36	0.89	1.06	1.03
	Charge Acceptance	0.88	0.88	0.89	0.88	0.81	0.50	0.40	0.38

[a] Test Runs 1 and 2 made at 52 °C, 3, 4 and 5 at 27 °C and 6, 7 and 8 at 0 °C.

[b] Based on plate weight, W/g.

3.2.4.3 Cycle-Life Tests

Cycle-life tests were made on the best positive plates (P089 and P092). A cycle consisted of a 20-A (0.28-A/cm^2) discharge for 15 sec followed by a 10-A (0.14-A/cm^2) charge for 30 sec. Before the cycle test, both plates were charged at 1 A (0.014 A/cm^2) or 2.7 V whichever limited, for one hour. The capacity of one plate (P089) was measured after each 100 cycles. Capacity was determined using a 5-A (0.070-A/cm^2) discharge. After measuring the capacity, the plate was charged at 2.5 A (0.035 A/cm^2) to a 2.7-V cut-off, then held at 2.7 V for 5 min. The other plate (P092) was subjected to 600 cycles after which the cell was charged at 1 A (0.014 A/cm^2) or 2.7 V for one hour. The test sequence was repeated until the plate failed. Plate failure was defined as the point at which the discharge voltage decreased to 1.5 V. The tests were conducted at 52 °C. High current densities were intentionally chosen to accelerate failure.

The results of the cycle-life test of Plate P089 are shown in Table 30 Even though the plate failed after 589 cycles, the plate could be restored by charging at 2.5 A (0.035 A/cm^2). However, the number of cycles to failure decreased with each recharge. After 900 cycles, the plate could not be reactivated. Plate P092 failed after 868 cycles. Changing the charge time from 30 to 32 sec to provide 15% overcharge restored the plate for an additional 125 cycles. Examination of the plates indicated that failure was due to loss of active material. Approximately 15 to 50% of the active material was lost from Plates P089 and P092, respectively. The cell containing Plate P092 showed evidence of an electrical short caused by bridging between the plates by active material accumulated at the bottom of the cell.

3.3 TEST CELLS

3.3.1 Cell Design and Fabrication

Two types of pasted-plate test cells were designed using the results of the components level tests and of the mathematical modeling of grid geometry. One (Type IA) emphasized high specific power while the other (Type IB) compromised power for the sake of life. Grid alloys selected for the test cells were 0.013% Li (Type IA cell) and 2.5% Sb-0.45% As (Type IB

Table 30. Cycle-Life Test Data for Components-Level Test Plate P089 at 52 °C

Cycle[a]	Capacity, A hr[b]	Remarks
---	1.14	Initially charged at 1 A (0.014 A/cm^2).
100	0.64	
200	0.63	
300	0.58	
	0.92	Stored (fully charged) over weekend at 52 °C
400	0.58	
500	0.56	
589	--	Failed, <1.5 V.
600	0.42	
672	--	Failed, <1.5 V.
700	0.32	
	0.83	Stored (fully charged) overnight at 52 °C.
750	--	Failed, <1.5 V.
800	0.26	
825	--	Failed, <1.5 V.
900	0.11	

[a] Discharged at 20 A (0.28 A/cm^2) for 15 sec, charged at 10 A (0.14 A/cm^2) for 30 sec.

[b] Determined at 5-A (0.070-A/cm^2) discharge rate, then charged at 2.5-A (0.035-A/cm^2) rate.

cell). Separators were sintered polyvinyl chloride (PVC) membranes (Ethyl Corporation), 0.020-in. (0.051-cm) thick with a 0.013-in. (0.033-cm) backweb. In the Type IB (long-life) cells, pairs of separators were heat-sealed together to form envelopes in which the positive plates were placed, whereas in the Type IA (high-specific-power) cells the separators were used singly in the conventional manner. Additives were not used in either cell.

Design parameters and projected operating characteristics of the pasted-plate test cells are the following:

Number of Positive Plates	10
Number of Negative Plates	11
Single Plate Area (10.8 cm × 10.8 cm)	233 cm^2
Grid Thickness	0.10 cm
Maximum Current	600 A
Maximum Current Density	2.6 A/cm^2
Minimum Cell Voltage	1.5 V
Approximate Cell Stack Size	4 cm × 17 cm × 15 cm

A grid mold was fabricated for the grid design that resulted from the mathematical modeling study described earlier in Section 3.1.1. Grids of 0.10- to 0.11-cm thickness were cast from Li and Sb-As alloys. (An outline of an actual grid was shown in Figure 5, Section 3.1.1.) Positive grids were pressed to 0.10 cm and negative grids to 0.089 cm before pasting. Connector straps and terminal posts were also cast and a burning comb for a 21-plate element was fabricated.

Five Type IA (Li-alloy grid) cells were fabricated. Their positive and negative group weights are summarized in Table 31. Typical grid weights were in the range of 28-33 g. The lighter grids were segregated for use in negative plates and the heavier for positive plates. Pastes were hand mixed in the laboratory using standard automotive oxide. The positive paste formula was PF-62 and the negative paste formula was PF-69. Wet densities of the pastes were 3.88 and 4.20 g/cm^3 for the positive and negative, respectively.

Five Type IB (As-Sb-alloy grid) cells were fabricated. Typical grid weights were in the ranges of 27-32 g for negatives and 32-35 g for positives,

Table 31. Group Weights for Type IA Cells[a]

	Positive Group Weights, g			Negative Group Weights, g		
Cell	Grids	Formed Plates	Active Material	Grids	Formed Plates	Active Material
1	295	663	368	300	665	362
2		657	362		660	360
3		651	356		656	356
4		653	358		657	357
5		644	349		656	356

[a] Each cell contains 10 positive and 11 negative plates. Weight of straps and posts not included.

with averaged weights of 30.4 g for negatives and 33.3 g for positives. Averaged group grid weights, group formed wiehgts, and active material per cell are given in Table 32. The positive and negative paste formulas were PF-66 and PF-73, respectively. Average wet paste densities were 4.0 and 4.45 g/cm^3 for the positive and negative, respectively.

Construction and assembly were the same as with the lithium-alloy cells except that the polyvinyl chloride separators were heat-sealed on three edges to form pockets (two separators per pocket) in which the positive plates were inserted. The foot was removed from the grid because, with the envelope separator construction, there is no danger of sediment collecting on the bridge ridge and shorting beneath a separator which may nct be properly seated on the ridge.

Plates were cured, dried and tank formed in the same way as were the components-level test plates. The formed plates were dry charged as before, then joined to connecting straps to form positive and negative groups and assembled into cells. All containers were cut from Group Size 22F automotive battery cases. Because the plates were not wide enough to fill the container, foamed polystyrene (closed pores) was used to fill the extra space. A photograph of a Type IB cell is shown in Figure 12. The cells were heavier than necessary because of excess volume in the cell compartment of the Group Size 22F container and because the containers were cut oversize for stability in handling and testing. Excess weight correction for calculation of specific power is estimated as 161 g as shown below.

Excess weight	
Extra plastic outside cell	90 g
Extra plastic in cell (excess length and width)	30
Styrofoam (space filler)	5
Extra electrolyte in sediment well	19
Extra connections	37
Total	181 g

Table 32. Group Weights for Type IB Cells[a]

		Positive Group Weights, g			Negative Group Weights, g	
Cell	Grids	Formed Plates	Active Material	Grids	Formed Plates	Active Material
1	333	691	358	334	654	320
2		691	358		654	320
3		692	359		654	320
4		692	359		656	322
5		692	359		656	322

[a] Each cell contains 10 positive and 11 negative plates. Weight of straps and posts not included.

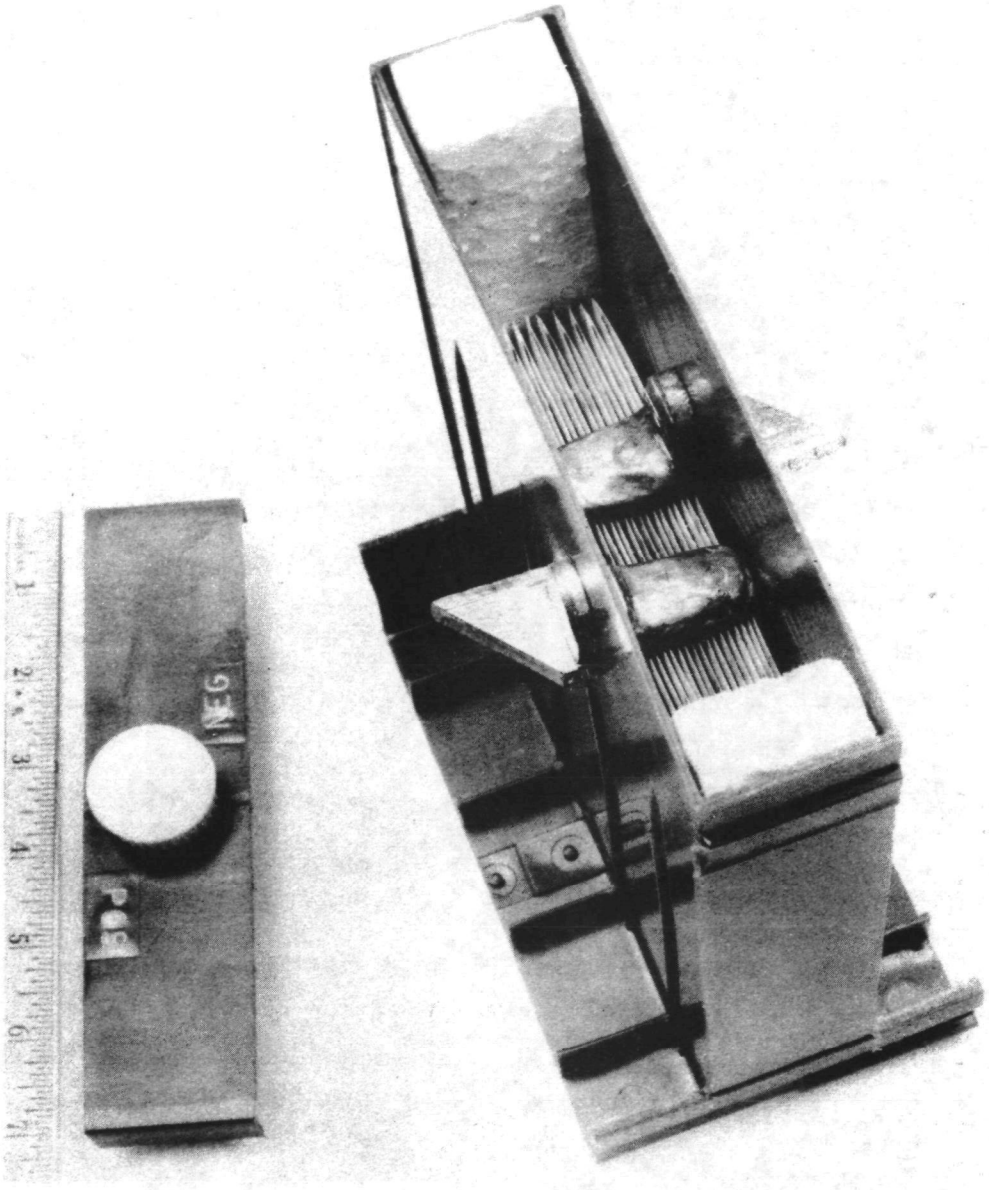

Figure 12. Type IB Test Cell.

Deficient Weight	
Top terminals and bushings	20
Net Excess Weight	161 g

3.3.2 Test Procedures

The cell test procedure was designed so that it would provide information for predicting the performance of a full-scale battery system. The overall test sequence conducted at 52 °C (125 °F) included three major steps:

Step 1. Performance Test for Specific Power. Peukert plots were obtained to establish initial performance characteristics of the test cells. Tests were made on all cells to establish manufacturing variability for each type of cell and were run three times on each cell to determine the extent of any burn-in effect. Discharge currents used were 600, 400, 200 and 100 A. Since each cell contained ten 233-cm^2 positive plates, the currents corresponded to current densities of 0.26, 0.17, 0.086 and 0.043 A/cm^2, respectively. Charge was at one-half the discharge currents to 2.7 V; then 5 min at 2.7 V.

Step 2. Cycle Test. One cell of each type, preferably the one which exhibited the highest specific power in Step 1 was to be subjected to 20,000 charge-discharge cycles. The cycling profile and power levels approximated those in Exhibit I of RFP No. EHSD 71-Neg. 100:

Cycle A

50-A (0.021-A/cm^2) discharge for 10.8 sec
25-A (0.011-A/cm^2) charge for 23 sec

Cycle B

365-A (0.16-A/cm^2) discharge for 25 sec
180-A (0.08-A/cm^2) charge for 50 sec

Cycle A was repeated 29 times followed by one Cycle B. The discharge and charge times were calculated to provide a 5% overcharge for the total of 29 "A" and 1 "B" cycles. Note that the

current densities in the cycle test (Step 2) were significantly lower than the 0.31-A/cm^2 discharge/0.15-A/cm^2 charge profile used in the accelerated cycle-life tests on the components level. Although the selected current densities were of reasonable magnitude, it should be noted that the test sequence was still a severe one since the cells were cycled continuously at a high ambient temperature (52 °C) and were not provided any additional charging at a lower rate.

Step 3. Performance Test. A repeat of Step 1 following 20,000 cycles in Step 2 was included in the test sequence to establish the effect of cycling on the figure of merit for specific power.

The figure of merit for the performance tests (both Steps 1 and 3) was the same as the one for specific power used in the components level tests:

$$(fm)_{sp} = i_{75}\bar{V}/W$$

where i_{75} is the current required to discharge the test cell to 1.5 V in 75 sec, $\bar{V}$ is the average cell voltage for the 75-sec discharge and W is the cell weight. The current value required for 75-sec discharge, i_{75}, is obtained from the Peukert plot (log discharge time vs. log discharge current).

Tests were implemented by using a cell tester which was designed and constructed around a 600-A, 40-V power supply (Christie Electric Corp., Model 1C040-600E245). The tester design was identical to the block diagram shown in Figure 10 for components-level tester, except for higher output power levels. Removable programming drums were used to program the tester for either the performance or cycle test schedule as described previously. The bipolar cells and batteries were tested using the components-level tester adjusted for the proper current levels. The test cells were thermostated at 51 °C (125 °F) using a constant temperature water bath. A view of the test station is shown in Figure 13.

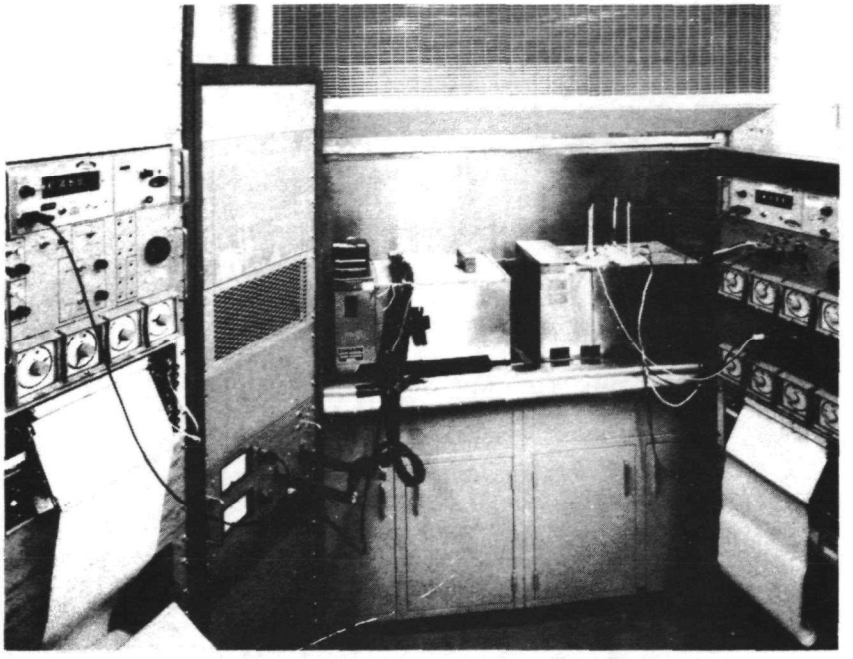

Figure 13. Battery Test Equipment. Left, cell tester; right, components-level tester; thermostated baths with cells in fume hood.

3.3.3 Tests and Results

3.3.3.1 Performance

The performance test was run at least three times for each cell and the results of the last test for each cell are assumed to be free of burn-in effects. Table 33 is a summary of the results for specific power whereas Table 34 shows the results of the last run for each cell. (Actual cell weights, uncorrected for excess weight, were used.) A test of a 61-A hr, Group Size 22F cell is included for comparison. It can be seen from Table 34 that the specific power of both Type IA and Type IB cells is approximately twice that of the Group Size 22F cell. To evaluate cell differences, the last run for each cell (Table 34) was used to analyze the standard errors and specific power output. The results are:

	Type IA	Type IB
Mean Specific Power, W/lb	147	140
Standard Error	2.24	11.04

The range of specific powers for Type IA cells is significantly larger than that for the Type IB cells. With this large variation and few test sample, the t-test does not indicate that the cell types are different in performance.

A comparison of the specific power for the separate runs on individual cells (Table 33) shows a large variation indicating a large test error. Components of this error may be a burn-in problem, changes in test procedures, inefficient test equipment, and unknown sources of variation. Ignoring an unequal number of runs, and assuming all tests are compatible, the overall average specific power for each cell was computed. The results are given in Table 35. Since the largest value for a Type IB cell is lower than the lowest Type IA cell value, it is concluded that the Type IA cell has higher specific power than the Type IB cell. The figures of merit in the above discussion are based on a 75-sec discharge time. For discharge times shorter than 75-sec the figure of merit increases because of the current-time relationship shown in Figure 14 which is a typical Peukert plot for a Type IA test cell. For example, for a 20-sec discharge, a current of 600 A can be maintained. This discharge time corresponds

Table 33. Summary of Performance Test Data for Pasted-Plate Cells

Cell	Specific Power, W/lb[b]	End-of-Discharge Voltage, V
IA-1[a]	145	1.0
	141	1.0
	134	1.0
	162	1.5
	160	1.5
IA-2	156	1.0
	152	1.0
	154	1.0
	155	1.5
IA-3	152	1.0
	151	1.0
	146	1.0
	149	1.5
IA-4	155	1.0
	149	1.0
	144	1.0
	147	1.5
	134	1.5
IA-5	154	1.0
	150	1.0
	145	1.0
	138	1.5
IB-1	130	1.0
	136	1.5
	142	1.5
IB-2	150	1.0
	138	1.5
	141	1.5
IB-3	141	1.0
	130	1.5
	141	1.5
	133	1.5
	137	1.5
IB-4	143	1.0
	133	1.5
	141	1.5
IB-5	144	1.0
	144	1.0
	138	1.5
	141	1.5

[a] Denotes Type-IA cell, Serial Number 1.

[b] Specific power based on discharge time to 1.5 V.

Table 34. Summary of Peukert-Plot Test Data for Pasted-Plate Test Cells[a]

Cell	i_{75}, A	$\bar{V}$, V	$(fm)_{sp}$, W/lb
IA-1	500	1.64	160
IA-2	480	1.63	155
IA-3	462	1.63	149
IA-4	418	1.60	134
IA-5	430	1.63	138
IB-1	452	1.63	142
IB-2	442	1.63	141
IB-3	428	1.63	137
IB-4	448	1.64	141
IB-5	440	1.65	141
22F[b]	270	1.56	70.4

[a] Last run.

[b] Group Size 22F, Gould Power Breed 22F-GP-61.

Table 35. Averaged Specific Power Values for Pasted-Plate Cells

Cell	Specific Power, W/lb
IA-1	148
IA-2	154
IA-3	150
IA-4	146
IA-5	147
IB-1	136
IB-2	143
IB-3	136
IB-4	139
IB-5	142

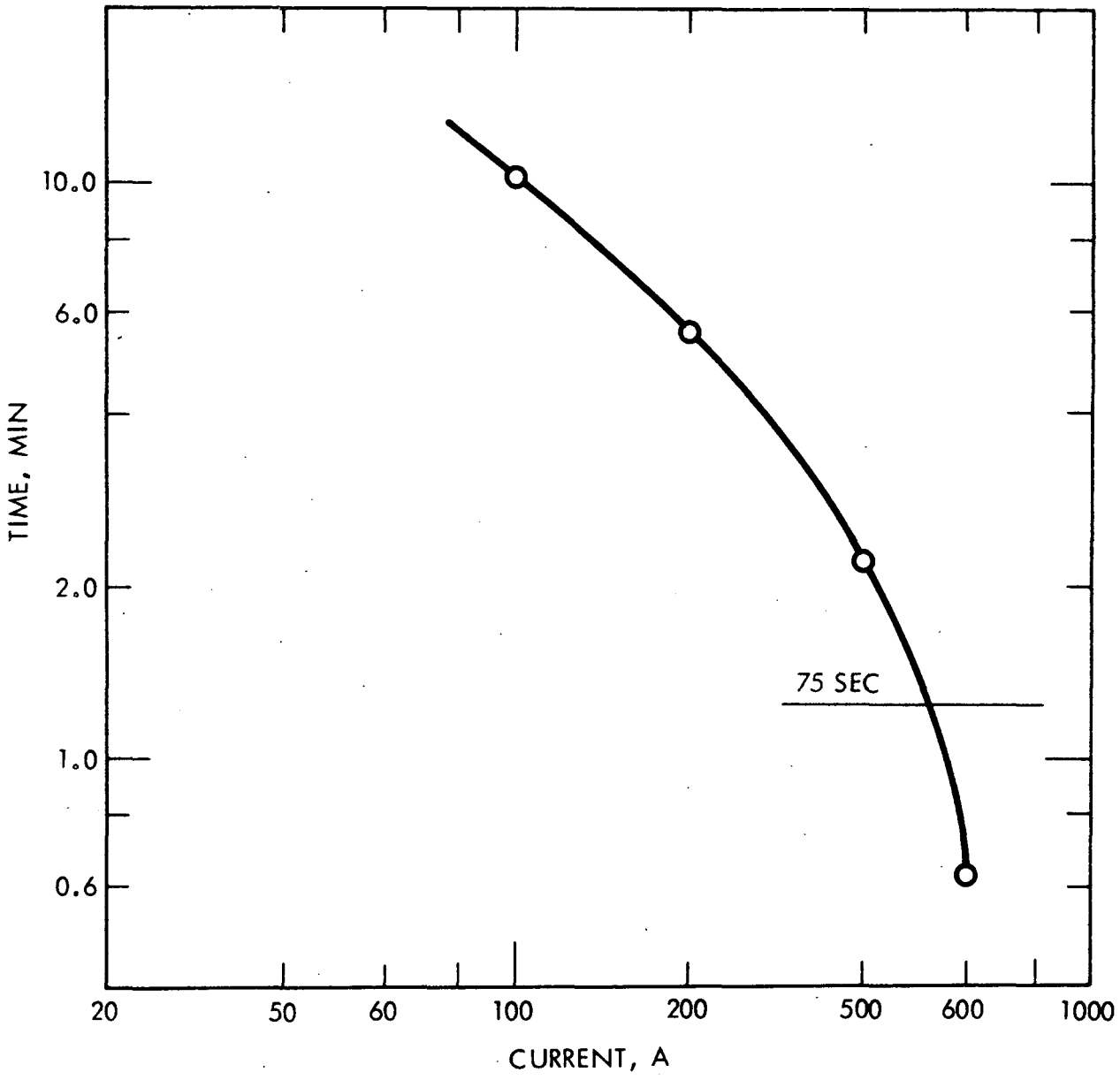

Figure 14. Typical Peukert Plot for Type IA Test Cell

roughly to the two 9-sec, 90.2-kW peak discharges for the power profile of the EPA specifications. The average voltage during this discharge is approximately 1.6 V so the specific power for a 20-sec discharge is approximately 188 W/lb or 205 W/lb based on corrected cell weights as discussed in Section 3.3.1.

3.3.3.2 Cycle Life

Cycle-life data was analyzed by plotting the end-of-discharge voltage for the "B" cycle as a function of the total number of cycles. These voltages were obtained every 300 cycles. When the end-of-discharge voltage reached 1.5 V the cell was considered to have failed since this was the minimum cell voltage given in the revised EPA specifications.

The comparison of the results for Cells IA-3 and IB-1 to those for a cell from a 61-A hr, Group Size 22F battery is shown in Figure 15. The cycle life to 1.5 V was approximately 10,500 cycles for Cell IB-1 and 8,000 cycles for Cell IA-3. This corresponds to 400 and 260 high power "B" cycles for Cell IB-1 and IA-3, respectively. Even though the revised EPA specifications call for 500 cycles at 70.5 kW, the power level for "B" cycles actually used in the cycle testing was 72.6 kW. Since the "B" cycle was repeated after 29 rather than 200 low power "A" cycles as required by EPA, the test used represents a more stringent cycle-life test. Although the end-of-discharge voltage for the Group Size 22F cell had decreased to 1.5 V at approximately 90 cycles, the cycle test was continued because the failure was attributed to the large iR drop due to the high resistance of 1.25 mΩ (compared to resistances of 0.58 and 0.62 mΩ for Cells IA-3 and IB-1, respectively). Degradation of the Group Size 22F cell beyond that point was slow, with the end-of-discharge voltage reaching 1.28 V at approximately 30,000 cycles (1,000 "B" cycles).

The end-of-discharge voltage for "A" cycles (10-kW discharge) remained above 2.0 V for all the cells tested for the entire duration of each test represented in Figure 15. Therefore, the cycle life of the cells was affected more by the high-power rather than low-power cycling. The results in Figure 15 were obtained without any additional low-rate charging. Cell IB-2 was run with attempts made to increase cycle life by introducing low-rate

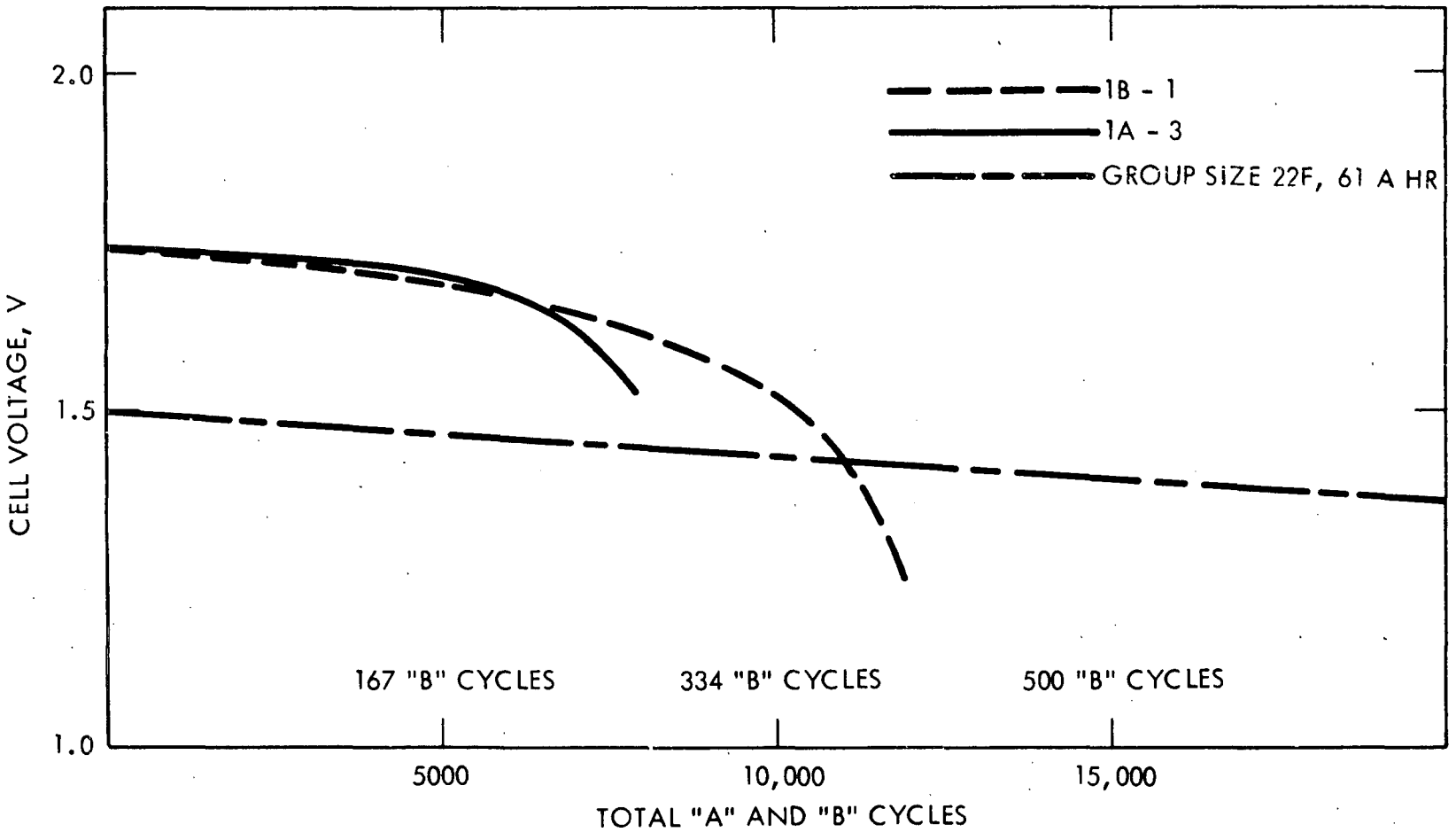

Figure 15. End-of-Discharge Voltage for Cycle B vs. Cycle Number for Test Cells

charging after approximately 2,000 and 9,000 cycles, but the end-of-discharge voltage still decreased to 1.5 V after 12,000 cycles. Cell IA-3 recharged after 8,000 cycles, also exhibited similar results with end-of-discharge voltage failing below 1.5 V several hundred cycles after resumption of cycling. Cell IA-2 was lost during test after 5,000 cycles because of a malfunction in the cell tester.

A post-mortem of both Type IB cells showed that the positive active material had become soft and that shedding had occurred. Insufficient charging in the cycling program probably contributed to the softness of the active material. Shorting through the separator was observed as evidenced by several spots of metallic lead being present on the positive plates. The lead spots were about 1.3 to 2 cm in diameter and about four were found in each test cell. The actual shorting through the separator (lead treeing) could be observed only by microscopic examinations. As expected, the grid was not noticeably corroded. The separator bags which enclosed the positive plates were not intact along the bottom edge, also providing a path for shorting. Shorting also contributes to shedding of the active material by causing the cell to run at a decreased state of charge.

Since the main failure mode was caused by shorting through the separator, it is felt that the results were not a realistic test of the new plates and great improvement would result from the use of other separators. Use of microporous separator materials such as Daramic (microporous, extruded polyethylene, W.R. Grace, Polyfibron Division), which have proven performance in heavy-duty industrial batteries, could prevent shorting and thus increase cycle life of the cell. Paper separators as used in Group Size 22F cells tested can also be investigated. Previous high-current cycle test results on the components level, Section 3.2.4.3, indicate that plates with paper separators which were cycled with a 2-A/in.^{2} (0.31-A/cm^2) discharge compared to 1 A/in.^{2} (0.16 A/cm^2) for the "B" cycles in the cell tests ran for 600 cycles before failure. Considering that the Group Size 22F cell has a long cycle life, but insufficient specific power, and that both Type I cells had sufficient specific power but short cycle life, a trade-off in design between these cells should result in a high-power cell with a long cycle life.

3.3.4 Summary and Recommendations

It is recommended that development of conventional lead-acid batteries be continued. This work should be directed toward a better understanding of the causes of failure of lead-acid batteries in hybrid vehicle duty and of the life that can be obtained.

The effect of separator and the method of testing on battery life should be investigated. The failures that have been observed so far in the program have all been caused by separator failure and the softening of the positive active material. This is greatly affected by the manner in which charging is accomplished, and especially by incomplete charging, which fails to re-cement the active material and leads to softening. The very stringent cycling conditions that have been used are probably useful as an accelerated test for comparing various cell designs but they hardly permit estimation of battery life to be expected in a hybrid vehicle.

At least one life test should be carried out under cycling conditions more representative of hybrid-vehicle duty, with more shallow cycles, which will allow more time for complete recharge after an occasional deep, full-power discharge. Also, the present cycling regime should be tried with provision for more complete recharge. For example, an occasional charge for a few hours could be interspersed in the cycling to assure complete recharge. State of charge should be monitored by measurement of electrolyte specific gravity.

Further development of conventional cells should stress the effect of various types of separators, alloys, lead oxides, and perhaps additives to the electrolyte (e.g., phosphoric acid, which has been observed to reduce softening of positive active material). Present grid design and size should be retained. Accelerated corrosion tests of this grid should be carried out at three temperatures to ascertain the temperature effect; it is recommended that the two lead alloys already selected (0.013% Li and 2.5% Sb-0.45% As) be compared with the conventional 4.5% Sb and that an improved quaternary alloy (0.07% Ag-1.5% Sb-1.6% Cd) also, be studied. Separators, oxides, and additives should be studied in component tests. Results of these studies should be utilized in the construction of improved test cells in which performance and life can be evaluated more definitively.

4. DEVELOPMENT OF BIPOLAR BATTERIES

4.1 ELECTRODE STUDIES

4.1.1 Objectives

The objectives in development of a bipolar lead-acid battery were to develop

- a light-weight electronically conductive substrate to which active material could be firmly attached and which would be inert in the cell environment,
- a method of attaching the active material utilizing Planté formation or pasting techniques, and
- a method of constructing a bipolar battery so that individual cells are sealed from each other.

The performance goals were to sustain a 2-A/in.^{2} (0.3-A/cm^2) discharge rate for 60 sec with a cell voltage $\geq$1.5 V and a recharge time of twice the previous discharge period. A specific power goal of 300 W/lb (137 W/kg) and a target life of 5 years was desired.

4.1.2 Conductive Substrates

Several approaches to develop a light-weight conductive substrate were evaluated. Considerations were given to conductive plastics and gold-plated titanium. Calculations of iR losses in a bipolar substrate due to its resistivity and thickness at 2 A/in.^{2} (0.31 A/cm^2) were made and are depicted in Figure 16. At the target current density, the iR loss will be 47 mV per cell if the substrate resistivity and thickness are 6 Ω cm and 0.010 in. (0.0254 cm), respectively. At a resistivity of 1 Ω cm and thickness of 0.025 in. (0.064 cm), iR loss will be 20 mV.

Gold-plated titanium was eliminated from considertion early in the program due to difficulites in achieving a pore-free, adherent gold plate and expected difficulties in working the titanium into a usable configuration. Commerically available conductive epoxies and thermoplastic materials were also found to be unsuitable because the usual conductive fillers (e.g., carbon, graphite, copper and silver) would react with the cell environment. Results of subjecting various conductive plastic materials to anodic polarization at the oxygen evolution potential in 1.260 sp gr

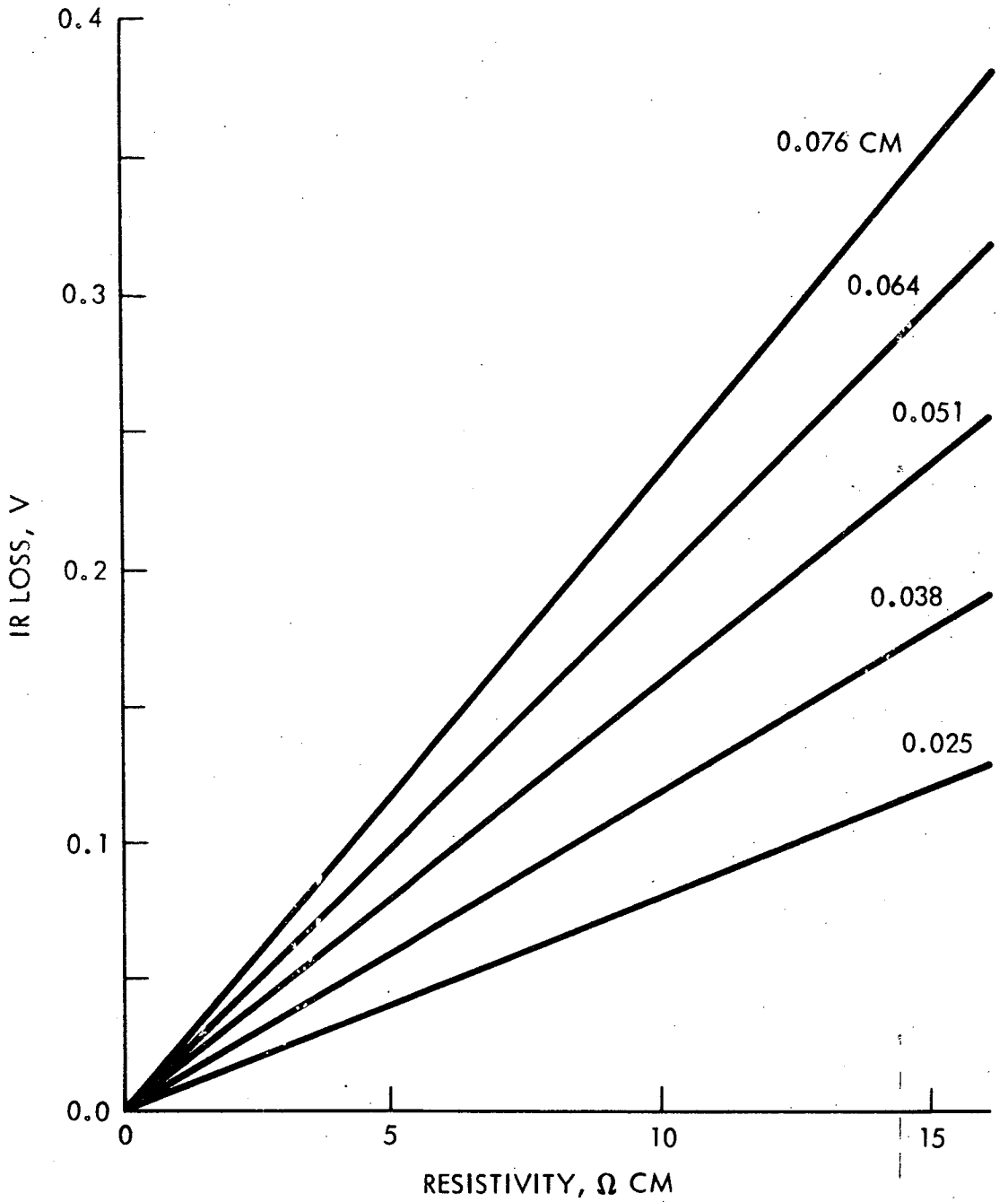

Figure 16. IR Loss in Bipolar Substrate at 0.31 A/cm^2 vs. Substrate Resistivity at Various Substrate Thicknesses

sulfuric acid at room temperature are shown in Table 36. It was clearly evident from these results that graphite or carbon black was definitely not acceptable as conductive fillers and that glassy or vitreous carbon would be acceptable. Vitreous carbon (a product of Beckwith Carbon Corp., Van Nuys, California 91406) is a distinct form of carbon which is amorphous, has a true density of 1.47 g/cm^3, a hardness of 7 on the Moh scale, and a resistivity of $\sim 10^{-3}$ Ω cm.

The development of a substrate material was therefore concentrated on the fabrication and evaluation of various plastics filled with finely divided vitreous carbon powder. Initially, substrates were fabricated using epoxy, TFE and FEP Teflon, polypropylene, polyethylene and fluorosilicone rubber filled with varying quantities of vitreous carbon. Polypropylene and polyethylene were eliminated from further consideration because their mechanical properties were seriously degraded when they were filled with vitreous carbon to the extent that the resistivity was acceptable. TFE and FEP Teflon and fluorosilicone rubber were also eliminated due to difficulties encountered in fabrication and expected difficulties in developing adequate seals with these materials. However, epoxy-vitreous carbon systems appeared promising and further efforts were concentrated on their development.

It was found that the lowest resistivities could be achieved by hot pressing the epoxy-vitreous carbon mixtures during the gel stage and oven curing. Some early results with CIBA 6010 resin and CIBA DP-152 and 951 (TETA, triethylenetriamine) are listed in Table 37. Data for CIBA 7079/972 and 1139/972 are included. Depending on the epoxy system used, temperatures of 100 to 175 °C and pressures of 2 to 10 tsi with press times of 5 to 15 min were required. The optimum hardner was found to be a methylene dianiline (MDA, supplied by CIBA Products Co. as CIBA 972). Several resins were found to be acceptable from a chemical resistance viewpoint; these included phenol Novolac liquid resin (CIBA EPN 1139) and conventional EPI-BIS resins (CIBA Araldite 6005 and 6010 liquid resins and CIBA Araldite 7072 solid resin). With the solid resin, the proper proportions of resin, hardner and vitreous carbon were mixed and ground to a fine powder and then compression molded. When liquid resins were used,

Table 36. Anodic Corrosion Test Data on Substrate Material[a]

Plastic	Conductor	Conductor, Vol %	Resistivity, Ω cm	Weight Change, %	Comment
Epoxy	Vitreous carbon	67	16.1	1.7	No visual effect, resistivity increased to 43.8 Ω cm.
Fluorosilicone rubber	Vitreous carbon	48	12.8	0.4	No visual effect, resistivity increased to 20.8 Ω cm.
Polypropylene	Vulcan XC72 graphite	23	3.1	-8.0	Sample corroded through at test clip contact.
---	Graphoil	--	8.5×10^{-4}	181	Original material is 61% porous; sample swelled from 0.025 to 0.06 cm in thickness.
Polypropylene	Vitreous carbon	38	65	--	Sample broke due to mechanical force.
Polyethylene	Carbon black	--	2.8	-1.4	Visible corrosion at the liquid line.
TFE	Graphite	85	0.4	--	Sample corroded through at test clip contact.

[a] Test run 4 days.

Table 37. Results of Conductive Plastic Fabrication Experiments

Epoxy	Vitreous Carbon, Wt %	Cure	Resistivity, Ω cm
CIBA 6010/152	40	Gravity, 40 °C, 4 hr	9.3×10^3
CIBA 6010/152	45	Gravity, 40 °C, 4 hr	2.4×10^3
CIBA 6010/152	50	Gravity, 40 °C, 4 hr	697
CIBA 6010/152	50	Gravity, 40 °C, 4 hr	179
CIBA 6010/152	55	Gravity, 40 °C, 4 hr	143
CIBA 6010/152	60	Gravity, 40 °C, 4 hr	65
CIBA 6010/152	60	Gravity, 40 °C, 4 hr	125
CIBA 6010/951	50	Gravity, 40 °C, 4 hr	6×10^5
CIBA 6010/951	55	Gravity, 40 °C, 4 hr	2.3×10^3
CIBA 6010/951	60	Gravity, 40 °C, 4 hr	4.8×10^3
CIBA 6010/152	71	Rolled, 50 °C, 2 hr	31.4
CIBA 6010/152	71	Rolled, 50 °C, 5 hr	16.1
CIBA 6010/152	80	Pressed, 60 °C, 1 hr	0.18
CIBA 6010/152	70	Gravity, 60 °C, 40 hr	6.6
CIBA 6010/152	80	Pressed at 1 tsi, 60 °C, 1 hr	0.13
CIBA 6010/152	80	Pressed at 1 tsi, 60 °C, 1 hr	0.2
CIBA 6010/152	75	Pressed at 3 tsi, 100 °C, 10 min	0.2
CIBA 6010/152	80	Pressed at 3 tsi, 100 °C, 10 min	0.2
CIBA 6010/152	80	Cold pressed at 6 tsi; press cured at 1/2 tsi, 100 °C, 10 min	0.12
CIBA 6010/152	77.5	Cold pressed at 6 tsi; press cured at 1/2 tsi, 100 °C, 10 min	0.29
CIBA 7079/972	60	Pressed at 10 tsi; heated to 150 °C, 15 min; hot pressed at 2 tsi, 150 °C, 10 min; cured at 100 °C, 16 hr; cured at 160 °C, 4 hr; annealed at 50 °C, 16 hr	1-2
CIBA 1139/972	60	Same as above	0.85

the proper proportions of resin, hardner and vitreous carbon were mixed with a solvent (acetone), the solvent evaporated, and the epoxy partially cured ("B-staged"). The resulting material was then ground to a fine powder and compression molded.

The initial substrates were compression molded using an aluminum mold where one die had a rib pattern and the other was a flat surface. These substrates contained 80 wt % vitreous carbon were 0.020-in. (0.051-cm) thick and had a 0.015- or 0.020-in. (0.038- or 0.051-cm) high raised grid pattern on one side. A 0.030-in. (0.076-cm) thick lead back plate to serve as the current collector was placed in the flat surface mold and bonded directly to the epoxy-vitreous carbon substrate. Lead tabs were burned onto the lead back plate and a layer of epoxy coating applied over the exposed lead surface. The overall dimensions of these bipolar half-plates were 2.25 in. × 2.44 in. (5.72 cm × 6.20 cm) and the rib width was 0.025 in. (0.064 cm). The epoxy-vitreous carbon substrate (without lead backing) weighed 4.0 g. A 0.125-in. (0.32-cm) wide edge was provided for sealing which left an active material area of $\sim$5 in.^{2} (32 cm^2).

The epoxy-vitreous carbon substrates as first developed had very high conductivity (resistivity <0.2 Ω cm) but attempts to form positive active material on these structures were unsuccessful. The problem was traced to corrosion at the interface between the substrate and the lead backing plate. It was found that the substrate contained pinholes or large pores which allowed sulfuric acid to contact the interface where corrosion occurred during formation of the active material. The corrosion product led to high resistance at the interface and caused buckling of the plate. The problem was eliminated by changing the material mixing procedure and reducing the vitreous carbon loading to 60 wt %. A small increase in resistivity occurred with reduction in carbon loading. The relation between carbon loading and resistivity is shown in Figure 17 for a CIBA 1139/972 substrate. At 60 wt % loading, a resistivity of 0.85 Ω cm was found which results in an iR loss of 13 mV for a 0.020-in. (0.051-cm) thick substrate at a current density of 0.31 A/cm^2. No further development of the basic conductive plastic was pursued.

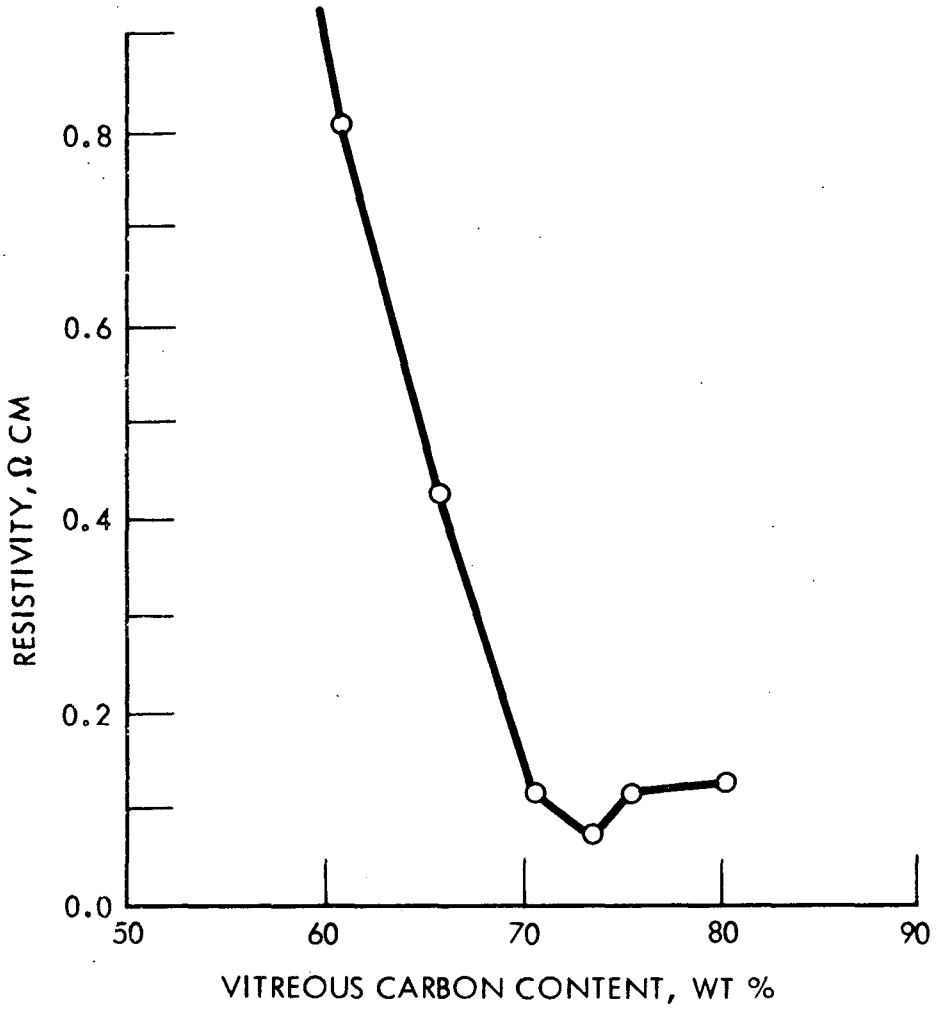

Figure 17. Resistivity vs. Vitreous Carbon Content of a CIBA 1139/972 Substrate

4.1.3 Electrode Development

Substrates for positive electrodes which were to be of the Planté type were fabricated in the same manner as described except that a 0.010-in. (0.025-cm) thick lead sheet was bonded to the front surface of the substrate during molding in place of the molded grid pattern. The 0.010-in. (0.025-cm) thick lead sheet was then cleaned and Planté formed in the usual manner. Several sets of Planté-type positive electrodes were produced. All of these electrodes were Planté formed to produce the active positive material, PbO_2, in an identical manner except for the formation time. A flooded cell consisting of a bipolar half-plate (electrode) and either another bipolar half-plate or a standard Pb 660 plate of opposite polarity was used to evaluate the performance of the electrode. The separator was microporous polyvinyl chloride with an overall thickness of 0.050-in. (0.13-cm) and 0.030-in. (0.08-cm) high ribs (Porvic-1, Electric Power Storage Limited, Essex, England). Electrolyte was 1.260 sp gr sulfuric acid. Results are listed in Table 38. The poor performance results listed for Plate PL1 were attributed to insufficient active positive material. A significant capacity increase was achieved by increasing the Planté formation time of the next two plates.

During the testing of Plate PL3, it was observed that increasing the electrolyte concentration from 35% H_2SO_4 (1.260 sp gr) to 42% (1.320 sp gr) caused a capacity decrease of 13% at the 2.5-A (0.08-A/cm^2) discharge rate and 26% at the 5.0-A (0.16-A/cm^2) discharge rate. Charging at a 2.71-V constant voltage with a maximum current limit of 2.5 A, compared to a charging at constant current of 2.5 A (0.08 A/cm^2), resulted in discharge times to 1.5 V at 5.0 A of 70 and 30 sec, respectively.

The improved performance of Plate PL4 is attributed to charging at a constant voltage of 2.71 V with a 4.5-A (0.14-A/cm^2) limit. The longest discharge time to 1.5 V at 5 A was 2.0 min and occurred at Cycle 42. The discharge rate was then changed to 10 A (0.31 A/cm^2), which resulted in the maximum discharge time (31 sec) occurring at Cycle 50. Discharge time or capacity then began to decrease (Cycle 100 -- 20 sec, Cycle 250 -- 4 sec, Cycle 440 -- <1 sec).

Table 38. Formation and Performance of Planté-Type Positive Plates Formed on Conductive Epoxy-Vitreous Carbon Substrates

Plate	Formation Time, hr	Increase in Thickness, cm	Discharge to 1.5 V		Total Number of Cycles
			Current Density, A/cm^2	Time, min	
PL1 (Pure Pb)	20	---	0.016	22.1	14[a]
			0.031	8.7	
			0.077	1.5	
			0.16	0.5	
PL3 (Pure Pb)	46	0.020	0.071	2.4	141[b]
			0.14	1.2	
PL4 (Pure Pb)	46	0.020	0.14	2.0	440[c]
			0.28	0.5	
PL5 and PL6 (Sb)	69[d]	0.030	---	---	---
PL7 and PL8 (Li)	50[d]	0.025	---	---	---

[a] Charged at constant current; capacity decreased rapidly with cycling. Active material was adherent at end of test.

[b] Charging at constant current yielded lower capacity than charging at constant voltage; higher sulfuric acid electrolyte concentration decreased capacity. Active material loose and shedding at end of test.

[c] Charged at constant voltage of 2.71 V; capacity decreased with cycling. Active material loose and shedding at end of test.

[d] Active material loose and shedding at the end of formation.

Further attempts to increase the performance of Planté positives by using lead alloys (to produce a more adherent active material) and longer formation times (to increase the quantity of active material) proved unsuccessful. It is believed that Plates PL3 and PL4 are close to the ultimate that can be achieved by this method. The Planté formation process is a delicately balanced empirical procedure which does not permit a great amount of variation.

The only known modification which might be attempted to improve the adherence and performance would be to deeply groove the lead sheet to enhance the surface area. This has never been done with lead sheets as thin as those being used in this project and great difficulty is expected. Even with 0.025-cm thick lead sheets a bipolar plate of the Planté type would weigh 26.6 g; that is 30% greater than a bipolar plate with 0.051-cm thick layers of pasted active material. The development of bipolar electrodes utilizing Planté formation was terminated and the effort concentrated on electrodes utilizing pasted active material.

Pasted positive plates were prepared by plating a thin film of lead on the grid structure of the conductive epoxy surface. The plates were then pasted with oxide, cured and electrochemically formed in sulfuric acid to produce the active PbO_2 material. Paste formulas and fabrication data are summarized in Table 39. The pasted positives initially fabricated could not be completely formed and exhibited poor performance characteristics, particularly at high rates as shown by the data in Table 40. The electrodes were tested using the same type cell described previously. Variations in oxides, curing conditions and forming conditions all failed to significantly improve the situation. The difficulty was finally traced to pinholes in the substrate material which permitted sulfuric acid to penetrate to the lead back plate, forming a high resistance interface by corrosion. Decreasing the carbon content of the conductive epoxy eliminated this problem. Plate PA9 with 73 wt % vitreous carbon in the substrate exhibited greatly improved high rate capacity and longer life. Comparison of the performance of Plates PA9 and PA10 indicates that cycling at lower rates to "condition" the electrode may be helpful. In an effort to further improve the performance and life of the positive electrodes, a

Table 39. Fabrication of Pasted-Plate Positives with Epoxy-Vitreous Carbon Substrates

Plate	Vitreous Carbon Content, wt %	Lead Layer Thickness, cm	Paste Formula Number/Oxide	Cure Time, hr
PA1	80	0.0013[a]	PF-66/SP102	89[b]
PA2	80	None	PF-66/SP102	89[b]
PA3	80	0.0013[a]	PF-66/SP102	61[b]
PA4	80	0.0013[a]	PF-35-A/SP103	60[b]
PA5	80	0.0013[a]	$K_2S_2O_8$ + PbO	5[b]
PA6	80	0.0013[a]	---	--
PA7 & PA8	80	0.0013[d]	PF-66/SP102	72[e]
PA9	73	0.0051[d]	PF-66/SP102	72[e]
PA10	73	0.0051[d]	PF-66/SP102	72[e]
PA11 & PA12	60	0.0025[d]	Special leady oxide	16[f]

[a] Substrate rib height, 0.038 cm.

[b] In air at room temperature and humidity.

[c] Formed negative converted chemically into positive.

[d] Substrate rib height, 0.051 cm.

[e] Wrapped in plastic.

[f] At 100% relative humidity and 60 °C.

Table 40. Formation and Performance of Pasted-Plate Positives with Epoxy-Vitreous Carbon Substrates

Plate	Formation Rate, mA/cm^2	Discharge to 1.5 V		Total Number of Cycles
		Current Density, A/cm^2	Time, min	
PA1	1.7[a,b]	0.00062	490	10
		0.078	<0.05	
PA2	1.7[a,c]	---	---	0
PA3	1.7[a,b]	0.078	0.43	12
PA4	0.6[a,b]	0.00062	465	7
PA5	0.6[a,d]	0.00062	351	9
PA6	---	---	---	0
PA7 & PA8	7[f,g]	0.0078	0.17	--
PA9	7[f]	0.016	46	628[h]
		0.031	20	
		0.078	5.2	
		0.16	1.5	
PA10	7[f]	0.031	0.25	16[i]
PA11	7[f]	0.016	63	9[j]
PA12	7[f]			6086

[a] Electrolyte, 1.060 sp gr.

[b] Poor formation, white spots or layer.

Table 40. Formation and Performance of Pasted-Plate Positives with Epoxy-Vitreous Carbon Substrates (Continued)

[c] Poor formation. X-ray diffraction analysis results, α-PbO_2, 10%; β-PbO_2, 38%; PbO (tetr.), 6%; $PbSO_4$, 23%.

[d] Poor formation; additional formation in 1.260 sp gr sulfuric acid at 50 °C unsuccessful.

[e] Chemical conversion incomplete.

[f] Electrolyte, 1.080 sp gr.

[g] Appeared well formed.

[h] Charged at a constant voltage of 2.55 V (0.16 A/cm^2). Discharged through 600 cycles at 0.16 A/cm^2; discharge time $\sim$1.5 min for first 20 cycles, then decreasing to <1 sec. Discharge time for Cycle 628 at 0.031 A/cm^2 was 11 min.

[i] Same charging mode as for Plate PA9. All discharges at 0.031 A/cm^2; discharge time for Cycle 16 down to 6.6 min.

[j] Charged at constant-voltage of 2.70 V for 2 hr. Test discontinued after 9 cycles (0.53 A hr, 39.8% of theoretical capacity) because of a short.

special leady oxide was used to fabricate Plates PA11 and PA12. A significant increase in capacity was observed for Plate PA11. However, testing was discontinued after a short developed during the ninth recharge.

The performance history of Plate PA12 is given in Table 41. All the performance testing was carried out at room temperature, and it is believed that no significant temperature increase occurred due to the testing. It should be noted that the discharge times [except at a current density of 1.5 A/in.^{2} (0.23 A/cm^2)] actually increased after 45 deep discharges. The end-of-discharge voltage in the "B" cycles [discharge at 1.0 A/in.^{2} (0.16 A/cm^2) for 25 sec] began at 1.75 V and then decreased with cycling. It appears that a full recharge was not possible in 50 sec, even though charging at constant voltage was used. After about 850 continuous "B" cycles, during which the end-of-discharge voltage had deteriorated to 1.0 V in <25 sec, another 100 "B" cycles with a constant end-of-discharge voltage of 1.65 V was achieved by increasing the recharge time to 75 sec.

"A"-cycle performance was better; after 2800 cycles of discharge at a constant current density of 0.16 A/in.^{2} (0.025 A/cm^2) for 10.8 sec, and charge at a constant current density of 0.08 A/in.^{2} (0.012 A/cm^2) for 22 sec, the end-of-discharge voltage was 1.89 V. However, during the next 2000 cycles the end-of-discharge voltage had deteriorated to 1.0 V in <10.8 sec of discharge. After a boost charge, the end-of-discharge voltage of the "A" cycle returned to a higher value (1.95 V). After this treatment, the cell was cycled with a 0.25-A/in.^{2} (0.039-A/cm^2) discharge and a 2.7-V constant-voltage charge for 2 hr. A capacity of about one-half that found initially in the same cycle mode was achieved. Upon disassembling the cell, it was noted that the active positive material was soft and porous, i.e., swelling had occurred and there was evidence of some material shedding.

Initially the plate contained 9.5 g of active material, 1.0 g of lead plating and 2.0 g of conductive substrate assignable to the positive bipolar component. The i_{75} value (75-sec rate to 1.5 V) and the average cell voltage, $\bar{V}$, were estimated to be 1.4 A/in.^{2} (0.22 A/cm^2) and 1.6, respectively.

The negative pasted bipolar electrodes were made with automotive leady oxide and paste formula PF-73. The electrodes were cured in air or wrapped

Table 41. Performance Data for Bipolar Positive Electrode PA12

Cycle	Current Density, A/cm^2	Discharge Time, sec to 1.75 V	to 1.50 V	to 1.00 V
1	0.31[a]	~1	36	62
6	0.23	27	64	78
2	0.16	74	124	135
3	0.088	255	286	297
7	0.022	1165	1198	1244
8-52	0.039	--	--	--
53	0.039	1282	1365	1397
54	0.31	0	13	65
55	0.23	--	62	127
58	0.16	43	157	216
59	0.088	297	442	474
60-110	B[b]	≥1.75 V at end of discharge		
111-896	B	Performance deteriorated to 1.0 V in <25 sec of discharge		
897-910	Various low-rate cycles	----------		
911-1011	Modified B[c]	End of 25-sec discharge constant at 1.65 V		
1012	A[d]	2.05 V at end of discharge		
1013-2947	A	----------		
2948	A	1.95 V at end of discharge		
2949-3849	A	----------		
3848	A	1.89 V at end of discharge		

Table 41. Performance Data for Bipolar Positive Electrode PA12 (Continued)

Cycle	Current Density, A/cm^2	Discharge Time, sec to 1.75 V	to 1.50 V	to 1.00 V
3850-5850	A	Performance deteriorated to 1.0 V in <10.8 sec of discharge		
5851	Low-rate boost charge	----------		
6064	A	1.95 V at end of discharge		
6065-6086	0.039	----------		720

[a] Charged at 2.70 V for 2 hr.

[b] "B" Cycle:
Discharged at 0.16 A/cm^2 for 25 sec, charged at 2.71 V (0.11 A/cm^2 maximum) for 50 sec.

[c] Modified "B"-Cycle:
Charge time increased to 75 sec.

[d] "A"-Cycle:
Discharged at 0.025 A/cm^2 for 10.8 sec, charged at 0.012 A/cm^2 for 22 sec.

in plastic. Electrolyte used during formation was 1.060 or 1.080 sp gr sulfuric acid and formation rates varied from 1 to 7 mA/cm^2. All of the negative electrodes produced had a very uniform appearance. Single-electrode measurements of assembled test cells indicated that the cells were limited by the positive bipolar electrode. No signficant changes were observed after the negative electrodes were cycled. The capacity to total discharge of a negative electrode prepared by pasting ~4.5 g active material onto a substrate with 0.038-cm high ribs was 0.375 A hr at the 20-hr rate, approximately 56% of theoretical capacity. A wide latitude is permissible in the processing of negative electrodes and no performance problems with the negative electrodes are expected.

4.2 ELECTRODE AND BATTERY EVALUATION

4.2.1 Fabrication

Bipolar half-plates (electrodes) and batteries were fabricated in order to determine their performance figures of merit on both the components and test cell levels as was done with the conventional (prismatic) plates and batteries. Two negative electrodes (N3 and N4) and two positive electrodes (P4 and P6) were fabricated for single-electrode tests. The positive electrodes for single-electrode testing were produced in the same manner as Plates PA11 and PA12 (Section 4.1.3) and used the same special leady oxide. After formation, the positive plates were washed and air dried. The negative electrodes used the same substrate material (conductive substrate composed of CIBA 7072 epoxy resin and CIBA 972 hardener with 60 wt % vitreous carbon) as the positive electrodes. The negative paste was automotive leady oxide and paste formula PF-73. Negatives were formed under the same conditions as the positive electrodes. After formation the negatives were washed, the water removed in boiling Stoddard solvent, and then air dried. Each electrode contained 4.0 g of conductive substrate (of which half is assignable for bipolar electrode considerations), a 0.030-in. (0.076-cm) thick pure lead backplate and a tab. The conductive substrate was plated with a 0.001-in. (0.0025-cm) thick layer of lead which weighed 1.0 g. The backplate and lower portion of the tab of the positive electrodes were lacquer-coated to prevent oxidation during testing. Weights of the single electrodes are listed in Table 42.

Table 42. Single Bipolar Electrode Weights

	Weights, g	
Electrode	Active Material	Bipolar Portion
N3	4.9	7.9
N4	4.8	7.8
P4	7.4	10.4
P6	7.7	10.7

A test cell was constructed by sealing the edges of a positive and negative electrode, separated by a Teflon (TFE) spacer, 0.060-in. (0.15-cm) thick, with epoxy. The epoxy used was CIBA 6010 resin with TETA hardener with Thixin added in sufficient quantity to produce a non-flowing mixture. The electrodes were the same as described above. The Porvic-1 separator (described in Section 4.1.3) was inserted after the epoxy had cured and the Teflon spacer had been removed. The positive bipolar portion of the cell weighed 10.6 g and the negative portion 8.0 g.

Two two-cell batteries were fabricated in essentially the same manner except the active material on the electrodes was unformed. The end electrodes were the same as the lead-backed electrodes described previously. The center electrodes of the batteries were true bipolar elements composed only of conductive vitreous carbon-epoxy substrate with active material pasted on both sides. The electrodes were separated by Teflon spacers and the edges were sealed in the same manner as the cell. Porvic-1 separators were inserted after the epoxy had cured and the Teflon spacers had been removed. A lead wire was sealed in place with epoxy to contact the center bipolar plates for voltage readings. Weights of the electrodes in the batteries are listed in Table 43.

A photograph of the two-cell bipolar battery is shown in Figure 18.

4.2.2 Tests and Results

The bipolar half-plates (electrodes) were assembled in "flooded" cell configuration using a Porvic-1 separator and Pb 660 plates of opposite polarity as auxiliary electrodes. The cell was filled with 1.260 sp gr sulfuric acid and tests conducted at 51 °C (125 °F). The test sequence was similar to that used for the components-level plate test (Section 3.2). The results of the test are listed in Table 44.

For the negative electrode, the i_{75} value was >0.33 A/cm^2 for both electrodes tested. The figure of merit for specific power was 2.30 W/g. This may be compared to a best value of 1.90 W/g for the pasted plates described in Section 3.2. The target performance was 60 sec of discharge at 0.31 A/cm^2 with a cell voltage greater than 1.5 V; the bipolar negative electrodes yielded 90 sec at that rate, 50% better than the target value.

Table 43. Type II (Bipolar) Battery Electrode Weights

Battery	Electrode	Weight, g	
		Paste[a]	Bipolar Portion
1	End negative	5.1	8.1
	End positive	6.9	9.9
	Bipolar element	9.9	14.8
2	End negative	5.0	8.0
	End positive	8.5	10.5
	Bipolar element	9.3	15.6

[a] Paste weight includes both negative and positive pastes on the bipolar elements.

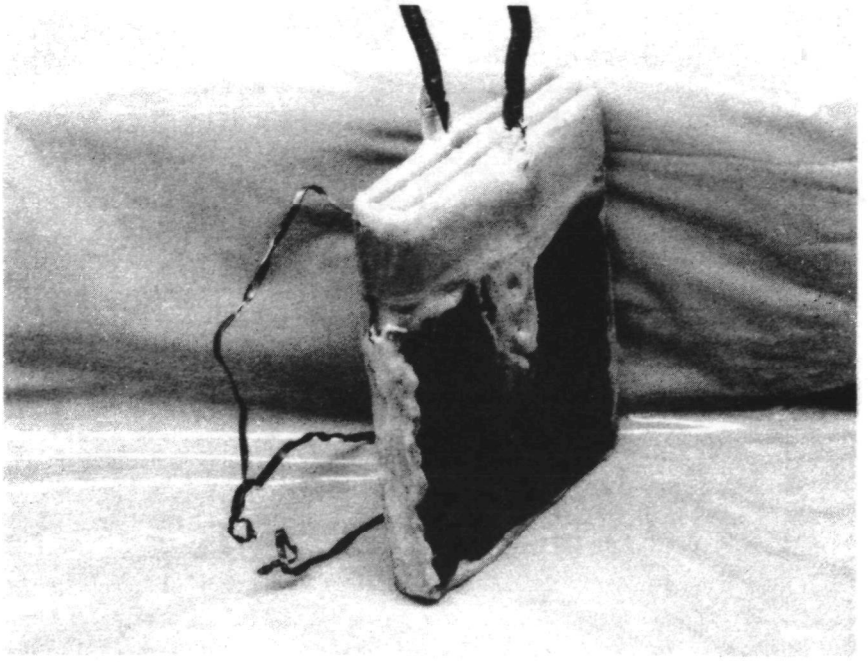

Figure 18. Two-Cell Bipolar Battery. Extra lead for monitoring center bipolar plate.

Table 44. Performance Test Data on Bipolar Test Plates

Electrode	Resistance, mΩ[a]	Discharge to 1.5 V			$i_{75'}$, A/cm^2	$(fm)_{sp}$, W/g
		Current, A	Current Density, A/cm^2	Time, min		
P4	>100				---	---
P6	25.5[b]	15	0.47	0.34	0.26	1.26
		10	0.31	1.0		
		5	0.16	2.6		
		2.5	0.08	5.6		
N3	20	15	0.47	0.7	0.36	2.30
		10	0.31	1.6		
		5	0.16	4.1		
		2.5	0.08	12.7		
N4	21	15	0.47	0.64	0.33	2.30
		10	0.31	1.4		
		5	0.16	3.8		
		2.5	0.08	12.0		

[a] At 1 kHz.

[b] Increased to 50 mΩ on standing overnight at open circuit.

The positive electrode yielded 60 sec at 0.31 A/cm^2 discharge with a cell voltage $\geq$1.5 V. This also meets the target value. The i_{75} value for the positive electrode was 0.26 A/cm^2 and it had a figure of merit of 1.26 W/g. This may be compared with the best figure of merit of 1.77 W/g for the pasted plates described in Section 3.2. It was noted that the active material became soft and some shedding occurred and that electrode resistance increased.

The test cell described in Section 4.2.1 could not be evaluated because of high internal resistance (150 mΩ). The high internal resistance was probably due to a high contact resistance at the interface between active material and the substrate.

Difficulties were encountered when attempts were made to form the electrodes in the two-cell bipolar batteries. One cell in each of the batteries would not accept a charge and a possible short in the unformed cell was suspected. In an effort to repair the short and prevent a recurrance of the problem, the separators were removed and the battery was rinsed in water and Stoddard solution at 105 °C and dried. New separators were then inserted and sealed with epoxy at the bottom of the cells to prevent bridging of the sediment. Even though this procedure eliminated the short problem, the unformed cell could not be completely formed. It is believed that sulfation of the paste had occurred while the active material was immersed in the forming acid during the initial attempts to form the plates.

4.3 SUMMARY AND RECOMMENDATIONS

The following conclusions can be reached:

- Conductive plastic substrates can be fabricated using vitreous carbon and various epoxy systems which will be chemically inert in a lead-acid cell environment. These substrates have a resistivity of $\leq$1 Ω cm and a density of $\sim$1.4 g/cm^3 and can be fabricated in a thickness of $\sim$0.025 in. (0.064 cm).

- A sufficient quantity of active material cannot be formed by known Planté methods to meet the performance requirements of 2 A/in.^{2} (0.31 A/cm^2) for 60 sec. The difficulty is fundamental because shedding of the active material occurs after some point and efforts to produce a more adherent structure by alloying the lead base material failed.

- o Performance of negative bipolar-type plates exceeded our target of 2 A/in.^{2} (0.21 A/cm^2) for 60 sec. Figure of merit for the positive bipolar-type plates was 30% lower than for the best conventional positive plate tested. Cycle life of the best bipolar positive plate was 6000 cycles including 60 deep discharges to 1.0 V. This is believed to be about equivalent to what would be expected from a good conventional positive plate. Most bipolar positive plates had short lives due to softening of the active material.

In view of these conclusions, it is recommended that:

- A variety of thermoplastic materials be evaluated as alternates for epoxy in a conductive plastic substrate. The objective would be to reduce manufacturing time and to fabricate a thinner substrate with greater strength. Candidate materials are chlorinated polyvinyl chloride, chlorinated polyethers, polyvinylidene fluoride, polyphenylene oxide and other thermoplastics.

- Development should continue in the area of positive oxides, pasting and formation techniques, and adhesion of the active material to the substrate.

- Methods of sealing bipolar plates into a cell and of sealing the cells of a battery together should be developed further. Candidate methods are a) use of rubber gaskets and compressing between end plates, and b) sealing of bipolar substrates to plastic frames followed by sealing of frames to each other by ultrasonic, solvent or thermal welding techniques.

5. PROJECTIONS AND RECOMMENDATIONS

5.1 PRISMATIC CELLS

5.1.1 Duty Cycle and Design Requirements

Several considerations impact the performance specifications for a hybrid-vehicle battery. They are vehicle acceleration and cruise performance, vehicle weight and volume, and battery durability. Many of the battery requirements can be generated from the design criteria developed by EPA and stated in "Vehicle Design Goals - Six Passenger Automobile," Revision B, Advanced Automotive Power Systems Development Division, Environmental Protection Agency, 11 February 1971. The following discussion is based on those goals and is augmented by information generated during a parallel TRW effort, "Cost and Emission Studies of Heat Engine/Battery Hybrid Family Car," Contract No. 68-04-0058, Environmental Protection Agency.

5.1.1.1 Battery Power Requirements

Peak Power

Figure 19 shows the road horsepower and cruise road horsepower for a 4,000-pound vehicle as a function of vehicle velocity. These curves were generated from performance goals described in Paragraph 8 of the EPA design goals document.

In order to translate the vehicle performance goals into power levels at the battery terminals, it was necessary to adjust the loads in Figure 19 for the effects of power train inefficiencies between battery and road. Using data generated in the Cost and Emission Studies, it was possible to construct vehicle velocity-battery power-time relationships for various hybrid configurations, engine power settings and battery characteristics. Figure 20 shows a case in which the vehicle velocity varies as a function of time according to the revised EPA battery specifications (detailed in Section 2.1). The particular vehicle modeled in this case was a series-connected hybrid, with a single gear ratio between the motor and wheels. The car has the capability of meeting or exceeding all the vehicle design goals and has a top speed (engine power only) of close to 90 mph which is reached in 25 sec after the start of the acceleration. The battery power-time relationships for specific velocity-time schedules, or the reverse, are small functions of the specific configuration chosen; however, the values of Figure 20 are quite representative of hybrid-vehicle demands.

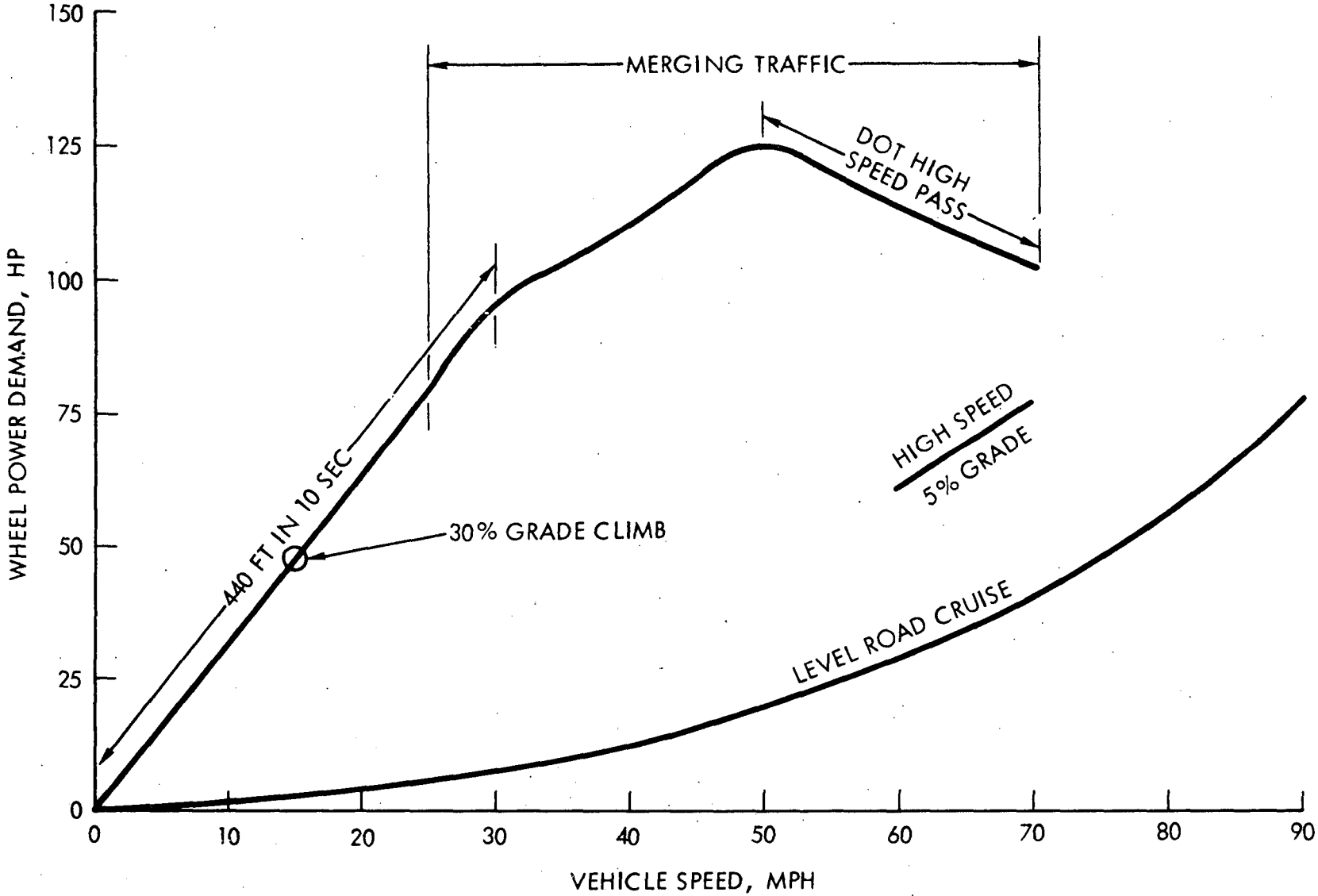

Figure 19. Wheel Power Demands for a 4,000-lb Car

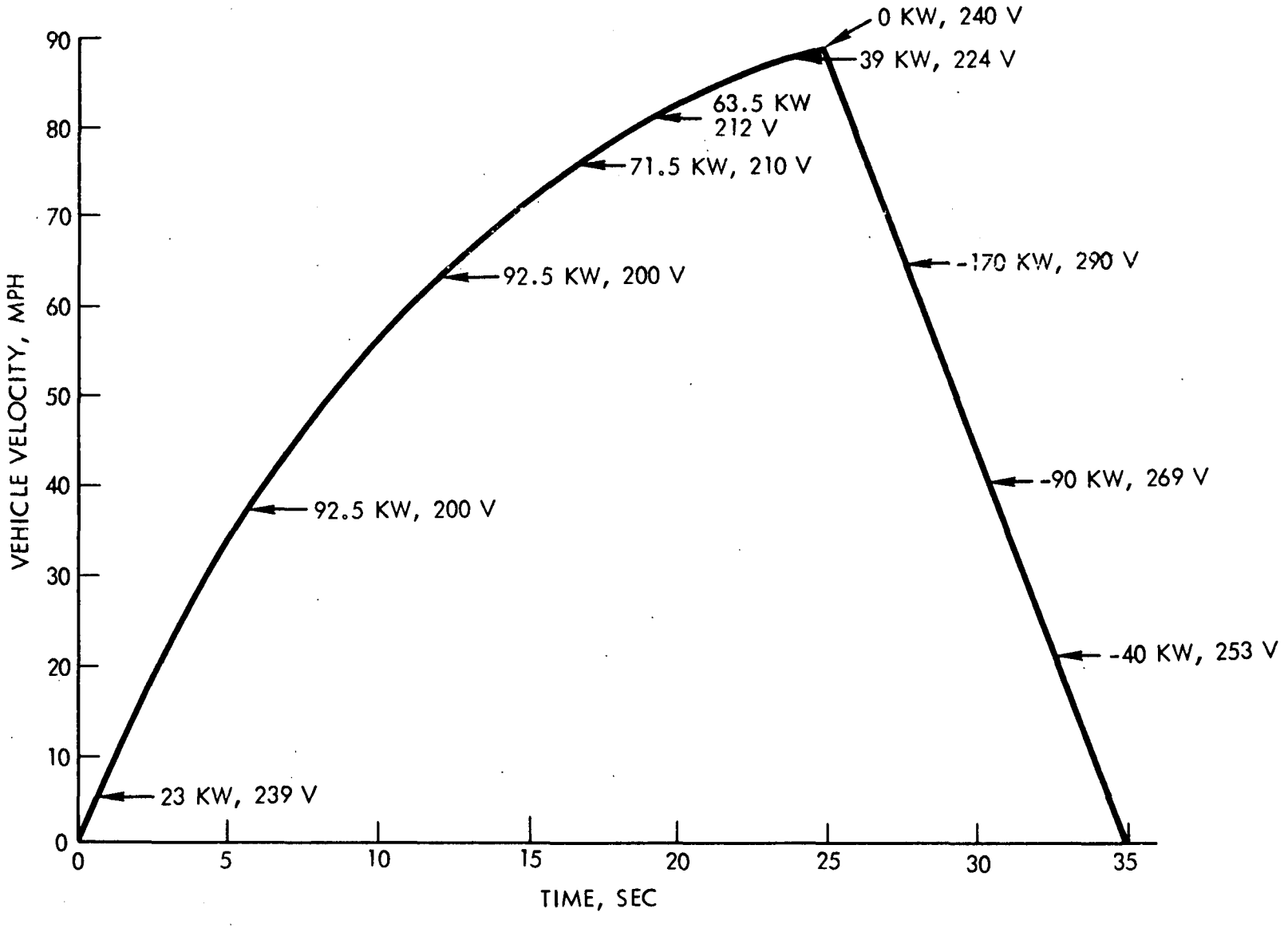

Figure 20. EPA Battery Power Profile for a 4,000-lb Series Hybrid Vehicle

The revised EPA battery specifications identify a 39-kW recharge rate for 90 sec. In reviewing the modes of power train operation, it is difficult to develop a circumstance in which this situation could arise. For example, Figure 20 shows that a panic stop from 90 mph in 10 sec could produce charge power levels at the battery in excess of 200 kW, but for periods of only a few seconds. Extended hill descents could last for 90 sec but the 39-kW power level for charging is difficult to construe.

Average Power

Analyses conducted during the Cost and Emission Studies contract contributed to an understanding of hybrid power-train components performance on a representative driving cycle. Average battery power and current are 9.4 ± 0.6 kW and 3.9 ± 0.2 A, respectively, during charge; and 11.3 ± 2 kW and 50 ± 10 A, respectively, during discharge. The averages are defined in terms of the average of all similar events; that is, the 9.4-kW charge power means the average power during all charging events is 9.4 kW.

A histogram for the battery charge and discharge currents during a typical driving mission is shown in Figure 21. During approximately 70% of the vehicle operating time the battery is being charged. The most probable battery current is approximately 50 A charge. Extremely high charge or discharge rates are not experienced. Such data are useful in constructing battery test cycles to simulate actual operating experiences.

While the ratio of charge to discharge time in the revised EPA specification is in agreement with the histogram ratio experienced in hybrid-vehicle operation, the time spent in high-rate charging seems unrealistic. There is some question as to the need for a full recharge after every discharge. For example, it is not clear that each 70.5-kW discharge should be associated with a 39-kW recharge which restores the battery to its original energy state. Rather, TRW's experience in operating its electromechanical transmission system is that the higher power level charge events occur in a quasi-tapered charge manner. With reference to Figure 20, the charging level during deceleration rapidly decreases as the vehicle slows down. Further time correlations are necessary to completely define the discharge-charge cycles which would represent actual battery usage.

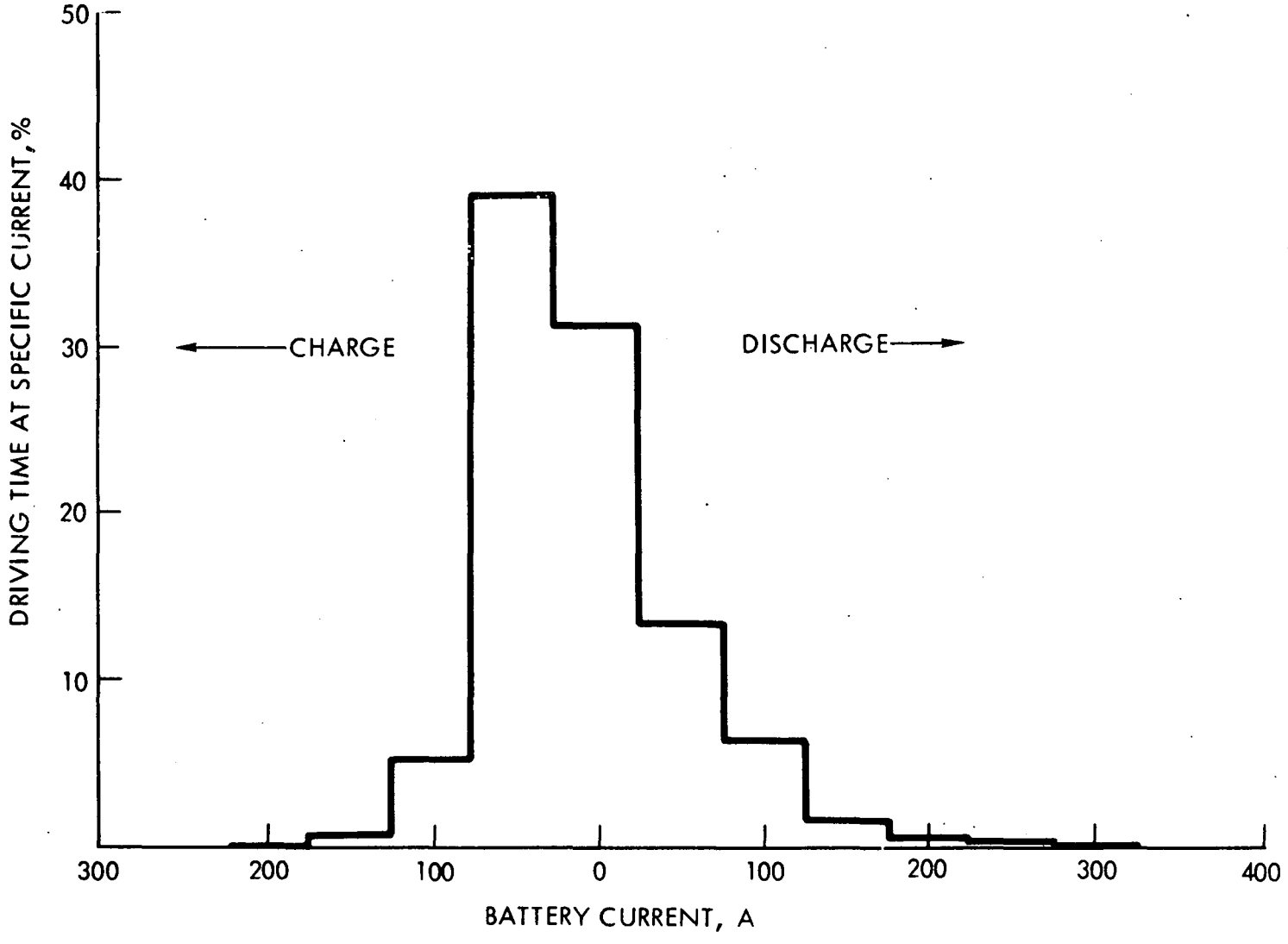

Figure 21. Typical Histogram of Battery Current during a Driving Cycle

5.1.1.2 Battery Weight and Volume

Paragraph 2 of the EPA design goals specifies a maximum power-train weight of 1,600 lb and a desirable weight of 1,300 lb, the latter consistent with current automotive practice. Analyses of the series and parallel hybrid systems suggest power-train weights of 1,090 and 840 lb, respectively, without battery. Table 45 compares the battery weights and peak specific powers for series and parallel systems for maximum and conventional power-train weights. It appears that the battery specific power requirements for the 1,600-lb power train can be met for both systems, although the series system may be marginal. Both systems, especially the series, will find it difficult to meet the lower power-train weight of a conventional vehicle without substantial improvement in battery specific power.

Due to the high density of lead-acid batteries no particular volume problems are anticipated. Furthermore, the ability to modularize the battery package into small distributed packages will aid in vehicle design flexibility.

5.1.2 Projected Characteristics of Cell and Full-Size Battery

On the basis of results for test cells, it is estimated that a cell of identical design except with 17 plates instead of 21 plates would meet the revised EPA power and capacity requirements. Weight of a six-cell battery in a custom-designed polypropylene container would be about 23.5 lb (10.7 kg) and the container would be about 8-in. long × 5.5-in. wide × 6.75-in. high (20.3 cm × 14.0 cm × 17.1 cm).

The full-size battery would consist of 22 six-cell units connected in series to give a nominal 264 V. Weight and volume would be 525 lb (239 kg) and 5.5 ft^3 (0.16 m^3), respectively. Life of the battery is expected to be three to five years.

5.1.3 Availability and Development

It is estimated that the cost of this battery to the original equipment manufacturer at a production rate of 100 batteries/day (2,200 12-V units) would be approximately $440. Production could begin in 1973.

A full-size battery could be produced in 1972 on a developmental basis. The biggest problem would be acquisition of polypropylene containers,

Table 45. Battery-Weight Constraints for Hybrid-Vehicle Systems (92.5-kW Peak Power Demand)

Hybrid System	Power Train Weight, lb	Battery Weight, lb	Specific Power, W/lb
Series	1,600	510	180
Parallel	1,600	760	120
Series	1,300	210	435
Parallel	1,300	460	200

for which a mold would have to be designed and fabricated. An existing container could be used, as was done in the case of the test cells, with considerable sacrifice in space utilization and with a weight penalty of perhaps 10%.

5.2 BIPOLAR BATTERY

Results achieved in the present program have demonstrated that a lightweight conductive substrate can be pasted and formed to produce a bipolar plate having current capability of 2 A/in.^{2} (0.31 A/cm^2) for one minute to a 1.5-V per cell cutoff. Discounting this by one-third to 1.4 A/in.^{2} (0.22 A/cm^2) to allow for losses normally encountered in scale-up, leads to an estimate of a total weight of 430 lb (195 kg) and a total volume of 3.3 ft^3 for a full-size battery system. The battery would consist of six modules, 6.6 in. × 7.8 in. × 15.5 in. (16.8 cm × 19.8 cm × 39.4 cm) which contain 134 cells each. The entire module would be served by addition of water to a single trough serving all cells. Other details are the following:

Bipolar Plate Size

- Active Material — 6.2 in. × 6.2 in. × 0.020 in. (15.7 cm × 15.7 cm × 0.051 cm)
- Substrate — 6.4 in. × 6.4 in. × 0.025 in. (16.3 cm × 16.3 cm × 0.064 cm)
- Plastic Frame — 6.6 in. × 7.8 in. × 0.115 in. (16.8 cm × 19.8 cm × 0.292 cm)

Contains reservoir, separator and vent.

268-V Module

- Size — 6.6 in. × 7.8 in. × 15.5 in. (16.8 cm × 19.8 cm × 39.4 cm)
- Volume — 800 in.^{3} (0.013 m^3)
- Weight — 70 lb (32 kg)

Complete Battery

	Prototype	Projected
• Modules	6	4
• 75-Sec Current	320 A	304 A
• Average Voltage	220 V	227 V
• 75-Sec Energy	7000 kJ	6900 kJ
• Volume	0.093 m^3	0.062 m^3
• Weight	195 kg	136 kg

We estimate that a prototype battery of this type could be built in 1973, with production in 1975.

Over a longer term it is expected that current capability can be increased to 2 A/$in.^2$ resulting in a 33% reduction in size, to four modules instead of six. This leads to the projected battery, weighing 300 lb (136 kg) and having a volume of 2.2 ft^3 (0.062 m^3). It is estimated that a prototype battery with these characteristics could be built in 1975 or earlier.

5.3 FUTURE WORK

5.3.1 Program Plan

It is recommended that development of both conventional and bipolar lead-acid batteries be continued. Work on conventional batteries should be directed toward a better understanding of the causes of failure of lead-acid batteries in hybrid-vehicle duty and of the life that can be obtained.

Limited optimization studies of the components of a conventional lead-acid cell have resulted in the fabrication and testing of cells that will produce an average power of 150 W/lb for 75 sec. This is almost twice the performance of conventional cells. While we do not believe we can continue to improve performance at this rate we do believe that additional optimization can result in a battery producing 200 W/lb for 75 sec without seriously changing current manufacturing methods or impacting the cost. The most serious question really concerns the lifetime of these high specific power batteries. Therefore we propose to perform life

studies at the components level to obtain the best compromise between lifetime and performance.

The failures that have been observed so far in the program have all been caused by softening of the positive active material. This is greatly affected by the manner in which charging is accomplished, and especially by incomplete charging, which fails to re-cement the active material and leads to softening. The very stringent cycling conditions that have been used are probably useful as an accelerated test for comparing various cell designs but they hardly permit estimation of battery life to be expected in a hybrid vehicle. Some life tests should be carried out under cycling conditions more representative of hybrid vehicle duty, with more shallow cycles, which will allow more time for complete chargeback after an occasional deep, full-power discharge.

We also believe that the longer term development of bipolar electrodes eventually will result in a long life lead-acid battery, compatible with hybrid-vehicle demands, which will produce 300 watts per pound. Thus our proposed program is divided into three parallel tasks, Tasks 1, 2 and 4 plus a design task, Task 3:

Task 1 Optimization Studies of Conventional Cells
Task 2 Life Studies of Conventional Cells
Task 3 Design and Performance Projections
Task 4 Development of Bipolar Battery

A detailed design will be made of a lead-acid battery capable of meeting the revised EPA requirements for a full size hybrid heat-engine/electric automobile.

5.3.2 Work Statement

TASK 1. OPTIMIZE CONVENTIONAL CELLS

1.1 Screen Cell Components

The highly successful program of optimization of the cell components instituted in the current program will be continued.

The effect of separator composition, thickness and design on performance will be tested along with increased pellet size (fewer structural members in the grid), use of inert binders in the pellets and the new grid design (4.25 in. × 4.25 in.) developed under the current program. The performance test will be the same as used in the current program and the same figure of merit,

$$(fm)_{sp} = i_{75}\bar{V}/W$$

where i_{75} is the current required to discharge a cell to 1.5 V in 75 seconds, $\bar{V}$ is the average cell voltage for this discharge, and W is the plate weight, will be used for evaluation.

The statistically designed performance test will consider information obtained during the current program. For example, interactions will be assumed negligible and use will be made of the estimate of experimental variation obtained to minimize the total number of tests necessary to achieve the test objectives. Preliminary considerations indicate the use of a Latin Square Design. As in the current program, tests will be performed in sequential steps to provide monitoring points so that the effectiveness of the test can be assessed as it proceeds.

Separators to be used in this study will be of various designs and will be acquired by purchase or by manufacture. These separators will be of various thicknesses no larger than about 0.020 in. and will be of various materials selected for low resistance and/or long battery life. Candidate materials are polyvinyl chloride and polypropylene with and without ribs. One or more separators may contain glass mats to aid in retention of active material.

1.2 Perform Computer-Assisted Modeling of Cells

A computer model developed under the current program for the plates will be extended to include the whole cell. The model of the plate will be refined to include the effect of pellet resistance, electrolyte resistance, state of charge, separator resistance and the number and size of plates.

TASK 2. LIFE-TEST CONVENTIONAL COMPONENTS AND CELLS

2.1 Perform Cycle-Life Study of First Generation Test Cells

Cycle-life test of a test cell started under the current program (first generation test cell) will be continued. The test program will be revised to include a recharge cycle and to match more closely the discharge cycle described by EPA. The test cell will be cycled 200,000 times or until failure whichever comes first. A cell will be considered to have failed when the cell voltage drops to 1.5 V. A Group Size 22F automotive SLI battery will be submitted to an identical test for comparison.

Although no catastrophic failure is anticipated, there is possibility of minimal degradation. As an example of data analysis, the end-of-discharge voltage can be plotted as a function of the number of cycles. The data will be plotted for each cell type and if a degradation trend is noted, the data will be subjected to a standard regression analysis to determine the curve which best describes the trend. This curve will be used to predict the number of cycles to an end-of-discharge voltage of 1.5 V. If the voltage reaches this value, the cell is considered to be in a failed condition. The magnitude of the coefficient of variation, $\sigma_w/\bar{x}$, between cells obtained from the specific power performance tests in the current program can be assumed to be the magnitude of variation between cells on the cycle axis so that a probability distribution of failure can be ascertained, if degradation is detected.

2.2 Perform Cycle-Life Tests on Components

Plates and separators which have been subjected to the performance test (Task 1.1) will be cycled using a form of an accelerated life test. Each component will be tested for the same number of cycles after which its performance will again be determined as described in Task 1.1 Difference in performance will be used as a criteria for measuring degradation as a function of cycling.

2.3 Perform Accelerated Corrosion Tests on Selected Grid Alloys

Four alloys will be prepared and cast into grids and test rods. Grids will be of the special design developed in the current program and performance tested in optimized cells. Grids will be pasted and tested in sp gr 1.260 sulfuric acid electrolyte. Corrosion rate will be accelerated

by maintaining the test cell at elevated temperature and by maintaining the test specimen at a potential of 0.075 V relative to the equilibrium potential of the alloy in the electrolyte. Plate dimensions will be measured periodically in situ by means of a cathetometer to determine rate and amount of growth. Plate capacity will be measured periodically and the test will be discontinued when capacity has decreased to 50% of its initial value. Tests will be carried out at 160, 140, and 120 °F. Life to 50% capacity will be expressed in terms of equivalent time at 75 and 125 °F. Test rods will be examined metallographically to determine corrosion pattern.

The following alloys will be tested:

1. 0.013% Li-Pb
2. 2.5% Sb-4.5% As-Pb
3. 0.07% Ag-1.5% Sb-1.6% Cd-Pb
4. 4.5% Sb-Pb

TASK 3. PROJECT PERFORMANCE AND DESIGN FULL SCALE BATTERY

3.1 Fabricate and Test Optimized Cells

The results of Tasks 1 and 2 will be used to design second generation test cells. These cells will be fabricated and tested using a test procedure similar to the one used in the current program. The emphasis will be placed on performance data although accelerated life tests will be considered.

3.2 Design Full-Scale Battery System

Based on the above approved design requirements and the results of the cell tests performed in Tasks 1, 2 and 3.1, the characteristics of a full scale battery system for a hybrid automobile will be projected with emphasis on weight and cost reduction consistent with specified life requirement. A preliminary design of a full scale battery system for a hybrid heat-engine/electric vehicle shall be performed. Full consideration shall be given to operational and maintainability requirements as well as cost and size reduction.

TASK 4. DEVELOP LIGHTWEIGHT BIPOLAR BATTERY

Methods of forming bipolar electrodes using conductive plastic substrates will be investigated. Both pasting and direct formation of active materials will be studied.

Methods of incorporating bipolar electrodes into a battery will be investigated. Performance objectives are a maximum discharge current density of 2 A/in.^{2} sustained for one minute to 1.5 V per cell cutoff and recharge capability suitable for a hybrid power train. Target specific power is 300 W/lb and target life in a hybrid power train is five years. Electrodes will have at least 100-cm^2 active area.

Initially, epoxy-glassy carbon substrates previously developed will be used. Methods of sealing bipolar electrodes into a battery will be studied. Candidate methods are 1) use of rubber gaskets and compressing the electrodes between endplates, and 2) sealing bipolar electrodes to plastic frames followed by sealing the frames to each other. Battery design will permit easy servicing.

Alternate conductive substrates offering lower cost and greater strength will be investigated. Candidate substitutes for epoxy in the substrates include chlorinated polyethers, chlorinated polyvinyl chloride, polyvinylidene fluoride and polyphenylene oxides.

APPENDIX A

MATHEMATICAL MODELING-PASTE ELEMENT

The basic assumptions used in this discussion are:

1. Current flowing from electrolyte to paste element moves in the z-direction and is uniformly distributed with respect to x and y.

2. The paste element occuplies the region $0 \leq x < a$, $0 \leq y \leq b$ of the x-y plane, and is "thin" in the z-direction. Its conductivity, σ, is small compared to that of its boundary which is taken to be an equipotential, at electrostatic potential $\phi = 0$. However, σ is large compared with the conductivity of the electrolyte.

The starting point for the analysis is the divergence theorem for the current desnity, $\vec{J}$, in the pellet. This current moves in the x-y plane (i.e., it has no z-component). The theorem states that

$$\int \vec{J}\cdot\hat{n}\ dS = \int \nabla\cdot\vec{J}\ dV \qquad (1)$$

in which $\hat{n}$ is the unit normal to the surface element of area dS, and dV is a volume element in the paste. The two integrals in Equation (1) are readily evaluated. The integral on the left is the total current flowing out of the volume element of the paste. This is of course equal to the total current entering the volume element from the electrolyte. If the area of the element which faces the electrolyte is dA, and the current density in the electrolyte is J, then

$$\int \vec{J}\cdot\hat{n}\ dS = J\ dA \qquad (2)$$

Since, by assumption, J is independent of x and y, and since the plate is thin, $\nabla\cdot\vec{J}$ is constant, and therefore

$$\int \nabla\cdot\vec{J}\ dV = \theta\ dA\ \nabla\cdot\vec{J} \qquad (3)$$

where θ is the thickness of the plate. Combining Equation (1), (2) and (3)

$$\nabla \cdot \vec{J} = J/\theta. \tag{4}$$

The relation between $\vec{J}$, the electric intensity, $\vec{E}$, and electrostatic potential, ϕ, is

$$\vec{J} = \sigma \vec{E} = -\sigma \nabla \phi. \tag{5}$$

Combining Equation (5) with Equation (4),

$$\nabla^2 \phi = -J/\theta\sigma. \tag{6}$$

This is Poisson's equation for the electrostatic potential, and is to be solved with the condition $\phi = 0$ on the boundaries $x = 0,a$, and $y = 0,b$. The solution, which can be effected by, for instance, the method of separation of variables, is

$$\phi(x,y) = k \sum_{\substack{m,n=1 \\ m,n \text{ odd}}}^{\infty} \sum^{\infty} \frac{\sin (mx\pi/a) \sin (ny\pi/b)}{mn(m^2/a^2 + n^2/b^2)} \tag{7}$$

where

$$k = 16J/\pi^4\theta\sigma \tag{8}$$

The average value, $\bar{\phi}$, of ϕ is

$$\bar{\phi} = (1/ab) \int_0^a dx \int_0^b dy\, \phi(x,y) = 4ka^2 \sum_{m,n \text{ odd}} \sum 1/[m^2n^2(m^2 + n^2t^2)] \tag{9}$$

where $t = a/b$. By symmetry, it is necessary to tabulate the sum in Equation (9) in the range $0 \leq t \leq 1$ only. The double sum is reduced to a single sum by means of the identity

$$\sum_{m \text{ odd}} 1/[m^2(m^2 + u^2)] = (\pi/4)[\pi/2u^2 - (1/u^3) \tanh \pi u/2] \tag{10}$$

Combining Equation (9) and (10), with u = nt,

$$\bar{\phi} = (ka^2/\pi)\left[\pi^5/192t^2 - (1/t^3) \sum_{n\ odd} (1/n^5) \tanh \pi nt/2\right]. \qquad (11)$$

In deriving Equation (11), use has been made of the identity

$$\sum_{n\ odd} 1/n^4 = \pi^4/96.$$

In terms of the average potential, $\bar{\phi}$, defined by Equation (9), the equivalent series resistance of the pellet may be defined as

$$R = \bar{\phi}/abJ \qquad (12)$$

that is, the series resistance is equal to the ratio of average potential to total current, abJ.

The current leaving the pellet at its boundaries is next considered. The current per unit length through the edge y = 0 is

$$J_0(x) = \theta\sigma\ (\partial\phi/\partial y)_{y\,=\,0} \qquad (13)$$

which becomes, on using Equations (7) and (8),

$$J_0(x) = 16a^2J/\pi^3b \sum_{\substack{m,n\\ odd}} [\sin\ (mx\pi/a)]/[m^2(m^2 + n^2t^2)]. \qquad (14)$$

The total current through the boundary y = 0 is the integral of Equation (14):

$$I_y = \int_0^a J_0(x)\ dx = 32a^3J/\pi^4b \sum_{\substack{m,n\\ odd}} 1/[m^2(m^2 + n^2t^2)]. \qquad (15)$$

The total current, I_x, through the boundary at x = 0 can be obtained from Equation (15) and the conservation equation,

$$2(I_x + I_y) = Jab \qquad (16)$$

By the use of Equation (10), I_y may be written as a single sum:

$$I_y = (abJ/2)\left[1 - 16/\pi^3 t \sum_{n\ \text{odd}} (1/n^3)\ \tanh\ \pi nt/2\right]. \tag{17}$$

The sum in Equation (17) is as readily evaluated as that in Equation (11).

Comparison of Equations (16) and (17) shows that the fraction of the current into the pellet which departs through the boundary x = 0 is

$$I_x/2(I_x + I_y) = 8/\pi^3 t \sum_{n\ \text{odd}} (1/n^3)\ \tanh\ \pi nt/2 \tag{18}$$

Finally, the voltage drop in the grid element at the y = 0 boundary will be calculated. This boundary has been assumed to be an equipotential. However, actually there is a small voltage gradient along each grid element, the presence of which does not materially affect the previous results.

Let the grid element extending from x = 0 to x = a have resistance R, and assume that all of the current entering it from the pellet flows to the end at x = a. Then the current at x is

$$I(x) = \int_0^x J_0(x')\ dx' \tag{19}$$

where $J_0(x)$ is given by Equation (14). The voltage drop in the portion (x, x + dx) is then

$$R/a\ dx \int_0^x J_0(x')\ dx'$$

so that the total voltage drop is

$$V = (R/a) \int_0^a dx \int_0^x J_0(x')\ dx'. \tag{20}$$

Performing the indicated integration results in

$$V = (16a^3 JR/\pi^4 b) \sum_{\substack{m,n \\ \text{odd}}} 1/[m^2(m^2 + n^2 t^2)]. \tag{21}$$

The double sum in Equation (21) is the same as that in Equation (15). The result is, therefore,

$$V = (abJR/4)\left[1 - 16/\pi^3 t \sum_{n \text{ odd}} (1/n^3) \tanh \pi nt/2\right]. \qquad (22)$$

The sums which appear in Equation (11), (18) and (22) were evaluated on the Hewlett-Packard 9100B calculator, for a variety of values of t in the range $0 < t < 1$. Parabolic fits to these results were used in the plate-resistance computer program.

APPENDIX B

SAMPLE CALCULATIONS FOR ANALYSIS OF VARIANCE

The Mean Square is equal to the Sum of Squares divided by the degrees of freedom associated with the source of variation (see Tables 20 and 27).

Using data for Runs 1 through 4 of Table 18, the Sums of Squares were computed as follows:

a. Total Sum of Squares (TSS)

$$\begin{aligned} TSS &= \text{Sum of Squares of Individuals (SSI) - Correction Factor (C)} \\ &= \sum x^2 - (\sum x)^2/n \\ &= 39.8^2 + 36.8^2 + \ldots + 39.9^2 + 37.0^2 - 22186.10 \\ &= 22254.84 - 22186.10 \\ &= 68.74 \end{aligned}$$

Note: x denotes $i_{75}\bar{V}$.

b. Sum of Squares for Runs (SSR)

$$\begin{aligned} SSR &= [(\sum x)_1^2 + (\sum x)_2^2 + (\sum x)_3^2 + (\sum x)_4^2]/4 - C \\ &= (147.5^2 - 147.5^2 + 150.1^2 + 150.7^2)/4 - 22186.10 \\ &= 2.25 \end{aligned}$$

Note: subscripts denote Run numbers.

c. Sum of Squares for Plates (SSP)

$$\begin{aligned} SSP &= [(\sum x)_1^2 + (\sum x)_2^2 + (\sum x)_3^2 + (\sum x)_4^2]/4 - C \\ &= (154.9^2 + 148.0^2 + 151.2^2 + 141.7^2)/4 - 22186.10 \\ &= 23.48 \end{aligned}$$

Note: subscripts denote Plate numbers.

d. Sum of Squares for Permutation Order (SSO)

$$\begin{aligned} SSO &= [(\sum x)_1^2 + (\sum x)_2^2 + (\sum x)_3^2 + (\sum x)_4^2]/4 - C \\ &= (145.5^2 + 156.2^2 + 149.2^2 + 144.9^2)/4 - 22186.10 \\ &= 20.23 \end{aligned}$$

Note: subscripts denote Permutation Order number (Section 3.2.4.1).

e. Sum of Squares for Experimental Variation (SSE)

$$SSE = TSS - SSR - SSP - SSO$$
$$= 68.74 - 2.25 - 23.48 - 20.23$$
$$= 22.78$$

Since no significance was detected, all data (that is, all five runs) were used to obtain the averages given in Table 19.

Using data for Test Run 2 of Table 23, the Sums of Squares given in Table 27 were computed as follows:

a. Total Sum of Squares (TSS)

$$TSS = SSI - C$$
$$= \sum x^2 - (\sum x)^2/n$$
$$= 1.45^2 + 1.10^2 + \ldots + 0.99^2 + 1.01^2 - 22.144083$$
$$= 23.185653 - 22.144083$$
$$= 1.041570$$

Note: x denotes $(fm)_{sp}$.

b. Sum of Squares for Thickness (SST)

$$SST = [(\sum x)_1^2 + (\sum x)_2^2]/8 - C$$
$$= (10.500^2 + 8.323^2)/8 - 22.144083$$
$$= 0.296208$$

Note: subscripts 1 and 2 denote thicknesses T_1 and T_2, respectively.

c. Sum of Squares for Temperature (SSt)

$$SSt = [(\sum x)_1^2 + (\sum x)_2^2]/8 - C$$
$$= (8.293^2 + 10.530^2)/8 - 22.144083$$
$$= 0.312760$$

Note: subscripts 1 and 2 denote temperatures t_1 and t_2, respectively.

d. Sum of Squares for Grid Type (SSG)

$$SSG = [(\sum x)_1^2 + (\sum x)_2^2]/8 - C$$

$= (9.976^2 + 8.847^2)/8 - 22.144083$

$= 0.079665$

Note: subscripts 1 and 2 denote grid types G_1 and G_2, respectively.

e. Sum of Squares for Paste Density (SSP)

$SSP = [(\sum x)_1^2 + (\sum x)_2^2]/8 - C$

$= (10.436^2 + 8.387^2)/8 - 22.144083$

$= 0.262400$

Note: subscripts 1 and 2 denote paste densities P_1 and P_3, respectively.

f. Sum of Squares for Experimental Variation (SSE)

$SSE = TSS - SST - SSt - SSP - SSG$

$= 1.041570 - 0.296208 - 0.312760 - 0.262400 - 0.079665$

$= 0.090537$